NASA-CR-199493

NAGW- 1944
IN-43-CR
5056
P_161

A SIMULATION TO STUDY THE FEASIBILITY OF IMPROVING THE TEMPORAL RESOLUTION OF LAGEOS GEODYNAMIC SOLUTIONS BY USING A SEQUENTIAL PROCESS NOISE FILTER

BRIAN DAVIS HARTMAN

Department of Aerospace Engineering Sciences

University of Colorado at Boulder

August, 1995

(NASA-CR-199493) A SIMULATION TO STUDY THE FEASIBILITY OF IMPROVING THE TEMPORAL RESOLUTION OF LAGEOS GEODYNAMIC SOLUTIONS BY USING A SEQUENTIAL PROCESS NOISE FILTER (Colorado Univ.) 161 p

N96-11021

Unclas

G3/43 0068155

This report was prepared under

Grant No. NAGW-1944

for the

National Aeronautics and Space Administration

Washington, D.C.

by the

Department of Aerospace Engineering Sciences

The University of Colorado at Boulder

Boulder, Colorado

under the direction of

Dr. George W. Rosborough

ABSTRACT

A key drawback to estimating geodetic and geodynamic parameters over time based on satellite laser ranging (SLR) observations is the inability to accurately model all the forces acting on the satellite. Errors associated with the observations and the measurement model can detract from the estimates as well. These "model errors" corrupt the solutions obtained from the satellite orbit determination process. Dynamical models for satellite motion utilize known geophysical parameters to mathematically detail the forces acting on the satellite. However, these parameters, while estimated as constants, vary over time. These temporal variations must be accounted for in some fashion to maintain meaningful solutions.

The primary goal of this study is to analyze the feasibility of using a sequential process noise filter for estimating geodynamic parameters over time from the Laser Geodynamics Satellite (LAGEOS) SLR data. This evaluation is achieved by first simulating a sequence of realistic LAGEOS laser ranging observations. These observations are generated using models with known temporal variations in several geodynamic parameters (along track drag and the J_2, J_3, J_4, and J_5 geopotential coefficients). A standard (non-stochastic) filter and a stochastic process noise filter are then utilized to estimate the model parameters from the simulated observations.

The standard non-stochastic filter estimates these parameters as constants over consecutive fixed time intervals. Thus, the resulting solutions contain constant estimates of parameters that vary in time which limits the temporal resolution and accuracy of the solution. The stochastic process noise filter estimates these parameters as correlated process noise variables. As a result, the stochastic process noise filter has

PRECEDING PAGE BLANK NOT FILMED

the potential to estimate the temporal variations more accurately since the constraint of estimating the parameters as constants is eliminated.

A comparison of the temporal resolution of solutions obtained from standard sequential filtering methods and process noise sequential filtering methods shows that the accuracy is significantly improved using process noise. The results show that the positional accuracy of the orbit is improved as well. The temporal resolution of the resulting solutions are detailed, and conclusions drawn about the results. Benefits and drawbacks of using process noise filtering in this type of scenario are also identified.

CONTENTS

CHAPTER

1 INTRODUCTION 1

1.1 Overview 1

1.2 Model Errors 1

1.3 Orbit Determination Filters 2

1.4 Satellite Laser Ranging and LAGEOS 4

1.5 Thesis Objectives 4

1.6 Description of Chapters 5

2 FILTERING THEORY 7

2.1 Introduction 7

2.2 The Orbit Determination Problem 7

2.3 State Estimation 11

2.4 Standard Filtering 14

2.5 Standard SRIF Filtering 15

2.6 Process Noise SRIF Filtering 19

2.7 Conclusions 28

3 SATELLITE LASER RANGING AND LAGEOS 30

3.1 Introduction 30

3.2 Satellite Laser Ranging 30

3.3 The Laser Geodynamics Satellite 32

3.4 LAGEOS Geodetic Solutions 34

3.4.1 LAGEOS J_2 and J_3 Solutions 35

3.4.2 LAGEOS Along Track Drag Solutions..... 37

3.5 Proposed Benefits of Process Noise Filtering for LAGEOS..... 38

4 SIMULATION MODEL..... 41

4.1 Introduction..... 41

4.2 Measurement Model..... 42

4.2.1 Tracking Network..... 43

4.3 Dynamical Model..... 47

4.4 True Model Deviation Signals Added to Model Parameters..... 48

4.4.1 Drag Model Deviation Signal..... 49

4.4.2 J_2 and J_3 Model Deviation Signal..... 50

4.4.3 J_4 and J_5 Model Deviation Signal..... 52

4.5 Summary of Data Simulation..... 54

5 FILTERING RESULTS..... 56

5.1 Introduction..... 56

5.2 One Year Arc: C_t, J_2, and J_3 Model Deviation Signals..... 56

5.2.1 Standard SRIF Using Boxcars..... 57

5.2.2 Process Noise SRIF..... 65

5.3 One Year Arc: C_t, J_2, J_3, J_4, and J_5 Model Deviation Signals..... 76

5.3.1 Standard SRIF Using Boxcars..... 76

5.3.1.1 Effective J_2 and J_3 Model Deviation Signals..... 79

5.3.2 Process Noise SRIF..... 90

5.4 Three Year Arc: C_t, J_2, and J_3 Model Deviation Signals..... 102

5.4.1 True Model Deviation Signals for the Three Year Arc..... 103

5.4.1.1 Drag Model Deviation Signal..... 103

5.4.1.2 J_2 and J_3 Model Deviation Signal..... 104

5.4.2 Process Noise SRIF 106

6 CONCLUSIONS 115

6.1 Summary and Discussion 115

6.1.1 Benefits of Stochastic Filtering 117

6.1.2 Drawbacks of Stochastic Filtering 119

6.2 Recommendations for Future Work 121

BIBLIOGRAPHY 123

APPENDIX

A KEPLERIAN RESIDUALS FOR ONE YEAR BOXCAR ARC WITH C_t, J_2, AND J_3 MODEL DEVIATION SIGNALS 130

B KEPLERIAN RESIDUALS FOR ONE YEAR PROCESS NOISE ARC WITH C_t, J_2, AND J_3 MODEL DEVIATION SIGNALS 134

C KEPLERIAN RESIDUALS FOR ONE YEAR BOXCAR ARC WITH C_t, J_2, J_3, J_4 AND J_5 MODEL DEVIATION SIGNALS 138

D KEPLERIAN RESIDUALS FOR ONE YEAR PROCESS NOISE ARC WITH C_t, J_2, J_3, J_4 AND J_5 MODEL DEVIATION SIGNALS 142

FIGURES

FIGURE

2.1. White Noise and Random Walk Processes. 22

3.1. The Laser Geodynamics Satellite (LAGEOS), from *Smith et al.* [1991]. 32

3.2. Monthly Variations in the J_2 Gravitational Coefficient Computed from LAGEOS SLR Data from *Nerem et al.* [1993]. 36

3.3. Monthly Variations in the J_3 Gravitational Coefficient Computed from LAGEOS SLR Data from *Nerem et al.* [1993]. 37

3.4. 15 Day Estimates of the Along Track Acceleration for LAGEOS from *Tapley et al.* [1993]. 38

4.1. SLR Geometry. 43

4.2. Tracking Station Network for LAGEOS Data Simulation With 20° Visibility Masks Shown. 44

4.3a. Histogram of Simulated LAGEOS Laser Ranging Data. 45

4.3b. Histogram of Actual LAGEOS Laser Ranging Data. 45

4.4. True Model Deviation Signal for the C_t Parameter Based on Current Best Estimates. 50

4.5. True Model Deviation Signal for the J_2 Parameter Based on Current Best Estimates. 51

4.6. True Model Deviation Signal for the J_3 Parameter Based on Current Best Estimates. 52

4.7. True Model Deviation Signal for the J_4 Parameter Based on Current Models. 53

4.8. True Model Deviation Signal for the J_5 Parameter Based on Current Models....53

5.1. True C_t and Estimated C_t Using Boxcars....58

5.2. C_t Residuals Using Boxcars....58

5.3. True J_2 and Estimated J_2 Using Boxcars....59

5.4. J_2 Residuals Using Boxcars....59

5.5. True J_3 and Estimated J_3 Using Boxcars....60

5.6. J_3 Residuals Using Boxcars....60

5.7. Radial Residuals Using Boxcars....62

5.8. Transverse Residuals Using Boxcars....62

5.9. Normal Residuals Using Boxcars....63

5.10. 3-d Position Residuals Using Boxcars....63

5.11. Range Residuals Using Boxcars....64

5.12. True C_t and Estimated C_t Using Process Noise....66

5.13. C_t Residuals Using Process Noise....67

5.14. True J_2 and Estimated J_2 Using Process Noise....67

5.15. J_2 Residuals Using Process Noise....68

5.16. True J_3 and Estimated J_3 Using Process Noise....68

5.17. J_3 Residuals Using Process Noise....69

5.18. Radial Residuals Using Process Noise....70

5.19. Transverse Residuals Using Process Noise....70

5.20. Normal Residuals Using Process Noise....71

5.21. 3-d Position Residuals Using Process Noise....71

5.22. Range Residuals Using Process Noise....72

5.23. Radial Residuals Using Boxcars (a) and Process Noise (b)..... 73

5.24. Transverse Residuals Using Boxcars (a) and Process Noise (b)..... 74

5.25. Normal Residuals Using Boxcars (a) and Process Noise (b)..... 74

5.26. 3-d Position Residuals Using Boxcars (a) and Process Noise (b)..... 75

5.27. Range Residuals Using Boxcars (a) and Process Noise (b)..... 75

5.28. True C_t and Estimated C_t Using Boxcars with J_4 and J_5 Model Deviation Signals Present but not Estimated..... 77

5.29. C_t Residuals Using Boxcars with J_4 and J_5 Model Deviation Signals Present but not Estimated..... 77

5.30. True J_2 and Estimated J_2 Using Boxcars with J_4 and J_5 Model Deviation Signals Present but not Estimated..... 78

5.31. True J_3 and Estimated J_3 Using Boxcars with J_4 and J_5 Model Deviation Signals Present but not Estimated..... 78

5.32. Effective and Actual J_2 Model Deviation Signals..... 83

5.33. Effective and Actual J_3 Model Deviation Signals..... 83

5.34. True Effective J_2 and Estimated J_2 Using Boxcars with J_4 and J_5 Model Deviation Signals Present but not Estimated..... 84

5.35. Effective J_2 Residuals Using Boxcars with J_4 and J_5 Model Deviation Signals Present but not Estimated..... 85

5.36. True Effective J_3 and Estimated J_3 Using Boxcars with J_4 and J_5 Model Deviation Signals Present but not Estimated..... 85

5.37. Effective J_3 Residuals Using Boxcars with J_4 and J_5 Model Deviation Signals Present but not Estimated..... 86

5.38. Radial Residuals Using Boxcars with J_4 and J_5 Model Deviation Signals Present but not Estimated..... 87

5.39. Transverse Residuals Using Boxcars with J_4 and J_5 Model Deviation Signals Present but not Estimated. 87

5.40. Normal Residuals Using Boxcars with J_4 and J_5 Model Deviation Signals Present but not Estimated. 88

5.41. 3-d Position Residuals Using Boxcars with J_4 and J_5 Model Deviation Signals Present but not Estimated. 88

5.42. Range Residuals Using Boxcars with J_4 and J_5 Model Deviation Signals Present but not Estimated. 89

5.43. True C_t and Estimated C_t Using Process Noise with J_4 and J_5 Model Deviation Signals Present but not Estimated. 91

5.44. C_t Residuals Using Process Noise with J_4 and J_5 Model Deviation Signals Present but not Estimated. 92

5.45. True Effective J_2 and Estimated J_2 Using Process Noise with J_4 and J_5 Model Deviation Signals Present but not Estimated. 92

5.46. Effective J_2 Residuals Using Process Noise with J_4 and J_5 Model Deviation Signals Present but not Estimated. 93

5.47. True Effective J_3 and Estimated J_3 Using Process Noise with J_4 and J_5 Model Deviation Signals Present but not Estimated. 93

5.48. Effective J_3 Residuals Using Process Noise with J_4 and J_5 Model Deviation Signals Present but not Estimated. 94

5.49. Radial Residuals Using Process Noise with J_4 and J_5 Model Deviation Signals Present but not Estimated. 95

5.50. Transverse Residuals Using Process Noise with J_4 and J_5 Model Deviation Signals Present but not Estimated. 96

5.51. Normal Residuals Using Process Noise with J_4 and J_5 Model Deviation Signals Present but not Estimated.....96

5.52. 3-d Position Residuals Using Process Noise with J_4 and J_5 Model Deviation Signals Present but not Estimated.....97

5.53. Range Residuals Using Process Noise with J_4 and J_5 Model Deviation Signals Present but not Estimated.....98

5.54. Radial Residuals Using Boxcars (a) and Process Noise (b) with J_4 and J_5 Model Deviation Signals Present but not Estimated. 99

5.55. Transverse Residuals Using Boxcars (a) and Process Noise (b) with J_4 and J_5 Model Deviation Signals Present but not Estimated. 100

5.56. Normal Residuals Using Boxcars (a) and Process Noise (b) with J_4 and J_5 Model Deviation Signals Present but not Estimated. 100

5.57. 3-d Position Residuals Using Boxcars (a) and Process Noise (b) with J_4 and J_5 Model Deviation Signals Present but not Estimated. 101

5.58. Range Residuals Using Boxcars (a) and Process Noise (b) with J_4 and J_5 Model Deviation Signals Present but not Estimated. 101

5.59. True Model Deviation Signal for the C_t Parameter Based on Current Best Estimates.....104

5.60. True Model Deviation Signal for the J_2 Parameter Based on Current Best Estimates.....105

5.61. True Model Deviation Signal for the J_3 Parameter Based on Current Best Estimates.....106

5.62. True C_t and Estimated C_t Using Process Noise.....107

5.63. C_t Residuals Using Process Noise.....107

5.64. True J_2 and Estimated J_2 Using Process Noise. 108

5.65. J_2 Residuals Using Process Noise. 108

5.66. True J_3 and Estimated J_3 Using Process Noise. 109

5.67. J_3 Residuals Using Process Noise. 109

5.68. Radial Residuals Using Process Noise. 111

5.69. Transverse Residuals Using Process Noise. 111

5.70. Normal Residuals Using Process Noise. 112

5.71. 3-d Position Residuals Using Process Noise. 112

5.72. Range Residuals Using Process Noise. 113

A.1. Semi-Major Axis Residuals Using Boxcars. 130

A.2. Eccentricity Residuals Using Boxcars. 131

A.3. Inclination Residuals Using Boxcars. 131

A.4. Argument of Periapse Residuals Using Boxcars. 132

A.5. Longitude of Ascending Node Residuals Using Boxcars. 132

A.6. Argument of Latitude Residuals Using Boxcars. 133

B.1. Semi-Major Axis Residuals Using Process Noise. 134

B.2. Eccentricity Residuals Using Process Noise. 135

B.3. Inclination Residuals Using Process Noise. 135

B.4. Argument of Periapse Residuals Using Process Noise. 136

B.5. Longitude of Ascending Node Residuals Using Process Noise. 136

B.6. Argument of Latitude Residuals Using Process Noise. 137

C.1. Semi-Major Axis Residuals Using Boxcars with J_4 and J_5 Model Deviation Signals Present but not Estimated. 138

C.2. Eccentricity Residuals Using Boxcars with J_4 and J_5 Model Deviation Signals Present but not Estimated. 139

C.3. Inclination Residuals Using Boxcars with J_4 and J_5 Model Deviation Signals Present but not Estimated.....139

C.4. Argument of Periapse Residuals Using Boxcars with J_4 and J_5 Model Deviation Signals Present but not Estimated. 140

C.5. Longitude of Ascending Node Residuals Using Boxcars with J_4 and J_5 Model Deviation Signals Present but not Estimated. 140

C.6. Argument of Latitude Residuals Using Boxcars with J_4 and J_5 Model Deviation Signals Present but not Estimated.....141

D.1. Semi-Major Axis Residuals Using Process Noise with J_4 and J_5 Model Deviation Signals Present but not Estimated. 142

D.2. Eccentricity Residuals Using Process Noise with J_4 and J_5 Model Deviation Signals Present but not Estimated.....143

D.3. Inclination Residuals Using Process Noise with J_4 and J_5 Model Deviation Signals Present but not Estimated.....143

D.4. Argument of Periapse Residuals Using Process Noise with J_4 and J_5 Model Deviation Signals Present but not Estimated. 144

D.5. Longitude of Ascending Node Residuals Using Process Noise with J_4 and J_5 Model Deviation Signals Present but not Estimated. 144

D.6. Argument of Latitude Residuals Using Process Noise with J_4 and J_5 Model Deviation Signals Present but not Estimated. 145

TABLES

TABLE

3.1. Orbit and Satellite Characteristics of LAGEOS.....33

4.1. Tracking Stations and Number of Passes and Observations Generated During the One Year Simulation.....46

4.2. Earth's Gravitational Coefficient and JGM-2 Coefficients (Unnormalized) used in Geopotential Model.....47

4.3. Amplitude and Phase of Seasonal Variations in J_4 and J_5 due to Atmospheric Mass Redistribution Without the Oceanic Inverted Barometer Effect (from *Chao and Au* [1991]).....54

5.1. RMS for C_t, J_2, and J_3 Residuals Using Boxcars.....61

5.2. RMS for RTN and Range Residuals Using Boxcars.....65

5.3. Values for the Time Correlation Constant τ, and Steady State Standard Deviation σ, for One Year Arc with C_t, J_2, and J_3 Model Deviation Signals.....66

5.4. RMS for C_t, J_2, and J_3 Residuals Using Process Noise and Boxcars.....69

5.5. RMS for RTN and Range Residuals Using Process Noise and Boxcars.....73

5.6. RMS for C_t, J_2, and J_3 Residuals Using Boxcars with J_4 and J_5 Model Deviation Signals Present but not Estimated.....86

5.7. RMS for RTN and Range Residuals Using Boxcars with J_4 and J_5 Model Deviation Signals Present but not Estimated.....90

5.8. RMS for C_t, J_2, and J_3 Residuals Using Process Noise and Boxcars with J_4 and J_5 Model Deviation Signals Present but not Estimated. 94

5.9. RMS for RTN and Range Residuals Using Process Noise and Boxcars with J_4 and J_5 Model Deviation Signals Present but not Estimated..... 98

5.10. RMS for C_t, J_2, and J_3 Residuals Using Process Noise. 110

5.11. RMS for RTN and Range Residuals Using Process Noise.....113

CHAPTER 1

INTRODUCTION

1.1 Overview

The current state of the art in filtering Earth orbiting satellite data has reached the point where temporal variations in the gravity field (particularly J_2 and J_3) appear to be observable. Determining these variations is of interest for determining global changes in mass distribution as well as for insight into interior mass properties. The desire to then obtain accurate estimates of these variations, as well as temporal variations in other geophysical parameters, provides the motivation for this study. In particular, it is of interest to determine if the relatively sparse, but accurate, laser range tracking of the LAGEOS satellite can be used to resolve these variations in the low degree coefficients of the Earth's gravity field with the use of a stochastic filter. Conventional filtering methods typically estimate these types of variations as piecewise constants over a given data arc [*Nerem et al.*, 1993]. This results in a discontinuous solution for the variations with limited temporal resolution (e.g. monthly). Stochastic filtering methods can estimate these variations as continuous process noise parameters which are correlated in time. This type of estimation procedure has the potential for resolving these variations much more accurately. This study analyzes the ability of a stochastic filter to recover and accurately estimate such variations.

1.2 Model Errors

A dynamical model is a mathematical representation of the forces acting on a physical system. If the dynamics of the system are known perfectly, then a dynamical model for the system can be used to determine the exact physical state of the system for

all time. Most physical systems cannot be modeled or observed perfectly, as is the case with Earth orbiting satellites. Errors in the dynamical model for a satellite result in differences between the true satellite state and the predicted satellite state based on the dynamical model. Many of these dynamical model errors are a result of not accurately knowing the values of physical parameters which help define the satellite dynamics mathematically. Geopotential coefficients, drag coefficients, and solar radiation pressure coefficients are some examples. Also, model errors may consist of unpredictable time variations in the model parameters which can not be modeled.

Likewise, errors may exist between the actual observation or measurement and the model used to determine a computed or predicted measurement based on the satellite state. These are measurement model errors. A computed measurement of the state is necessary to compare to the actual observed measurement of the state in order to compare the current actual state with the current predicted state. Errors due to moving laser stations (plate tectonics), clock errors, and atmospheric refraction are some examples of measurement model errors. There are also some model errors, such as polar motion errors, which may be considered both dynamical model errors and measurement model errors as these parameters are present in both models.

1.3 Orbit Determination Filters

By observing the satellite over time, the differences between the true (observed) state and the predicted state based on the dynamical model become apparent. Orbit determination is the process of obtaining the best estimate of the state of a satellite based on observations of that satellite. An orbit determination filter is used to combine the information from a set of observations into an estimate of the state while filtering out the errors associated with the observations and the dynamical model.

There are several types of orbit determination filters. The particular application usually dictates the specific filter which is most appropriate. For this study, the two main types of filters which are of concern are a standard (non-stochastic) Square Root Information Filter (SRIF) and a process noise (stochastic) SRIF. These two filters are compared and their ability to resolve specific model errors is assessed.

The satellite state parameters may be defined as the position and velocity of the satellite plus constant model parameters. These model parameters are defined as constants in the mathematical model, yet they may in fact vary in time. Such parameters must be defined as constants in the model since any variations are usually unpredictable. If variations of a particular model parameter are predictable, then these variations can be built into the model. The resulting dilemma is that of estimating unpredictable variations in model parameters as constants. The limitations inherent to this approach are obvious.

Standard non-stochastic filters estimate model parameters (used in the dynamical and measurement models) as constants. Process noise stochastic filters can estimate these model parameters as stochastic, time varying parameters correlated in time. Generally, stochastic filters are most often used to estimate extra accelerations which account for the total effect of the individual model errors for various parameters combined [*Yunck et al.*, 1990; *Wu et al.*, 1992; *Yunck et al.*, 1994]. These stochastic acceleration estimates result in an estimated state which is much closer to the true state (position and velocity). The estimates of the constant parameters of the state that are used in the dynamical and measurement models are generally no closer to the true values, however. This is due to the fact that the errors in these parameters have not been estimated, but rather the net effect of these errors has been estimated as additional accelerations. This study focuses on the ability of a stochastic orbit determination filter to estimate time varying model parameters directly and simultaneously with the satellite

state, and the associated accuracies of the estimates of the model parameters and the satellite orbit.

1.4 Satellite Laser Ranging and LAGEOS

Satellite laser ranging (SLR) is a satellite observational technique which has developed and matured over the last couple of decades. The observable used in SLR is a range measurement from a ground based laser station to the satellite. This range measurement is based on the round trip travel time of a laser pulse and the constancy of the speed of light. Current precisions for SLR measurements are at the sub-centimeter level [*Kolenkiewicz et al.*, 1991]. This highly accurate type of measurement results in geodynamic solutions which are more accurate than those solutions using other types of ground-based measurements.

Launched in 1976, the Laser Geodynamics Satellite (LAGEOS) has been a popular target for SLR. Due to its high altitude (approximately 5900 km), the LAGEOS orbit is highly predictable and fairly easy to model [*Cohen and Smith*, 1985]. The high altitude results in smaller effects from atmospheric drag or the higher frequency geopotential terms. Thus, LAGEOS solutions are less sensitive to model errors from drag and gravity than lower altitude satellites, and more accurate geodynamic solutions are possible.

1.5 Thesis Objectives

The main objective of this thesis is to assess the ability of a sequential process noise filter to resolve specific model deviation signals embedded in simulated LAGEOS SLR data. The accuracies of the estimated model deviation signals and the satellite state are analyzed by comparing them to the known truth used in the simulated orbit. Specifically, model deviation signals in an along track drag parameter and the second

and third degree zonal geopotential coefficients (J_2 and J_3) are introduced into a simulated one year orbit and temporally resolved by a stochastic filter. Comparisons are made to a solution generated with a standard non-stochastic filter. Also, solutions are generated in the presence of additional model deviation signals (J_4 and J_5), which are not estimated. A simulated three year orbit with model deviation signals present in C_t, J_2, and J_3 is also processed just using the stochastic filter. The three year arc is not processed using the standard non-stochastic filter. The ability of a stochastic process noise filter to resolve variations over this longer three year arc is assessed. The advantages and disadvantages of using a stochastic filter to generate a LAGEOS geodynamic solution are addressed as well.

This research will benefit future geodetic and geodynamic studies which attempt to temporally resolve satellite model parameters. The feasibility of this approach is assessed as it is related to orbit determination and satellite geodynamics. The specific benefits and drawbacks of sequential process noise filtering in determining these solutions will help to refine the role of this type of filtering in future analyses. This study will also benefit orbit determination studies considering the use of process noise parameters and stochastics in general in estimating model errors.

1.6 Description of Chapters

Chapter two reviews the basic aspects of filtering theory. The orbit determination problem is presented and state estimation theory is summarized. The square root information filter (SRIF) is developed both with and without correlated process noise. The standard SRIF (without process noise) and the stochastic (process noise) SRIF are the two orbit determination filters compared in this analysis.

Chapter three discusses the satellite laser ranging technique (SLR) and the Laser Geodynamics Satellite (LAGEOS) and their roles in geodynamics. Some current

LAGEOS geodynamic solutions are presented and possible benefits of stochastic filtering of LAGEOS data are detailed.

Chapter four details the simulation model used in the generation of the simulated LAGEOS data. The measurement model and tracking station network are presented along with the dynamical model. The specific model deviation signals inserted into the simulated data are presented as well.

Chapter five details the results obtained from filtering the simulated data with both the standard and the stochastic filter. The temporal resolution of the model deviation signals estimated by each filter are compared. The accuracies of each filter in estimating the satellite orbit are also compared.

Chapter six discusses the conclusions drawn based on the results of filtering the simulated data. Benefits and drawbacks of using process noise to estimate variations of parameters from their nominal values are discussed. Finally, recommendations for future studies related to this research are made.

CHAPTER 2

FILTERING THEORY

2.1 Introduction

By observing a physical system, an estimate of the state of the system can be made based on the observations. The state of the system defines what the system is doing or looks like at any given time. Generally, the measurements or observations of the system usually contain some type of noise. Filtering or estimation is the process of determining the best estimate of the state of the system (by some measure) from these noisy observations. By "filtering" out the noise on the observations, a "best estimate" of the state can be made which is often more accurate than the noise on the observations.

In the process of determining the best estimate of a satellite state, observations of the satellite are required. These observations are processed in such a way as to filter out the errors associated with them as the state of the satellite is estimated. This chapter describes the theory associated with this process, which is commonly referred to as filtering.

2.2 The Orbit Determination Problem

If the forces acting on a satellite have been modeled perfectly and the initial conditions of the satellite are known exactly, then the state of the satellite can be found for all time by integrating its equations of motion. A general form for the equations of motion is

$$\ddot{\mathbf{r}} = \mathbf{F}(\mathbf{r},\dot{\mathbf{r}},\mathbf{p},t) \tag{2.1}$$

where $\mathbf{r}$ and $\dot{\mathbf{r}}$ are the geocentric position and velocity of the satellite, $\mathbf{p}$ are constant parameters contained in the mathematical force model for the satellite's dynamics, and t is the integration time. In general, however, neither the dynamical force model nor the true initial conditions are known exactly. Perfect dynamical force models do not exist, and the constant parameters $\mathbf{p}$ in the force model have errors as well as possibly unpredictable changes over time. True initial conditions usually differ from those calculated *a priori*, so even a "perfect" dynamical force model for the satellite will predict a trajectory that differs from the true trajectory as a result of this initial condition error. Also, some accelerations may not be modeled at all by the chosen dynamical force model. As a result, observations during the satellite's orbit must be made in order to determine or verify its subsequent trajectory. Since the state variables associated with a satellite ($\mathbf{r}$ and $\dot{\mathbf{r}}$) cannot be observed directly, other measurements such as a range or a range rate must be made. The satellite state can then be estimated based on these measurements. This is known as the orbit determination problem.

Due to inherent measurement errors in making observations of the satellite, the trajectory estimated based on the observations will be different than the satellite's true trajectory, even if the dynamical force model for the motion of the satellite is perfect. Errors in the measurement model, which relates the satellite observations to the satellite state, also exist. The observation vector $\mathbf{Z}$ of the satellite at time t is usually a nonlinear function of the satellite state ($\mathbf{r}$ and $\dot{\mathbf{r}}$), a set of measurement model parameters $\mathbf{b}$, plus some random measurement noise $\mathbf{e}_z$:

$$\mathbf{Z} = \mathbf{G}(\mathbf{r},\dot{\mathbf{r}},\mathbf{b},t) + \mathbf{e}_z \tag{2.2}$$

Thus, the satellite state and the observations are related in a nonlinear manner, denoted by the function $\mathbf{G}$. By linearizing this nonlinear function about a known reference trajectory, the orbit determination problem can be simplified [*Smith et al.*, 1962]. If the

reference trajectory and the true trajectory are sufficiently close during the time interval of concern, then the actual trajectory can be expanded in a Taylor series about the reference trajectory for each point in time. By truncating this expansion after the first order terms, the state *deviation* from the reference trajectory may be represented by a set of linear differential equations. Likewise, the observation deviation may be linearly related to the state deviation. Thus, the nonlinear problem of determining the satellite's state can be transformed to a linear problem which determines the satellite's state deviation from some reference state (trajectory).

To summarize mathematically, at time t, the deviations in the satellite state and observations are:

$$\mathbf{x}(t) = \mathbf{X}(t) - \mathbf{X}^*(t) \tag{2.3}$$

$$\mathbf{z}(t) = \mathbf{Z}(t) - \mathbf{Z}^*(t) \tag{2.4}$$

where $\mathbf{X}(t)$ is the true satellite state; $\mathbf{X}^*(t)$ is the reference state based on a specified dynamical force model; $\mathbf{x}(t)$ is the state deviation from the reference state $\mathbf{X}^*(t)$; $\mathbf{Z}(t)$ is the observation vector; $\mathbf{Z}^*(t)$ is the computed observation vector based on the reference state $\mathbf{X}^*(t)$; and $\mathbf{z}(t)$ is the observation deviation from the computed observation $\mathbf{Z}^*(t)$.

By using the deviations defined in equations 2.3 and 2.4, and dropping the time dependence of the state and observation deviation for notational simplicity, equations 2.1 and 2.2 may be linearized as

$$\dot{\mathbf{x}} = A(t)\mathbf{x} \tag{2.5}$$

$$\mathbf{z} = H\mathbf{x} + \mathbf{e}_z \tag{2.6}$$

where

$$A(t) = \frac{\partial \mathbf{F}}{\partial \mathbf{X}}(\mathbf{X}^*,t) \tag{2.7}$$

$$H = \frac{\partial \mathbf{G}}{\partial \mathbf{X}}(\mathbf{X}^*,t) \tag{2.8}$$

For the $n\times 1$ state vector $\mathbf{X}$, an $n\times n$ state transition matrix Φ is defined

$$\Phi(t,t_j) = \frac{\partial \mathbf{X}(t)}{\partial \mathbf{X}(t_j)} \tag{2.9a}$$

with

$$\dot{\Phi}(t,t_j) = A(t)\Phi(t,t_j) \ , \ \Phi(t_j,t_j) = I \tag{2.9b}$$

and

$$\Phi(t_j,t) = \Phi^{-1}(t,t_j) \tag{2.9c}$$

Thus, the linearized system (equation 2.5) has the general solution

$$\mathbf{x}(t) = \Phi(t,t_j)\mathbf{x}(t_j) \tag{2.10}$$

If desired, by using this result and choosing an arbitrary epoch time t_o, the linearized observation-state relation (equation 2.6) may also be written

$$\mathbf{z} = H_o\mathbf{x}_o + \mathbf{e}_z \tag{2.11}$$

where

$$H_o = H\Phi(t,t_o) \text{ and } \mathbf{x}_o = \mathbf{x}(t_o) \tag{2.12}$$

For an $m \times 1$ observation deviation vector $\mathbf{z}$, H is a $m \times n$ matrix. Thus, observation deviations at any time t are linearly related to state deviations at that time or at some epoch time t_o.

2.3 State Estimation

Least squares filters are the most commonly used filters for orbit determination problems since they provide the best estimates of the state when the uncertainty is due to Gaussian or normally distributed noise. They minimize the square of the difference between the observed measurement and the expected measurement computed from an observational model based on the state of the reference trajectory.

Observations can be filtered in two basic modes: batch or sequential. Depending on the specific problem and application, data is filtered as an entire batch, sequentially, or a combination of both. A batch filter estimates the state at an epoch time based on all the observations taken over a given time interval. A sequential filter processes the observations one by one, estimating either the current state or some epoch state after each observation. By processing the observations sequentially, many large matrix inversions and multiplications are avoided since the size of the observation deviation vector $\mathbf{z}$ is dependent only on the number of observations at the current time rather than the number of observations over the entire time interval. When computer

storage is limited, the batch method is less favorable due to the necessity to store all the observations and iterate through the data until a solution is converged upon. Batch methods, however, are easy to implement and less sensitive to erroneous data points. While still quite simple to implement, sequential filters are more sensitive to erroneous data and numerically more unstable. Sequential algorithms are often used in applications where computer storage is a limitation.

In general, a "standard" filter is most frequently used to estimate the state of satellites and model parameters. *Tapley et al.* [1993] and *Nerem et al.* [1994] are two typical examples of recent satellite solutions that estimate geodynamic parameters. Nearly all current satellite solution methods use some type of standard least squares orbit determination filter to estimate satellite states and model parameters. When epoch values for the satellite position and velocity are used, a standard filter estimates all of the parameters in the state vector as constants, which are inherently assumed to be time invariant. The epoch satellite position and velocity define the satellite state at a specific epoch time, and the model parameters may be defined in either the dynamical force model (such as geopotential coefficients or drag coefficients) or the measurement model (such as tracking station positions). Errors inevitably enter into the solution or estimate when model parameters are constants in the dynamical or measurement model, but in reality, vary in time by some measurable, yet unpredictable amount. This type of error is often referred to as model error. That is, the system is not performing or behaving like the predicted model. This problem can be minimized somewhat by using multiple piecewise constants which represent the particular variation as a group of consecutive discontinuous constants, each representing a shorter time interval than the entire time period of interest. The effectiveness of this approach is dictated by many properties, including the observability of the variation the type, amount, and density of available data, and the frequency of the variation.

Another type of filter, called a "process noise" or "stochastic" filter, can be used to address this type of error. A process noise filter estimates specified "constant" parameters as stochastic, time varying parameters. *Lichten* [1990a, 1990b] details procedures that involve process noise for estimating geodynamical parameters using Global Positioning System (GPS) data. *Lichten* [1992] and others have presented solutions which involve the use of process noise parameters in satellite orbit estimation. Even though the parameters are modeled as constants in the dynamical force model or the measurement model, the filter allows the estimates for these parameters to vary in time. The parameters can vary in a manner which is consistent with the information contained in the observations. Examples of phenomena which can be approximated quite well by process noise parameters are solar radiation pressure, mismodeled drag effects, leaky attitude control systems, moving tracking stations, polar motion and Earth rotation parameters, clock errors, atmospheric path delays, gravity field model errors, and linearization errors. Thus, a process noise filter is capable of reducing or eliminating many types of model error.

Often, process noise filters are utilized to lump all model errors into additional acceleration parameters or a specific model parameter to reduce the negative effect of the total model error on the estimate of the orbit. Reduced dynamic tracking techniques have utilized this approach [*Yunck et al.*, 1990; *Wu et al.*, 1991; *Yunck et al.*, 1994; *Gold*, 1994]. This approach is used when the temporal variation of model parameters, or perhaps their actual values, is of little interest and the objective is only to improve the continuous estimate of the satellite position and velocity over time. By representing the cumulative effect of all model errors with an additional stochastic acceleration, this can be accomplished, and is referred to as the reduced-dynamic technique [*Yunck et al.*, 1990].

In contrast, estimates of particular parameters may be made stochastically to understand their temporal variations in addition to reducing the effect of the model error on the estimate of the orbit. This study focuses on the feasibility of this approach in accurately estimating some basic geodynamic parameters from LAGEOS data. Thus, eliminating various model errors associated with specific parameters through process noise filtering may lead to more accurate estimates of the satellite orbit, as well as better temporal estimates of the particular dynamical model parameters and measurement model parameters.

2.4 Standard Filtering

The determination of the best estimate of $\mathbf{x}$ satisfying the linearized observation-state relation (equation 2.6) is discussed. The least squares best estimate of $\mathbf{x}$ is that value which minimizes the sum of the squares of the computed observation residuals $\mathbf{e}_z$. A performance index J is defined

$$J = \mathbf{e}_z^{\mathrm{T}}\mathbf{e}_z = \| \mathbf{e}_z \|^2 \tag{2.13}$$

which must be minimized in a least squares sense to determine the best estimate of $\mathbf{x}$. The notation $\| \cdot \|$ is used to express the Euclidean norm of a vector ($\| \mathbf{a} \| = \sqrt{(\mathbf{a}^{\mathrm{T}}\mathbf{a})}$). Based on the observations $\mathbf{z}$ and specified values of $\mathbf{x}$, the squares of the observation errors $\mathbf{e}_z$ may be summed and minimized. Using equation 2.6, the performance index J may be written as

$$J = (\mathbf{z} - H\mathbf{x})^{\mathrm{T}}(\mathbf{z} - H\mathbf{x}) \tag{2.14}$$

This performance index is now minimized with respect to the state deviation $\mathbf{x}$:

$$\frac{\partial J}{\partial \mathbf{x}}(\hat{\mathbf{x}}) = 0 = -2H^{\mathrm{T}}(\mathbf{z} - H\hat{\mathbf{x}}) \tag{2.15}$$

or

$$H^{\mathrm{T}}H\mathbf{x} = H^{\mathrm{T}}\mathbf{z} \tag{2.16}$$

Equation 2.16 is often referred to as the normal equations. The value of $\mathbf{x}$ which minimizes the performance index J, and thus satisfies the normal equations, is the least squares best estimate of the state and denoted $\hat{\mathbf{x}}$. The error covariance matrix P that is associated with the best estimate $\hat{\mathbf{x}}$ is defined

$$P = \left(H^{\mathrm{T}}H\right)^{-1} \tag{2.17}$$

so

$$\hat{\mathbf{x}} = PH^{\mathrm{T}}\mathbf{z} \tag{2.18}$$

The error covariance matrix P is updated to the time of the new observations, if necessary (for current state filters), as follows:

$$P_{t_2} = \Phi(t_2,t_1)P_{t_1}\Phi^{-1}(t_2,t_1) \tag{2.19}$$

2.5 Standard SRIF Filtering

To achieve more stability, accuracy, and better numerical conditioning, factorized sequential filtering algorithms can be used [*Bierman*, 1977]. By updating a factorized variation of the covariance matrix for the system, the algorithm exhibits improved numeric behavior with less sensitivity to divergence or erroneous data points. This is mainly a result of reducing the numerical ranges of the values of the covariance matrix (10^{-n} to 10^{n} $\Rightarrow$ $10^{-n/2}$ to $10^{n/2}$). Square root factorizations, first introduced by *Potter* (cf. *Battin*, 1964), are common and quite useful in sequential filter algorithms.

A current state sequential square root filter is used in this study, and is described below.

The basic aspects of a commonly used square root filter, known as the square root information filter (SRIF), are outlined. In a SRIF, the square root of the information matrix associated with the linearized system is operated on rather than the covariance matrix. The complete formulation for the SRIF is detailed in *Lawson and Hanson* [1974] and *Bierman* [1977].

If the linearized system deviation defined by equation 2.10 has an associated error covariance matrix P, then its associated information matrix Λ, is defined as

$$\Lambda \equiv P^{-1} = R^{\mathrm{T}}R \tag{2.20}$$

where R is the square root of the information matrix and is upper triangular in form. The *a priori* error covariance and estimate $\left[\widetilde{P}\,\widetilde{\mathbf{x}}\right]$ are related to the *a priori* information array $\left[\widetilde{R}\,\widetilde{\mathbf{z}}\right]$ as follows:

Since

$$P = \left(R^{\mathrm{T}}R\right)^{-1} = R^{-1}R^{-\mathrm{T}} \tag{2.21}$$

the normal equations (equation 2.16) may be written

$$\widehat{\mathbf{x}} = \left(R^{\mathrm{T}}R\right)^{-1}R^{\mathrm{T}}\mathbf{z} = R^{-1}\mathbf{z} \tag{2.22}$$

Thus, the best estimate $\widehat{\mathbf{x}}$ must satisfy

$$R\mathbf{x} = \mathbf{z} \tag{2.23}$$

So $\tilde{R}$ and $\tilde{\mathbf{z}}$, which represent *a priori* values of R and $\mathbf{z}$, correspond to the following data equation for the system

$$\tilde{\mathbf{z}} = \tilde{R}\mathbf{x} + \tilde{\mathbf{e}}_z \tag{2.24}$$

where $\tilde{R}$ is square, $\mathbf{x}$ is the state of the system, and $\tilde{\mathbf{e}}_z$ has zero mean with unit covariance. The least squares solution to this *a priori* data equation and the equation for the new observations (equation 2.6) is desired.

The matrix $\tilde{R}$ is updated to the time of the new observations, if necessary (for current state filters), as follows:

$$\tilde{R}_{t_2} = \tilde{R}_{t_1}\Phi^{-1}(t_2,t_1) \tag{2.25}$$

By applying the orthogonal transformation method [*Givens*, 1959; *Householder*, 1964; *Schmidt*, 1967] to equations 2.24 and 2.6, the least squares solution of

$$\begin{bmatrix} \tilde{R} \\ H \end{bmatrix} \mathbf{x} = \begin{bmatrix} \tilde{\mathbf{z}} \\ \mathbf{z} \end{bmatrix} - \begin{bmatrix} \tilde{\mathbf{e}}_z \\ \mathbf{e}_z \end{bmatrix} \tag{2.26}$$

is also the least squares solution of

$$T\begin{bmatrix} \tilde{R} \\ H \end{bmatrix} \mathbf{x} = T\begin{bmatrix} \tilde{\mathbf{z}} \\ \mathbf{z} \end{bmatrix} - T\begin{bmatrix} \tilde{\mathbf{e}}_z \\ \mathbf{e}_z \end{bmatrix} \tag{2.27}$$

where T represents the orthogonal transformation matrix which preserves unit covariance characteristics of the error terms. The orthogonal transformation matrix T can be chosen such that

$$T\begin{bmatrix} \tilde{R} \\ H \end{bmatrix} = \begin{bmatrix} \hat{R} \\ 0 \end{bmatrix} \tag{2.28}$$

with $\hat{R}$ upper triangular.

Using the same T, the following can be defined:

$$T\begin{bmatrix} \tilde{\mathbf{z}} \\ \mathbf{z} \end{bmatrix} = \begin{bmatrix} \hat{\mathbf{z}} \\ \mathbf{e}_{ls} \end{bmatrix} \quad \text{and} \quad T\begin{bmatrix} \tilde{\mathbf{e}}_z \\ \mathbf{e}_z \end{bmatrix} = \begin{bmatrix} \hat{\mathbf{e}}_z \\ \mathbf{e}_{e_{ls}} \end{bmatrix} \tag{2.29}$$

As defined, $\mathbf{e}_{ls}$ represents the error in the least squares fit. Now equation 2.26 becomes

$$\begin{bmatrix} \hat{R} \\ 0 \end{bmatrix} \mathbf{x} = \begin{bmatrix} \hat{\mathbf{z}} - \hat{\mathbf{e}}_z \\ \mathbf{e}_{ls} - \mathbf{e}_{e_{ls}} \end{bmatrix} \tag{2.30}$$

Thus, the augmented observation array

$$\begin{bmatrix} \tilde{R} & \tilde{\mathbf{z}} \\ H & \mathbf{z} \end{bmatrix} \tag{2.31}$$

is transformed to

$$\begin{bmatrix} \hat{R} & \hat{\mathbf{z}} \\ 0 & \mathbf{e}_{ls} \end{bmatrix} \tag{2.32}$$

and observations can be accumulated sequentially with the *a priori* information array. After the final observation is accumulated (transformed), the least squares best estimate of the state $\hat{\mathbf{x}}$, is:

$$\hat{\mathbf{x}} = \hat{R}^{-1}\hat{\mathbf{z}} \tag{2.33}$$

This estimate is easily computed via backsubstitution rather than by matrix inversion since $\hat{R}$ is upper triangular. The filtered best estimate of the state deviations $\hat{\mathbf{x}}$, can be computed at any given time. The filtered best estimate of the state is thus based on all observations up to that particular time. Smoothed estimates can be computed for all times by mapping the state deviations to any previous time. Alternatively, the estimated

state deviations can be added to the reference state, and the estimated state at other times can be found by integrating the equations of state.

2.6 Process Noise SRIF Filtering

By using a process noise filter, many phenomena, unmodeled and mismodeled by the dynamical model or measurement model, can be accounted for in a more reasonable way. These unmodeled and mismodeled phenomena degrade the solution accuracy and are reflected in the measurement residuals (the difference between the measured observation and the estimated observation resulting from the solution). Process noise filtering can help prevent these model errors from corrupting the solution. The development of this sequential current state algorithm is based on the SRIF algorithm with correlated process noise, first introduced by *Andrews* [1968], and presented by *Bierman* [1977].

First order exponentially correlated process noise is often called colored noise. The process noise filter developed is based on this type of process noise, but other types of process noise can be incorporated into process noise filters. Colored noise can be described mathematically as:

$$\frac{dp}{dt} = -\left(\frac{1}{\tau}\right)p + \omega \tag{2.34}$$

where p is the process noise parameter, τ is the time constant of the process, and ω is white noise with zero mean. Equation 2.34 can be converted to a recursive form, which is useful in discrete time systems, such as the orbit determination problem:

$$p_{j+1} = m_j p_j + w_j \tag{2.35}$$

with

$$m_j = \exp[-(t_{j+1} - t_j)/\tau] \tag{2.36}$$

and

$$w_j = \int_{t_j}^{t_{j+1}} \exp[-(t_{j+1} - \xi)/\tau]\omega(\xi)d\xi \tag{2.37}$$

It can be shown that the variance q, associated with the process noise w, is:

$$q = (1 - m_j^2)\sigma^2 \tag{2.38}$$

where σ^2 is the steady state variance associated with p.

The state is now partitioned into process noise, dynamic, and bias parameters denoted by $\mathbf{p}$, $\mathbf{x}$, and $\mathbf{y}$ respectively. The bias parameters are simply constant (time invariant). The dynamical model for this partitioned, linearized state is:

$$\begin{bmatrix} \mathbf{p} \\ \mathbf{x} \\ \mathbf{y} \end{bmatrix}_{j+1} = \begin{bmatrix} M & 0 & 0 \\ \Phi_p & \Phi_x & \Phi_y \\ 0 & 0 & I \end{bmatrix} \begin{bmatrix} \mathbf{p} \\ \mathbf{x} \\ \mathbf{y} \end{bmatrix}_j + \begin{bmatrix} \mathbf{w}_j \\ 0 \\ 0 \end{bmatrix} \tag{2.39}$$

This corresponds to equation 2.10 for the standard SRIF development. The state transition matrices Φ_p, Φ_x, and Φ_y map state elements at time t_j to time t_{j+1}. I is a square unit matrix equal in size to the number of bias parameters $\mathbf{y}$. M is the process noise transition matrix and is assumed diagonal, with diagonals m, given by equation 2.36.

The value of m is dictated by the time constant for the process τ, in the following way:

$m = 0$	$\tau \rightarrow 0$	[white noise process - not correlated in time]
$0 < m < 1$	$0 < \tau < 1$	[colored noise process - somewhat correlated in time]
$m = 1$	$\tau \rightarrow \infty$	[random walk process - strongly correlated in time]

The behavior of the process noise parameters **p** are controlled mainly by the mapping elements m associated with each particular parameter. Each of the process noise parameters **p** can have an independent time constant τ (and corresponding m) and steady state standard deviation σ associated with it. A parameter behaves as white noise when $m = 0$, and as a random walk when $m = 1$. A parameter behaves like colored noise when m is between these two extremes. When a parameter is defined to model a random walk process ($m = 1$), the variance q for that particular parameter must be explicitly defined since no steady state exists and the steady state variance σ^2 for that parameter is undefined. Figure 2.1 shows a white noise and a random walk process generated using equation 2.35. Both processes shown in Figure 2.1 use an initial value of p=0 for the process noise parameter and the same process noise series w (zero mean, unit covariance) with a specific value of m.

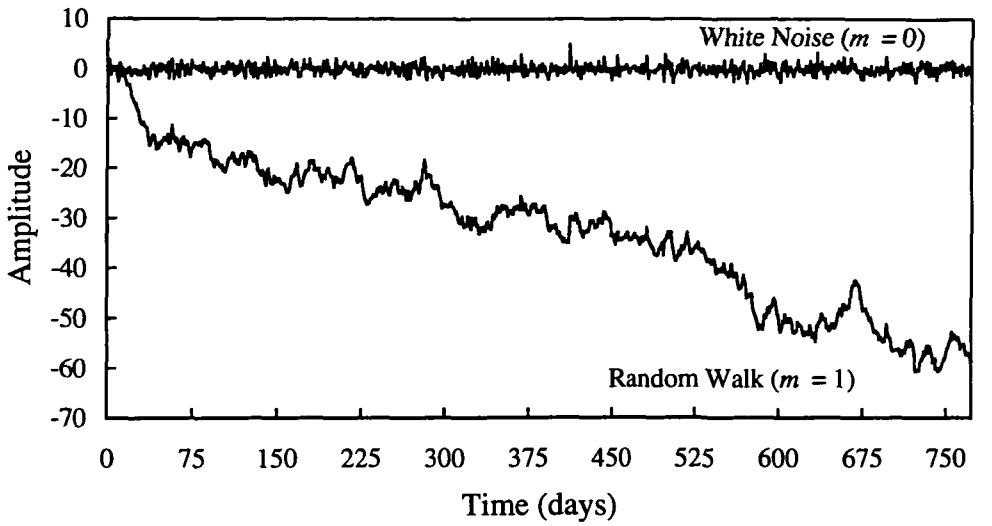

Figure 2.1. White Noise and Random Walk Processes.

Paralleling the development of the standard SRIF, the mathematical development of determining the least squares best estimate using the process noise SRIF algorithm follows (this development follows that of *Bierman* [1977]):

At time t_j, the data equation for R and $\mathbf{z}$ can be written:

$$\begin{bmatrix} \hat{R}_p & \hat{R}_{px} & \hat{R}_{py} \\ \hat{R}_{xp} & \hat{R}_x & \hat{R}_{xy} \\ 0 & 0 & \hat{R}_y \end{bmatrix} \begin{bmatrix} \mathbf{p} \\ \mathbf{x} \\ \mathbf{y} \end{bmatrix}_j = \begin{bmatrix} \hat{\mathbf{z}}_p \\ \hat{\mathbf{z}}_x \\ \hat{\mathbf{z}}_y \end{bmatrix} \tag{2.40}$$

$\hat{R}_{xp}$ is zero unless no data was processed at the last time update. If R is not at the time of the current observation (t_{j+1}), it must updated. The time update for R is a bit more complex in the process noise SRIF algorithm than that described by equation 2.25 in the standard SRIF algorithm. From equation 2.39:

$$\mathbf{x}_{j+1} = \Phi_x \mathbf{x}_j + \Phi_p \mathbf{p}_j + \Phi_y \mathbf{y} \tag{2.41}$$

Solving for $\mathbf{x}_j$ in terms of $\mathbf{x}_{j+1}$ and substituting this into equation (2.40):

$$\begin{bmatrix} \widehat{R}_p - (\widehat{R}_{px}\Phi_x^{-1})\Phi_p & \widehat{R}_{px}\Phi_x^{-1} & \widehat{R}_{py} - (\widehat{R}_{px}\Phi_x^{-1})\Phi_y \\ \widehat{R}_{xp} - (\widehat{R}_x\Phi_x^{-1})\Phi_p & \widehat{R}_x\Phi_x^{-1} & \widehat{R}_{xy} - (\widehat{R}_x\Phi_x^{-1})\Phi_y \\ 0 & 0 & \widehat{R}_y \end{bmatrix} \begin{bmatrix} \mathbf{p}_j \\ \mathbf{x}_{j+1} \\ \mathbf{y} \end{bmatrix} = \begin{bmatrix} \widehat{\mathbf{z}}_p \\ \widehat{\mathbf{z}}_x \\ \widehat{\mathbf{z}}_y \end{bmatrix} \quad (2.42)$$

But, $\mathbf{p}_{j+1}$ is needed in equation 2.42 as well. By using the *a priori* data equation for $\mathbf{w}_j$ this can be done:

$$R_w\mathbf{w}_j = \mathbf{z}_w \quad (2.43)$$

where

$$R_w = \frac{1}{\sqrt{\mathbf{q}}}$$

with R_w diagonal and $\mathbf{q}$ is the variance associated with the process noise $\mathbf{w}_j$, as defined in equation 2.38.

And from equation 2.39

$$\mathbf{w}_j = \mathbf{p}_{j+1} - M\mathbf{p}_j \quad (2.44)$$

so

$$R_w(\mathbf{p}_{j+1} - M\mathbf{p}_j) = \mathbf{z}_w \quad (2.45)$$

Now combining equation 2.45 with equation 2.42 to obtain the updated R and $\mathbf{z}$ at the next time, t_{j+1}:

$$\begin{bmatrix} -R_wM & R_w & 0 & 0 \\ (\widehat{R}_p - \overline{R}_{px}\Phi_p) & 0 & \overline{R}_{px} & (\widehat{R}_{py} - \overline{R}_{px}\Phi_y) \\ (\widehat{R}_{xp} - \overline{R}_x\Phi_p) & 0 & \overline{R}_x & (\widehat{R}_{xy} - \overline{R}_x\Phi_y) \end{bmatrix} \begin{bmatrix} \mathbf{p}_j \\ \mathbf{p}_{j+1} \\ \mathbf{x}_{j+1} \\ \mathbf{y} \end{bmatrix} = \begin{bmatrix} \mathbf{z}_w \\ \widehat{\mathbf{z}}_p \\ \widehat{\mathbf{z}}_x \end{bmatrix} \quad (2.46)$$

where

$$\overline{R}_{px} = \widehat{R}_{px}\Phi_x^{-1} \quad \text{and} \quad \overline{R}_x = \widehat{R}_x\Phi_x^{-1} \tag{2.47}$$

Now, using an orthogonal transformation to upper triangularize $[R\ \mathbf{z}]$ and eliminate $\mathbf{p}_j$:

$$T\begin{bmatrix} -R_wM & R_w & 0 & 0 & \mathbf{z}_w \\ (\widehat{R}_p - \overline{R}_{px}\Phi_p) & 0 & \overline{R}_{px} & (\widehat{R}_{py} - \overline{R}_{px}\Phi_y) & \widehat{\mathbf{z}}_p \\ (\widehat{R}_{xp} - \overline{R}_x\Phi_p) & 0 & \overline{R}_x & (\widehat{R}_{xy} - \overline{R}_x\Phi_y) & \widehat{\mathbf{z}}_x \end{bmatrix} = \begin{bmatrix} R_p^* & R_{pp}^* & R_{px}^* & R_{py}^* & \mathbf{z}_p^* \\ 0 & \widetilde{R}_p & \widetilde{R}_{px} & \widetilde{R}_{py} & \widetilde{\mathbf{z}}_p \\ 0 & \widetilde{R}_{xp} & \widetilde{R}_x & \widetilde{R}_{xy} & \widetilde{\mathbf{z}}_x \end{bmatrix} \tag{2.48}$$

Since $\mathbf{y}$ is a bias, it is unaffected by the mapping from t_j to t_{j+1} and need not be included in the time update for R and $\mathbf{z}$ or in the orthogonal transformation:

$$\left[\widehat{R}_y\ \widehat{\mathbf{z}}_y\right]_j = \left[\widetilde{R}_y\ \widetilde{\mathbf{z}}_y\right]_{j+1} \tag{2.49}$$

The quantities superscripted by * are not used to obtain filtered estimates, but are critical if smoothing is to be done following the filtering. The $\widehat{\ }$ quantities from the previous time are now represented by the $\widetilde{\ }$ quantities at the current time, completing the time update for R and $\mathbf{z}$.

Next, the measurement accumulation is written:

$$T\begin{bmatrix} \tilde{R}_p & \tilde{R}_{px} & \tilde{R}_{py} & \tilde{\mathbf{z}}_p \\ \tilde{R}_{xp} & \tilde{R}_x & \tilde{R}_{xy} & \tilde{\mathbf{z}}_x \\ 0 & 0 & \tilde{R}_y & \tilde{\mathbf{z}}_y \\ & & & \\ & H & & \mathbf{z} \end{bmatrix} = \begin{bmatrix} \hat{R}_p & \hat{R}_{px} & \hat{R}_{py} & \hat{\mathbf{z}}_p \\ 0 & \hat{R}_x & \hat{R}_{xy} & \hat{\mathbf{z}}_x \\ 0 & 0 & \hat{R}_y & \hat{\mathbf{z}}_y \\ & & & \\ & 0 & & \mathbf{e}_{ls} \end{bmatrix} \tag{2.50}$$

where $\mathbf{z}$ is the observation deviation vector for the current time, H is the observation partials matrix, the $\hat{R}$ and $\hat{\mathbf{z}}$ partitions represent the updated R and $\mathbf{z}$ at the current time *after* accumulating the current observation, and $\mathbf{e}_{ls}$ represents the sum of squares of the error terms. At any given time, the best estimate is:

$$\hat{\mathbf{x}} = \hat{R}^{-1}\hat{\mathbf{z}} \tag{2.51}$$

where

$$\hat{\mathbf{x}} = \begin{bmatrix} \mathbf{p} \\ \mathbf{x} \\ \mathbf{y} \end{bmatrix} \qquad \hat{R} = \begin{bmatrix} \hat{R}_p & \hat{R}_{px} & \hat{R}_{py} \\ 0 & \hat{R}_x & \hat{R}_{xy} \\ 0 & 0 & \hat{R}_y \end{bmatrix} \qquad \hat{\mathbf{z}} = \begin{bmatrix} \hat{\mathbf{z}}_p \\ \hat{\mathbf{z}}_x \\ \hat{\mathbf{z}}_y \end{bmatrix}$$

Again, since $\hat{R}$ is kept in upper triangular form, a matrix inversion is not necessary to compute the best estimate of the state deviations. The best estimate, $\hat{\mathbf{x}}$, can be found directly via backsubstitution. Similarly, the error covariance matrix $\hat{P}$ for the estimate $\hat{\mathbf{x}}$ is

$$\hat{P} = \hat{R}^{-1}\hat{R}^{-T} \tag{2.52}$$

This best estimate of the state deviations $\hat{\mathbf{x}}$, is referred to as a filtered estimate. It represents the best estimate at that particular time based on all observations up to and including the observation at that time. Smoothed estimates represent the best estimate at a given time based on all of the observations, both before and after the time of the estimate. Smoothing is the process of determining these smoothed estimates once all the observations have been processed.

If these smoothed estimates of the state at other times are desired, then the smoothing parameters saved at each time (from equation 2.48) may be used. Given $[\mathbf{p}_j, \mathbf{x}_j, \mathbf{y}_j]$, then $[\mathbf{p}_{j-1}, \mathbf{x}_{j-1}, \mathbf{y}_{j-1}]$ can be found as follows. Since $\mathbf{y}$ is a constant, its smoothed estimate equals its filtered estimate:

$$\mathbf{y}_{j-1} = \mathbf{y}_j \tag{2.53}$$

Using equations 2.46 and 2.48, the smoothed estimate of $\mathbf{p}$ is

$$\mathbf{p}_{j-1} = \frac{[\mathbf{z}_p^*]_j - \mathbf{p}_j[R_{pp}^*]_j - \mathbf{x}_j[R_{px}^*]_j - \mathbf{y}_j[R_{py}^*]_j}{[R_p^*]_j} \tag{2.54}$$

and using equation 2.39, the smoothed state estimate is

$$\mathbf{x}_{j-1} = \Phi_x^{-1}[\mathbf{x}_j - \Phi_p\mathbf{p}_{j-1} - \Phi_y\mathbf{y}_{j-1}] \tag{2.55}$$

Using these recursive equations, smoothed estimates of the state can be found for all previous times. This smoothing process is slightly more complex when stochastic parameters are present than smoothing for the standard SRIF which only involves integrating the equations of state backwards or mapping state deviations using the state transition matrix Φ.

Filtered estimates of the error covariance matrix P at any given time are found by using equation 2.52. Once all the observations have been processed, the error covariance matrix at previous times may be desired (smoothed error covariance values). This requires the knowledge of either the information matrix R at any previous time so that P may be found via equation 2.52 or the knowledge of P directly by way of mapping from the final time. The mapping of the information matrix R, based on R at the final time after all observations have been processed, may be done by using the time update for R backwards. While equations 2.46 and 2.48 are used to update R forward in time during the filtering, they may be used for backwards mapping by substituting t_{j-1} for t_{j+1} in calculating the state transition matrices. Given the final information matrix R at the final time based on all observations (equation 2.51), equations 2.46 and 2.48 may be used to propagate R to previous times. Then, the $\tilde{}$ quantities resulting from equation 2.48 represent R at the previous time rather than the current time, and the $\hat{}$ quantities represent the current time rather than the previous time.

Alternatively, P from the final time may be mapped directly to other times by using the generalized error covariance update relation:

$$P_{j+1} = \begin{bmatrix} M & 0 & 0 \\ \Phi_p & \Phi_x & \Phi_y \\ 0 & 0 & I \end{bmatrix} P_j \begin{bmatrix} M & 0 & 0 \\ \Phi_p & \Phi_x & \Phi_y \\ 0 & 0 & I \end{bmatrix}^{\mathrm{T}} + \begin{bmatrix} I_p \\ 0 \\ 0 \end{bmatrix} Q \begin{bmatrix} I_p \\ 0 \\ 0 \end{bmatrix}^{\mathrm{T}} \qquad (2.56)$$

Recall, the state transition matrices Φ_p, Φ_x, and Φ_y map state elements at time t_j to time t_{j+1}, M is the process noise transition matrix and is assumed diagonal with diagonals m given by equation 2.36, and Q is the diagonal error covariance matrix for the process noise w with diagonals given by equation 2.38. I is a square unit matrix equal in size to the number of bias parameters $\mathbf{y}$ and I_p is a square unit matrix equal in size to the number of process noise parameters $\mathbf{p}$. In order to map P to previous times using equation 2.56, the substitution of t_{j-1} for t_{j+1} must be made in calculating the state transition matrices and Q.

The process noise SRIF algorithm parallels the standard SRIF algorithm with the exception of the propagation of R and the smoothing portion which are both different from the standard SRIF algorithm since stochastic parameters ($\mathbf{p}$) are involved. The time variation of each process noise parameter is controlled with a time constant τ, and a steady state variance σ^2, for the parameter. As τ increases and σ decreases, the corresponding parameter stays more constant from one time to the next. As τ decreases and σ increases, the corresponding parameter becomes more time varying. These two parameters are "tuned" or chosen depending on the expected time variation of the process the process noise parameter is modeling.

2.7 Conclusions

The basic attributes of the standard and stochastic filters are now summarized. As mentioned previously, the inherent disadvantage of using a standard filter to estimate temporal variations of parameters is the fact that a standard filter must estimate these variations as constants. In order to minimize this inadequacy, a parameter may be divided into multiple "sub-parameters", each of which represents the original parameter for a particular and unique time interval during the period of interest. For example, over a one year data arc, the solar radiation pressure coefficient of a satellite may be

estimated using 52 consecutive parameters, each representing a unique one week period during the data arc. The consecutive joining of these 52 discontinuous sub-parameters over the one year time period represents the year long estimate for the parameter. Based on the appearance of the consecutive joining of these discontinuous sub-parameters, this type of solution is denoted a "boxcar" solution for the purposes of this study. For parameters which are not purely kinematic in nature, this involves adding each of these sub-parameter boxcars to the satellite state vector. Thus, the computational price for filtering a two year arc instead of a one year arc doesn't merely double, but grows geometrically depending on the number of parameters that are estimated with shorter boxcars. For data arcs spanning long time periods such as six months or more, estimating the variations of parameters in this fashion can be quite tedious and computationally laborious. Further, splitting a parameter into multiple boxcars does not guarantee improved recovery or resolution of the variation. The ideal minimum time interval for a parameter depends on many things, including the sensitivity of the satellite to variations in the parameter, data type and density, and the observability of the variation in the satellite measurement. As an example, using boxcars that span time intervals less than one month for variations in gravity coefficients generally does not improve the recovery of these variations.

In contrast, by estimating variations in a parameter as stochastic process noise parameters, no increase in the size of the satellite state vector is needed. Since the parameter is inherently stochastic as opposed to constant, no additional sub-parameters are required. As shown in the development of the process noise SRIF, stochastic estimates of the process noise parameters are obtained at every observation time. If the variation in a parameter is recoverable via this approach, the estimation of the variation may be significantly simplified computationally.

CHAPTER 3

SATELLITE LASER RANGING AND LAGEOS

3.1 Introduction

Some basic principles of the satellite laser ranging technique are discussed. The specific role of the Laser Geodynamics Satellite (LAGEOS) in satellite laser ranging is outlined as well. Some current solutions based on LAGEOS data are also presented. Benefits of processing LAGEOS data using process noise filtering techniques are also proposed.

3.2 Satellite Laser Ranging

Satellite Laser Ranging (SLR) is a highly accurate and precise tracking method used for orbit determination of satellites. Ground based tracking stations measure the distance (range) from the satellite to the station by using lasers. The time it takes the photon pulse from the ground based laser to travel to the satellite and back is converted to a range measurement by using the constancy of the speed of this light pulse. In the case of satellites designed for laser ranging targeting, the laser pulse is reflected by a cluster of cube-corner reflectors located on the satellite surface. The precision of SLR is now at the sub-centimeter level [*Kolenkiewicz et al.*, 1991; *Tapley et al.*, 1993; *Degnan*, 1994], and through the formation of laser normal points, can reach a few millimeters [*Degnan*, 1994] (see *Smith et al.* [1991] for a detailed discussion on normal point formation and processing). The accuracy of SLR ranging systems is also at the sub-centimeter level [*Degnan*, 1985, 1993, 1994], and the number of tracking stations around the world has been increasing consistently over the past two decades. By integrating these highly accurate and precise SLR measurements from multiple tracking

stations with a dynamical model for the motion of the satellite, numerous model parameters can be determined to a high degree of precision via a least squares orbit determination filter. These parameters include those describing the satellite's motion, positions of the tracking stations, tectonic plate motions, both spatial and temporal variations of the Earth's gravity field, Earth rotation and polar motion parameters, Earth and ocean tides, variations in the center of mass of the total Earth system, and other geodetic parameters used in the dynamic and measurement models [*Degnan*, 1994]. The accuracies of geodetic and geophysical results obtained through satellite observations are directly related to, and often limited by, the accuracies of the observables used in obtaining the results. The accuracy of the SLR observable has enabled the quality of geophysical and geodetic results to improve significantly through the use of laser target satellites.

3.3 The Laser Geodynamics Satellite

The Laser Geodynamics Satellite (LAGEOS), launched by NASA from the Western Test Range in California on May 4, 1976, is a passive, spherical, artificial satellite. Figure 3.1 shows LAGEOS which resembles a large cannonball covered with retroreflectors.

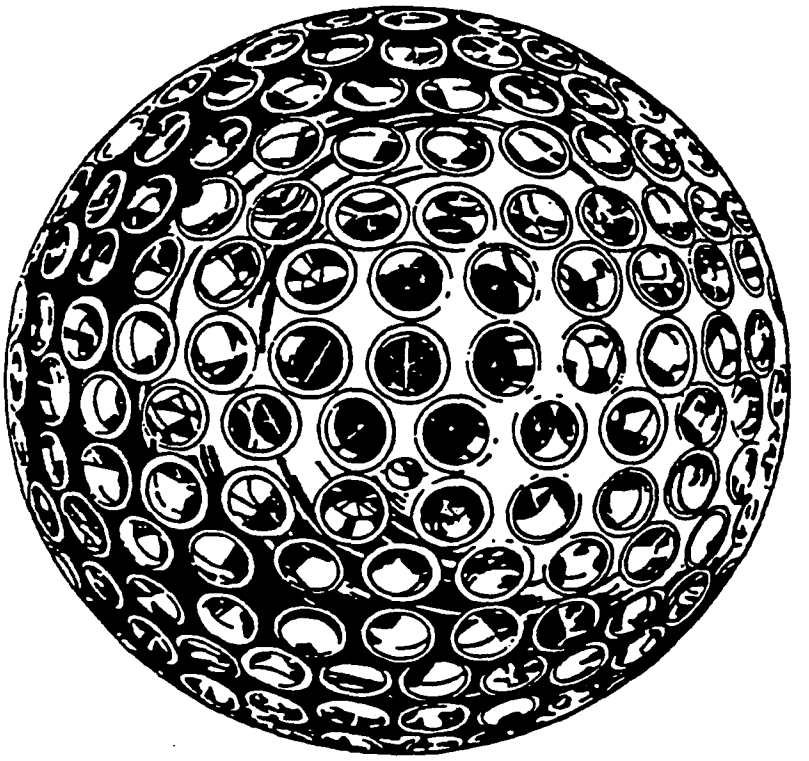

Figure 3.1. The Laser Geodynamics Satellite (LAGEOS), from *Smith et al.* [1991].

As outlined by *Fitzmaurice et al.* [1977] and *Cohen and Smith* [1985], Table 3.1 shows the orbit and satellite characteristics of LAGEOS. It is covered with cube-corner reflectors, 422 made of fused silica and four made of germanium. It was designed specifically and exclusively as a long-term laser ranging target to improve geophysical and geodetic solutions through the use of SLR data.

Table 3.1. Orbit and Satellite Characteristics of LAGEOS.

Diameter	60 cm
Mass	411 kg
Fused silica retroreflectors	422
Germanium retroreflectors	4
Inner core material	Beryllium copper
Outer spherical shell material	Aluminum
Semimajor Axis	12265 km
Eccentricity	0.004
Inclination	109.8°
Perigee altitude	5858 km
Apogee altitude	5958 km
Perigee rate	-0.214°/day
Orbital period	225.3 minutes
Node rate	+0.343°/day
Semimajor axis decay rate	−1.1 mm/day

LAGEOS is in a highly stable, nearly circular Earth orbit, at an altitude of approximately 5900 km. This high altitude, along with the satellite's simple spherical shape and high mass density, minimize the effects of drag, solar radiation pressure, and other nonconservative forces. The effects of the short-wavelength geopotential coefficients, which are not known to the accuracy of the long-wavelength coefficients, are also minimized in this high altitude orbit. Thus, the motion of LAGEOS is quite predictable based on current satellite dynamical models. With both highly accurate range observations and a very predictable trajectory, LAGEOS is ideal for determining tracking station positions and distances between stations, geopotential coefficients, tidal amplitudes, nonconservative force parameters, polar motion parameters, Earth rotation parameters, tectonic plate motions, and other model parameters. Moreover, the temporal variations of such solutions can be determined more accurately and precisely

than from other satellites not specifically designed for precise orbit determination purposes. Many of the geodetic solutions obtained from LAGEOS data have also been verified by independent very long baseline interferometry (VLBI) and GPS techniques [*Kolenkiewicz et al.*, 1985; *Himwich et al.*, 1993; *Dickey*, 1993; *McCarthy*, 1993].

3.4 LAGEOS Geodetic Solutions

Advances in SLR techniques have led to improvements in dynamic satellite geodesy methods and geodynamic solutions. By observing a satellite using SLR methods, its motion as it moves through the Earth's geopotential field can be monitored. Thus, by modeling the satellite's orbital motion due to gravitational and non-gravitational forces, SLR observations provide a link or connection between the satellite and the tracking stations observing the satellite. The parameters describing the satellite's motion, the locations of the tracking stations, and other parameters in the model are estimated by minimizing the difference between the model orbit and the actual orbit in a least squares fashion through the use of the SLR observations.

LAGEOS, being designed specifically for satellite geodesy and geodynamics research, has provided improved estimates of tracking stations and their motions since its mission began in 1976. One of the most current solutions is reported by *Tapley et al.* [1993]. Improved estimates of other geophysical parameters and their time variations have been made using LAGEOS SLR data as well. *Lerch et al.* [1985], *Marsh et al.* [1988], *Marsh et al.* [1990], *Nerem et al.* [1994], and others have detailed improvements in the Earth's gravitational field from LAGEOS data. Tidal parameters [*Christodoulidis et al.*, 1986], Earth rotation and polar motion parameters [*Tapley et al.*, 1985; *Pavlis et al.*, 1988; *Caporali et al.*, 1990; *Tapley et al.*, 1993], and secular variations in J_2 [*Yoder et al.*, 1983; *Rubincam*, 1984; *Cheng et al.*, 1989; *Gegout et al.*, 1991] have also been estimated based on LAGEOS data. *Rubincam* [1984] and others

have used LAGEOS data to study postglacial rebound. The estimates made from LAGEOS SLR observations are more meaningful than most other data types due to the accuracy of both the observations and the predicted orbit, which translates to improved accuracy of the estimates. The utilization of LAGEOS for satellite geodesy and geodynamics research has led to many advancements and achievements which would not have occurred as quickly without the benefit of LAGEOS.

3.4.1 LAGEOS J_2 and J_3 Solutions

Temporal variations in the low degree zonal harmonics of the Earth's gravitational field are observable using SLR [*Shum et al.*, 1987; *Cheng et al.*, 1989, 1990]. Some examples of the geophysical processes contributing to these variations are luni-solar tides, nontidal variations in the distribution of atmospheric mass and ocean water mass, meteorological mass redistribution, and postglacial rebound of the solid Earth [*Chao et al.*, 1987; *Cheng et al.*, 1989; *Chao and Au*, 1991]. Continental water storage and snow cover/loading can cause variations in the gravitational field also [*Chao et al.*, 1987; *Chao and O'Connor*, 1988]. The seasonal gravitational variations (annual and semiannual), however, are dominant and are mainly due to solar influences on the Earth's mass distribution. The primary solar influences include the seasonal redistribution of atmospheric mass, the seasonal redistribution of hydrospheric mass, and solar annual and solar semiannual solid Earth and ocean tides [*Chao and Au*, 1991].

An example of a current solution for the temporal variations of the J_2 and J_3 gravitational coefficients based on LAGEOS SLR data is that of *Nerem et al.* [1993]. As they detail, monthly estimates of the nontidal, nonsecular J_2 and J_3 variations are computed for the period from 1980 to 1990. Figure 3.2 presents the monthly estimates for the J_2 variation and Figure 3.3 shows the monthly estimates for the J_3 variation that

they computed. These solutions compute a constant J_2 and J_3 variation for every month during the 10 year period. Using the terminology described in the previous chapter, these are referred to as monthly boxcars. A resolution of one month is typical for solutions of temporal variations in gravitational coefficients based on SLR data.

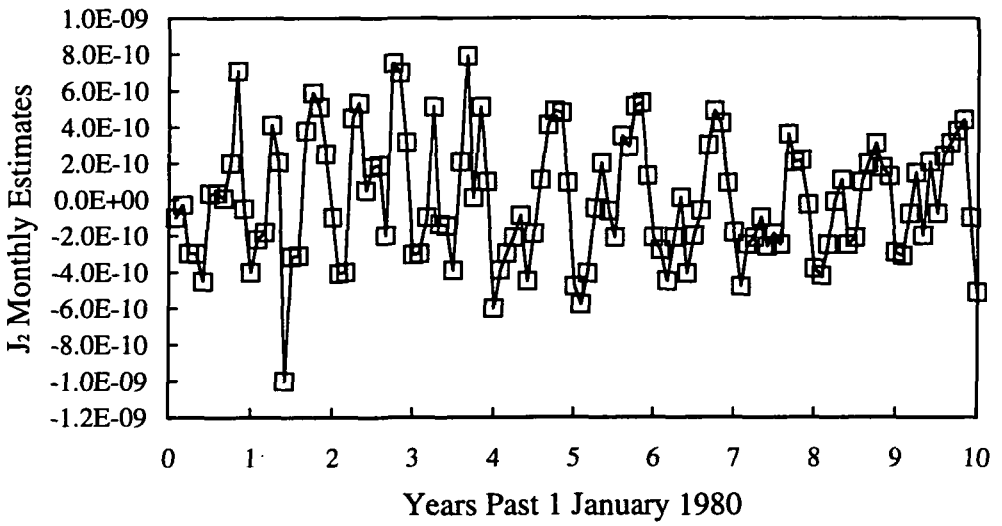

Figure 3.2. Monthly Variations in the J_2 Gravitational Coefficient Computed from LAGEOS SLR Data from *Nerem et al.* [1993].

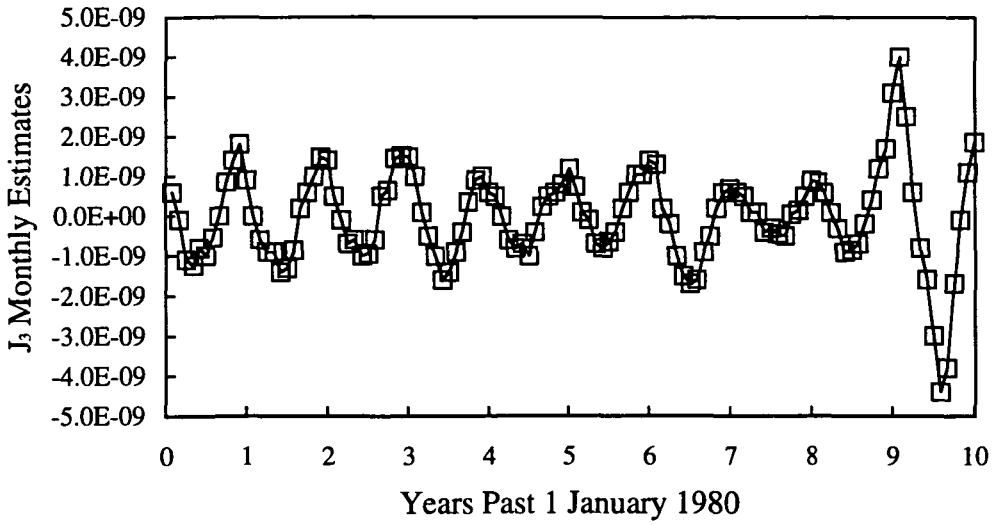

Figure 3.3. Monthly Variations in the J_3 Gravitational Coefficient Computed from LAGEOS SLR Data from *Nerem et al.* [1993].

3.4.2 LAGEOS Along Track Drag Solutions

After subtracting most of the known forces acting on LAGEOS, there is still an along track deceleration (drag) which has been observed and reduces the semimajor axis by about 1 mm per day (see *Tapley et al.* [1993] for a more detailed look at the long term estimates of this drag and an interesting discussion on the drag in general). Previous studies have addressed the possible origins and proposed models for this drag [*Rubincam*, 1982, 1987, 1988, 1990], which are mostly thermal in nature.

A current solution for the anomalous along track drag on LAGEOS is computed by *Tapley et al.* [1993]. This along track drag remains after most of the known forces acting on LAGEOS are taken into account. Estimates of this along track drag are necessary when estimating other geodynamic or geodetic parameters from LAGEOS SLR data to prevent this acceleration from aliasing into estimates. Typically, the along track drag is estimated every 15 days (15 day boxcars). Figure 3.4 shows the boxcar

estimates computed by *Tapley et al.* based on LAGEOS data from May 30, 1976 to May 30, 1993. The along track drag has a mean of –3.5 picometer/s^2 over the arc.

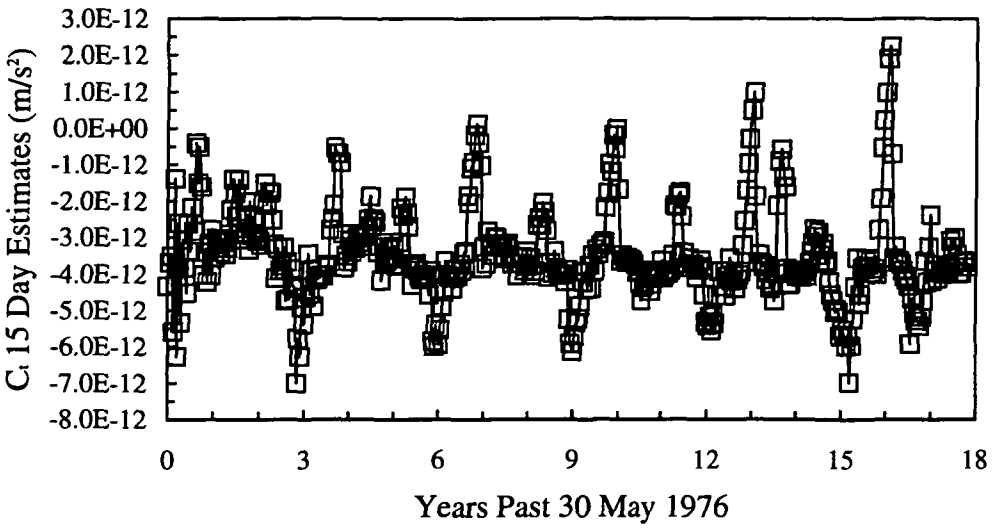

Figure 3.4. 15 Day Estimates of the Along Track Acceleration for LAGEOS from *Tapley et al.* [1993].

3.5 Proposed Benefits of Process Noise Filtering for LAGEOS

Most LAGEOS data analysis techniques determine geodetic and geodynamic parameters by solving for them as if they were constants over the specific time interval of the data arc through the use of a standard filter. For example, *Smith et al.* [1985], estimate polar position values and variations in universal time every 5 days, and tracking station locations and other parameters every 30 days. *Smith et al.* [1991] estimate parameters as constants over fixed time intervals as well. Aside from being linked from one time interval to the next by the satellite orbital parameters, these constant parameters are effectively decoupled from one time interval to the next. In other words, the estimates for the constants over the time interval are primarily based

on the observations made during the time interval Estimates of purely kinematic parameters are based entirely on observations made during the particular time interval, while estimates of dynamic parameters are still linked from one time interval to the next by the satellite orbit. If these parameters, in reality, do not change over the given time interval, then model error is not introduced into the solution. If, however, these parameters do vary over the given time interval, then model error will corrupt the solution. By limiting the time interval such that the given parameters do not change in any measurable way over that interval, then model error can be kept at a minimum. A time series of a specific parameter can then be constructed by joining the consecutive fixed interval estimates of the parameter (boxcars). The fundamental drawback to generating temporal solutions in this manner is the actuality that estimates will degrade if the time interval for the boxcar estimate is either too short or too long. If the time interval is too short, then accurate estimates may not be possible given the available data or the observability of the variation. If the time interval is too long, then the parameter may vary significantly from the constant estimate over the interval, thus resulting in adverse effects from model error. The shorter boxcar time intervals may be desirable from a resolution perspective, while the longer boxcar time intervals may help to reduce the effects of measurement noise and erroneous data.

By estimating these parameters stochastically using a process noise filter, long data arcs may be used to generate a solution from LAGEOS SLR data without the division of the arc into smaller arcs for the estimates of known time varying parameters. The strength of the solution may be enhanced by using a long time interval (the length of the entire arc for each parameter), and the temporal resolution of the solution of the parameters may also improve. Along with the entire geodynamic solution, the estimate of the satellite orbit over time may be improved as well. The time variations of

parameters are found by using the entire long arc of data, even though the parameters may change significantly over the long interval. For example, variations in gravity field coefficients or variations in tracking station positions could be estimated with improved resolution by using long arcs spanning years to decades rather than the same long arcs divided into shorter monthly time intervals for these parameters. An estimate for each process noise parameter is computed at every time that an observation is made over the data arc. Thus, the estimate at *each* individual time for a process noise parameter is based on the observations made over a rough, adjustable time interval centered on the time of the estimate. The length of this rough time interval, or correlation window, is determined by a time constant τ, for the particular parameter. Effectively, observations made outside of this correlation window in time have little or no effect on the estimate made at the time at the center of the window. Parameters which are highly correlated in time (slowly varying) may have longer correlation windows than parameters which vary more rapidly in time. Depending on the observability of the particular variation in the observation, a parameter may be estimated more accurately as a process noise parameter. For variations which are not effectively observed in the satellite observations, the process noise estimates may be no more accurate than standard, consecutive fixed interval estimates. The possible benefits of estimating particular parameters stochastically based on LAGEOS SLR data are assessed in this study.

CHAPTER 4

SIMULATION MODEL

4.1 Introduction

Model errors of some type exist within any real satellite observation. This is a result of the fact that the actual forces causing the motion of the satellite differ from the forces that can be represented in a mathematical force model. One can not know the true variations from the dynamical force model. This results in an imperfect knowledge of the true trajectory of a satellite if real observations are used. The best one can do is determine the best estimate of the trajectory, which is limited by how well your model represents the true trajectory.

To fully understand how well model errors can be resolved by estimating parameters stochastically, the model errors themselves must be known. In this study, the true temporal variations of the particular parameters being estimated must be known perfectly before conclusions can be drawn as to the effectiveness of particular filtering methods in estimating these variations. Thus, simulated LAGEOS SLR observations are generated with specific temporal variations of parameters (referred to hereafter as model deviation signals or model signals) built into the model used in generating the observations. This permits the direct comparison of the estimates to the known truth.

LAGEOS SLR data is generated for a period of one year for this study. Solutions obtained by processing this simulated one year arc both with stochastic and non-stochastic filtering techniques are compared. The process by which this data is generated is now detailed. A three year LAGEOS SLR data arc, processed only by the stochastic filter, is also generated following the same simulation procedure. The laser

ranging measurements are computed based on a specified tracking network of laser ranging stations and a satellite in the same orbit as LAGEOS, acting under a specified dynamical model. This chapter details the models used and the process by which the simulated observations are generated.

4.2 Measurement Model

The measurement used in the simulation is a range observable, which corresponds to a typical SLR measurement. The magnitude of the difference between the satellite position vector and the tracking station position vector is determined:

$$Z = \| \mathbf{r}_s - \mathbf{r}_t \| \tag{4.1}$$

where Z is the SLR measurement (range), $\mathbf{r}_s$ is the satellite position vector, and $\mathbf{r}_t$ is the tracking station position vector. This measurement simply represents the distance (range) from the tracking station to the satellite. Figure 4.1 shows the geometry of the SLR measurement. The actual determination of real laser range measurements is a bit more complex, as it involves corrections for atmospheric refraction, instrument delays, relativistic effects, and the finite speed of light.

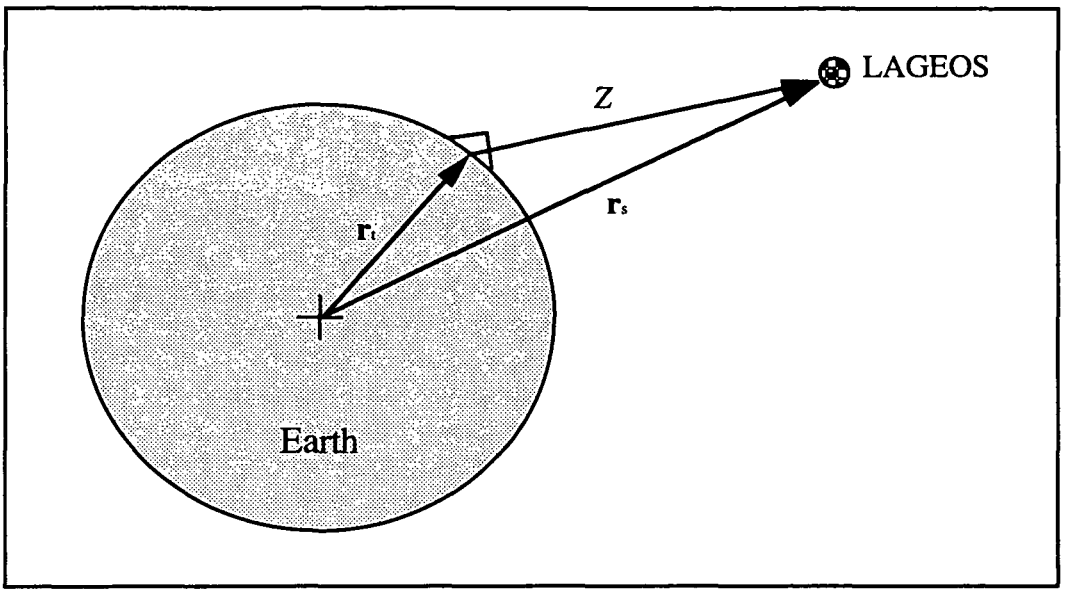

Figure 4.1. SLR Geometry.

The final, corrected laser range measurement is what is computed geometrically in equation 4.1 and used in this simulation. Finally, white noise with 1 cm RMS is added to all measurements once generated. This random error corresponds to the current ideal levels of accuracy and precision associated with SLR observations. Actual data may suffer from biases which are being ignored in this simulation.

4.2.1 Tracking Network

Typically, dozens of laser ranging tracking stations are able to track LAGEOS using the SLR technique. Over 100 tracking station sites around the world have made laser ranges to LAGEOS since its launch. In generating the simulated observations for this study, only eight tracking stations are used. This conservative tracking network was chosen to represent a worst case tracking scenario. Also, using a subset of the actual tracking network will reveal any problems that might result from the lack of a dense data distribution.

Figure 4.2 shows the tracking station network. Six of the eight tracking stations are located in the northern hemisphere. This reflects the fact that the majority of SLR tracking stations are in the northern hemisphere.

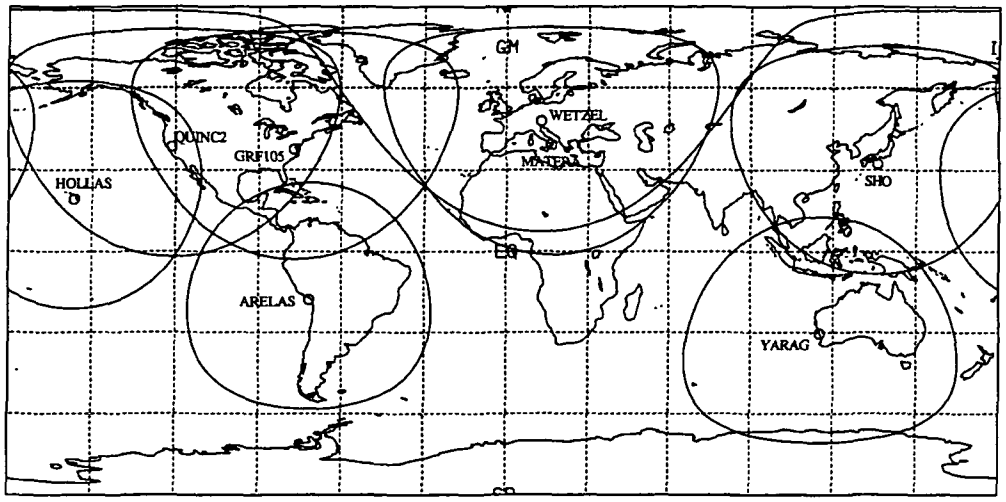

Figure 4.2. Tracking Station Network for LAGEOS Data Simulation With 20° Visibility Masks Shown.

The tracking stations operate from 6:00 PM to 6:00 AM local time. Four of the northern hemisphere stations track five days per week (Monday through Friday), as is the case with many NASA stations, while the rest of the stations track every day.

Observations are generated every three minutes (representing compressed normal point observations) for a specific tracking station only if the tracking station is operating during the particular pass, and the satellite is above 20° elevation. All observations are decimated by randomly eliminating 75% of the passes in an attempt to model data outages due to weather problems or inoperative tracking stations. Figure 4.3a shows the histogram of the simulated LAGEOS data over the one year simulation

period and Figure 4.3b shows a histogram of actual LAGEOS data over the same time period.

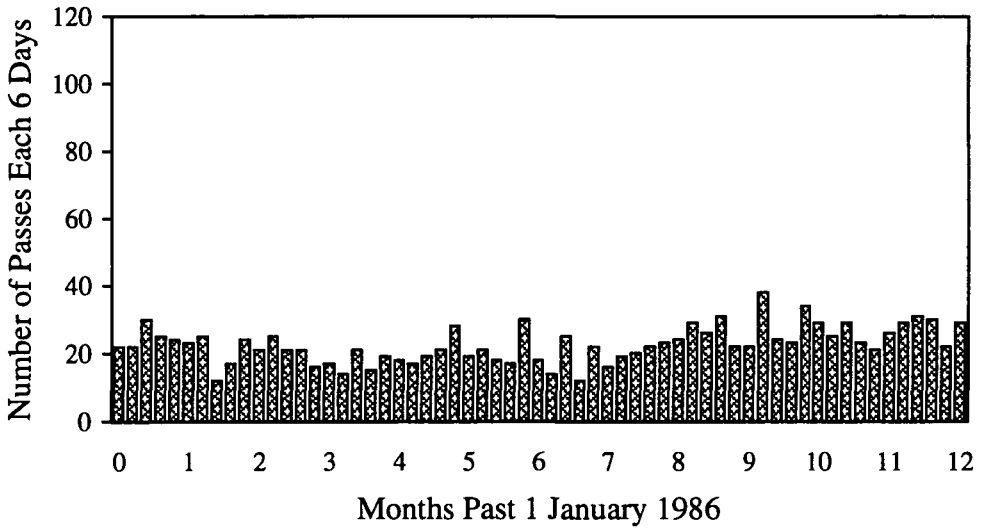

Figure 4.3a. Histogram of Simulated LAGEOS Laser Ranging Data.

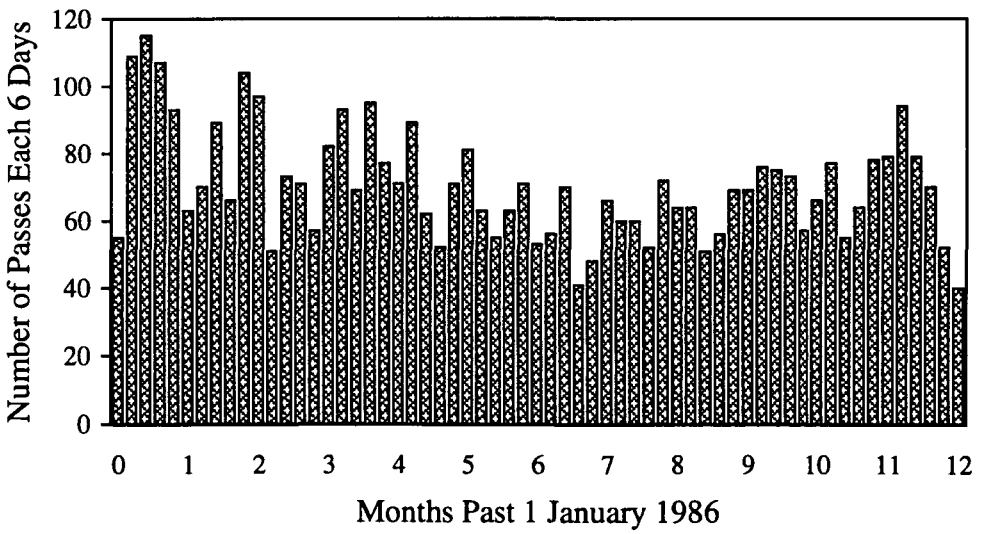

Figure 4.3b. Histogram of Actual LAGEOS Laser Ranging Data.

The simulation generates a conservative amount of data relative to the actual amount of LAGEOS data that is available from the same time period. The number of passes in each six days during the simulated LAGEOS arc is approximately one-half the number of passes in each six days during the actual LAGEOS arc. This ensures that any conclusions drawn based on the results of this simulation will not be improperly due to excessive or unrealistic data density. Table 4.1 shows the number of passes and observations for each of the tracking stations during the one year simulation. The days of the week that the stations operate is also summarized.

Table 4.1. Tracking Stations and Number of Passes and Observations Generated During the One Year Simulation. Station operation schedule is also summarized.

Tracking Station	Station ID	Number of Passes	Number of Observations	Station Operation Schedule
GRF105 (GSFC, USA)	7105	151	1897	Monday-Friday
QUINC2 (Quincy, USA)	7109	143	1777	Monday-Friday
HOLLAS (Maui, USA)	7210	118	1403	Monday-Friday
WETZEL (Wettzell, Germany)	7834	135	1765	Monday-Friday
ARELAS (Arequipa, USA)	7907	186	2261	Monday-Sunday
MATERA (Matera, Italy)	7939	208	2712	Monday-Sunday
SHO (Simosato, Japan)	7838	201	2491	Monday-Sunday
YARAG (Yaragadee, Australia)	7090	238	2586	Monday-Sunday
Totals		1380	16892	

4.3 Dynamical Model

A simplified dynamical force model is used in this study. The gravitational forces are modeled by a central body term (μ, the Earth's gravitational coefficient) and the zonal nonspherical geopotential coefficients up to degree five (J_2, J_3, J_4, and J_5). The reference value for μ is taken from *Ries et al.* [1992], and the zonal coefficients are taken from the JGM-2 [*Nerem et al.*, 1994] gravity model. Thus, the geopotential model is longitudinally symmetric. Table 4.2 summarizes the geopotential model used.

Table 4.2. Earth's Gravitational Coefficient and JGM-2 Coefficients (Unnormalized) used in Geopotential Model.

Coefficient	Nominal Value	Standard Deviation (σ)
μ	398600.4415 km^3/s^2	0.0008 km^3/s^2
J_2	1082627.0 x 10^{-9}	0.244 x 10^{-9}
J_3	−2532.308 x 10^{-9}	0.690 x 10^{-9}
J_4	−1620.430 x 10^{-9}	0.780 x 10^{-9}
J_5	−227.0711 x 10^{-9}	0.521 x 10^{-9}

The anomalous along track drag observed in the LAGEOS orbit is an ideal parameter to estimate stochastically since the forces causing the drag are not completely understood. In this study, this particular along track drag is considered the total drag. An empirical drag model is used to model this acceleration. The empirical function used is

$$\mathbf{D} = C_t \frac{\dot{\mathbf{r}}}{\| \dot{\mathbf{r}} \|} \tag{4.2}$$

where C_t is the along track parameter for the drag acceleration. The nominal average value for C_t used in this study is the mean of the observed value, or -3.5×10^{-12} m/s^2 (-3.5 picometer/s^2) [*Tapley et al.*, 1993].

The satellite state deviation vector, **x**, that is used in the simulation is

$$\mathbf{x} = [\, C_t \; J_2 \; J_3 \; J_4 \; J_5 \; \mu \; x \; y \; z \; \dot{x} \; \dot{y} \; \dot{z} \,]^{\mathrm{T}}$$

It is noted that estimates of this state vector are state *deviations* from the reference state based on the dynamical force model.

4.4 True Model Deviation Signals Added to Model Parameters

The dynamical model parameters described above remain fixed in the model throughout the filtering process. However, specific temporal variations, or model deviation signals, are introduced into the C_t, J_2, J_3, J_4, and J_5 model parameters in the dynamical force model as the simulated SLR measurements are generated. The temporal estimates of the these signals after filtering may then be compared to the known true model deviation signals present in the data. Again, these model deviation signals are *not* modeled in the dynamical model used in the filtering of the data. They are only added to the constant nominal values of the respective model parameter during the generation of the simulated data.

Some basic assumptions are made in defining these realistic model deviation signals. In general, the temporal signals are based on previously reported estimates or models of the temporal variations for the particular parameters. The true model deviation signals for C_t, J_2, and J_3 are based on previously reported estimates. While unknown, it is presumed that these parameters vary in some continuous manner. The previously reported estimates for these signals are then interpolated using a natural cubic spline in order to produce a smooth, continuous signal to use for the truth in this

study. The natural cubic spline interpolation forces the interpolation through the support points (previously reported estimates) while generating a smooth function. The true model deviation signals for J_4 and J_5 are based on proposed models. The true signal used for these parameters is inherently continuous since it is based on a model. No assumptions are made as to the expected averages (biases) of the model deviation signals for each of the parameters. While there is no expectation that the averages for these model deviation signals will be zero, no separate estimate is made for these biases. That is, the total model deviation signal for each parameter is estimated as a single deviation in the filtering process rather than a bias plus a variation from the bias. This approach should be valid as long as the biases of the model deviation signals remain on the order of magnitude of the variations from the bias, which is the circumstance for the model deviation signals used in this study and detailed below.

All of the model deviation signals for the one year arc are based on estimates made during the one year period from January 1, 1986 to December 31, 1986. The true model deviation signals introduced into the simulated data are detailed below.

4.4.1 Drag Model Deviation Signal

For the along track drag parameter C_t, the model deviation signal shown in Figure 4.4 is added to the nominal C_t value of -3.5 picometer/s^2 during the simulation of the observations.

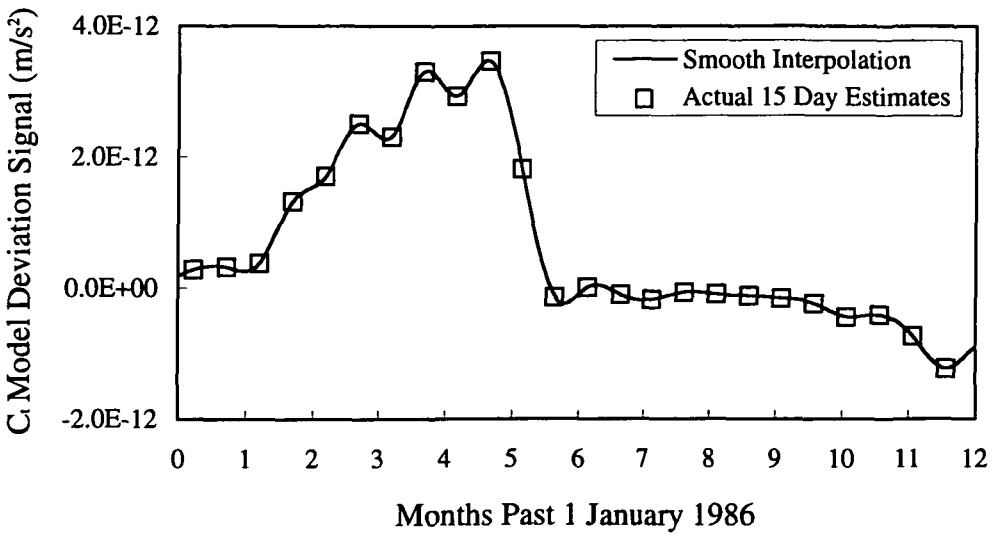

Figure 4.4. True Model Deviation Signal for the C_t Parameter Based on Current Best Estimates.

This model deviation signal is taken from *Tapley et al.* [1993] which gives 15 day estimates for the observed along track drag for LAGEOS over a 14 year period. The 15 day estimates falling between January 1, 1986 and December 31, 1986 are also shown in Figure 4.4 for reference. This one year of interpolated along track drag variation, with the average value subtracted out, is what is shown in Figure 4.4.

4.4.2 J_2 and J_3 Model Deviation Signal

The model deviation signal for the J_2 coefficient consists of a secular and nonsecular term. The model deviation signal for the J_3 coefficient is purely nonsecular. The secular rate used for J_2 ($\dot{J}_2$) is -2.6×10^{-11}/yr [*Nerem et al.*, 1993]. The total model deviation signal for each coefficient represents the nontidal temporal variations in J_2 and J_3.

The nonsecular part of the J_2 and J_3 model deviation signal is taken from *Nerem et al.* [1993] which gives monthly estimates for the nonsecular variations of J_2 and J_3 over the time period from 1980 to 1989. The estimates used are those they computed

from atmospheric pressure data (with no correction for the inverted barometer effect). These estimates are used in this study since they represent the current best estimates of the true J_2 and J_3 nonsecular variations. (Similar estimates of the J_2 and J_3 nonsecular variations exist based on LAGEOS SLR data, but are "effective" estimates as they include nonsecular variations from higher degree zonals which cannot be separated without independent data from satellites in different orbits.) Their monthly estimates for the nonsecular variations from January, 1986 to December, 1986 are interpolated with a natural cubic spline. This one year of interpolated J_2 and J_3 nonsecular variation, with the secular variation for J_2 added back, is what is shown in Figures 4.5 and 4.6 with the monthly estimates they are based on shown for reference (unnormalized). This is the total model deviation signal (total temporal variation) added to the nominal JGM-2 J_2 and J_3 values.

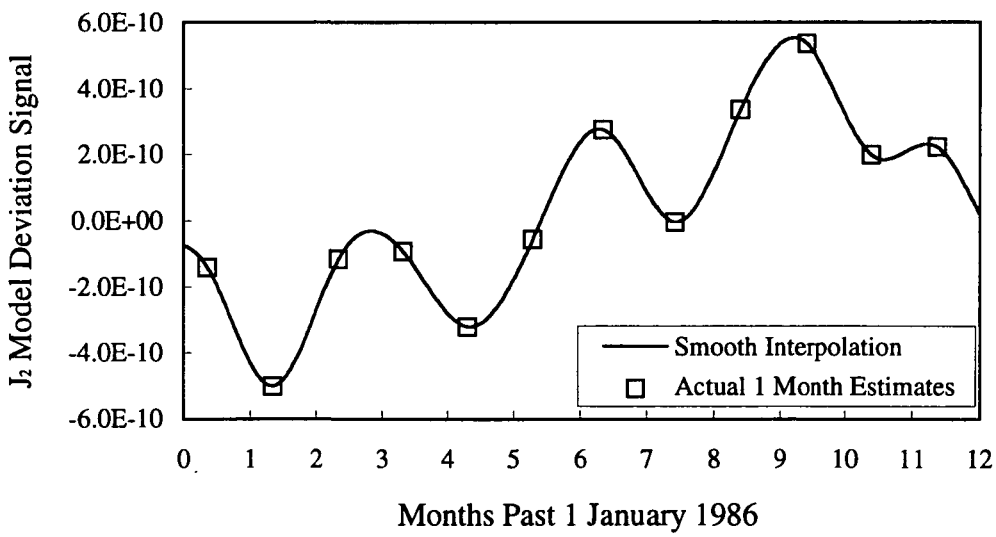

Figure 4.5. True Model Deviation Signal for the J_2 Parameter Based on Current Best Estimates.

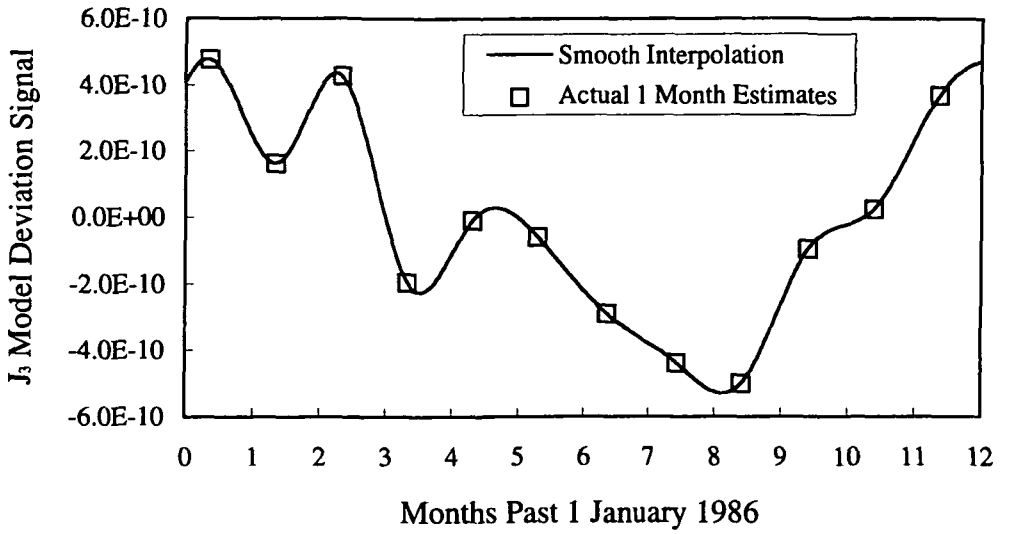

Figure 4.6. True Model Deviation Signal for the J_3 Parameter Based on Current Best Estimates.

4.4.3 J_4 and J_5 Model Deviation Signal

For the J_4 and J_5 coefficients, the model deviation signal shown in Figures 4.7 and 4.8 is added to the nominal JGM-2 J_4 and J_5 values (unnormalized). It should be noted that these model deviation signals are only included in part of this study, as discussed in chapter 5.

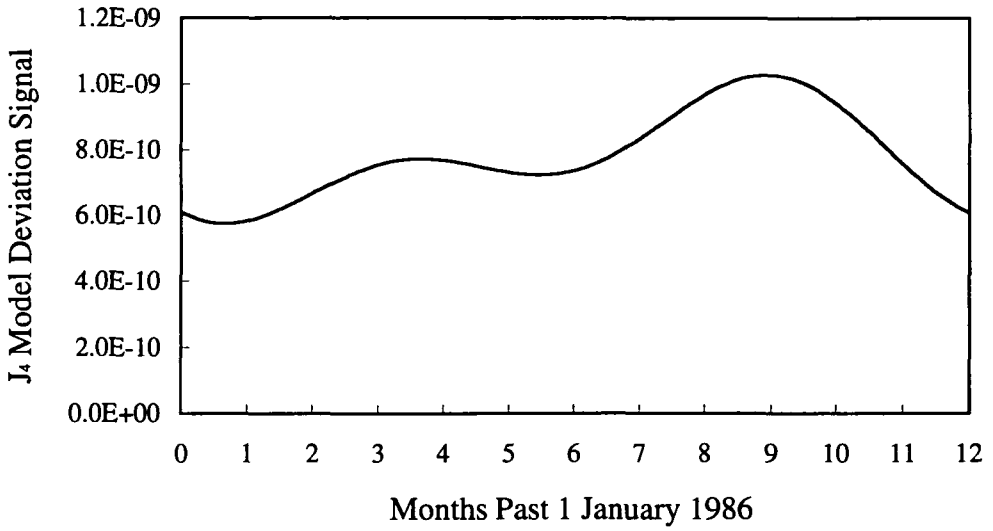

Figure 4.7. True Model Deviation Signal for the J_4 Parameter Based on Current Models.

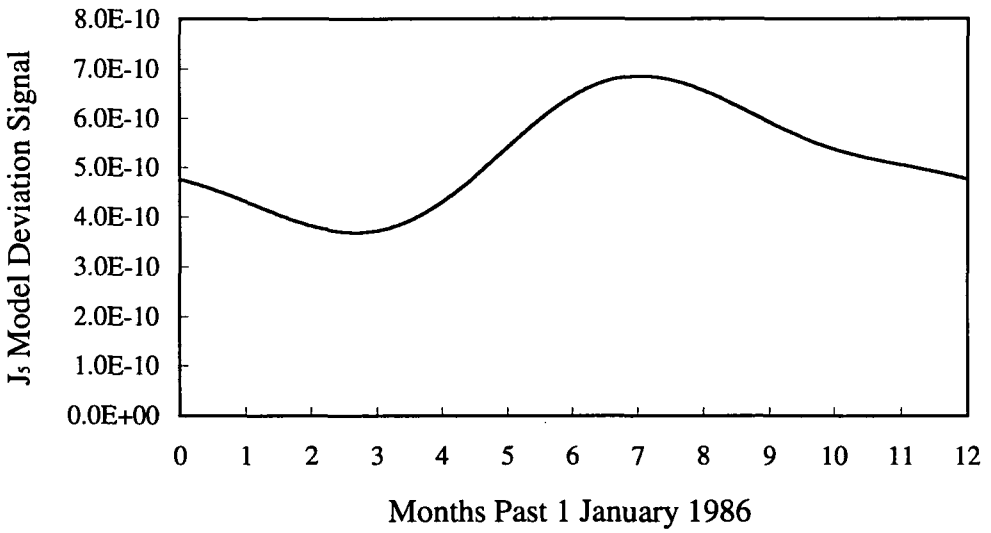

Figure 4.8. True Model Deviation Signal for the J_5 Parameter Based on Current Models.

These J_4 and J_5 model deviation signals are taken from *Chao and Au* [1991] which gives the amplitude and phase of the seasonal variations from the mean of J_4 and

J_5 (among other coefficients) based on global surface pressure data from 1980 to 1988. Table 4.3 details the characteristics which are pertinent to this study.

Table 4.3. Amplitude and Phase of Seasonal Variations in J_4 and J_5 due to Atmospheric Mass Redistribution Without the Oceanic Inverted Barometer Effect (from *Chao and Au* [1991]). Phase with respect to the sine convention with $t = 0$ on January 1.

	Annual Variation		Semiannual Variation	
Coefficient	Amplitude	Phase	Amplitude	Phase
J_4	1.52×10^{-10}	−155°	1.12×10^{-10}	−101°
J_5	1.38×10^{-10}	−143°	0.44×10^{-10}	62°

For this study, the temporal variations from January 1, 1986 to December 31, 1986 are computed from a function based on the amplitudes and phases noted above. Also, biases of 7.80×10^{-10} and 5.21×10^{-10} are included in the model deviation signals for J_4 and J_5 respectively. These biases represent the JGM-2 standard deviations (σ) for the reference values of J_4 and J_5 that are used in the dynamical model. This total model deviation signal (bias and temporal variation) is what is shown in Figures 4.7 and 4.8.

4.5 Summary of Data Simulation

To summarize, the satellite trajectory is numerically integrated using the dynamical model and the model deviation signals. These model deviation signals are continuous and based on a natural cubic spline interpolation of 15 day current estimates for C_t and one month estimates J_2 and J_3 for the period from 1 January 1986 to 1 December 1986. The continuous model deviation signals for J_4 and J_5 are based on current models. Range data from specified tracking stations to this trajectory is then computed at three minute intervals (based on observability and station operation criteria) and saved with 1 cm RMS random noise added to each range measurement. This data,

comprised of a time from epoch, tracking station number, and range measurement, makes up the simulated SLR data set used in this analysis.

CHAPTER 5

FILTERING RESULTS

5.1 Introduction

This chapter summarizes the solutions obtained from both the standard and stochastic orbit determination filtering modes. Both methods are used independently to determine solutions from the same set of simulated observations. A simulated one year data arc is processed both with and without the J_4 and J_5 model deviation signals present in the data. Also, a simulated three year data arc (without the J_4 or J_5 model deviation signals present) is processed using the stochastic filtering mode and the resulting solution is presented.

5.2 One Year Arc: C_t, J_2, and J_3 Model Deviation Signals

A simulated one year data arc with model deviation signals present in C_t, J_2, and J_3 and no model deviation signals present in J_4 or J_5 is processed. For both the standard and stochastic filtering methods, the one year data arc is processed with a single estimate made for the satellite state ($\mathbf{r}$ and $\dot{\mathbf{r}}$), and no correction made for μ, J_4, or J_5 (since no model deviation signal is present in the μ, J_4, or J_5 parameters, no correction is needed). In section 5.3, data that contains J_4 and J_5 model deviation signals is processed. For the standard SRIF mode, two iterations are performed in generating the solution. The reference trajectory for the second iteration uses the corrections from the first iteration. The estimates for C_t, J_2, and J_3 from the first iteration are used in the dynamical model during the second iteration as well. For the process noise SRIF mode, a preliminary correction is made only to the satellite state while fixing all other parameters. This gives a reference orbit that is sufficiently close

to the true orbit over the entire arc, thus minimizing linearization errors. A second iteration is performed using the process noise mode once this preliminary, non-stochastic correction is made.

5.2.1 Standard SRIF Using Boxcars

The standard SRIF is implemented using consecutive 15 day estimates for C_t throughout the arc. That is, a single, constant C_t estimate is made for the first 15 days of the arc, a second, constant C_t estimate for the second 15 days of the arc, and so on. This results in 24 consecutive C_t estimates over the one year arc. Thus, the solution for the C_t variation over the one year period is defined by joining these 24 C_t "boxcars" together. Again, the term boxcar is used henceforth to denote this type of solution based on its appearance as the discontinuous, constant estimates are consecutively joined together. Similarly, one month estimates are made for J_2 and J_3 throughout the one year arc. This results in 12 consecutive boxcars for the J_2 and J_3 solution over the one year arc. Thus, the simultaneous solution for the 24 C_t boxcars, the 12 J_2 boxcars, the 12 J_3 boxcars, and the satellite position and velocity is required.

First, the boxcar estimates for the C_t, J_2, and J_3 temporal variations are compared to the truth. Figure 5.1 shows the true C_t and the estimated C_t and Figure 5.2 shows the C_t residuals, or the true C_t minus the estimated C_t.

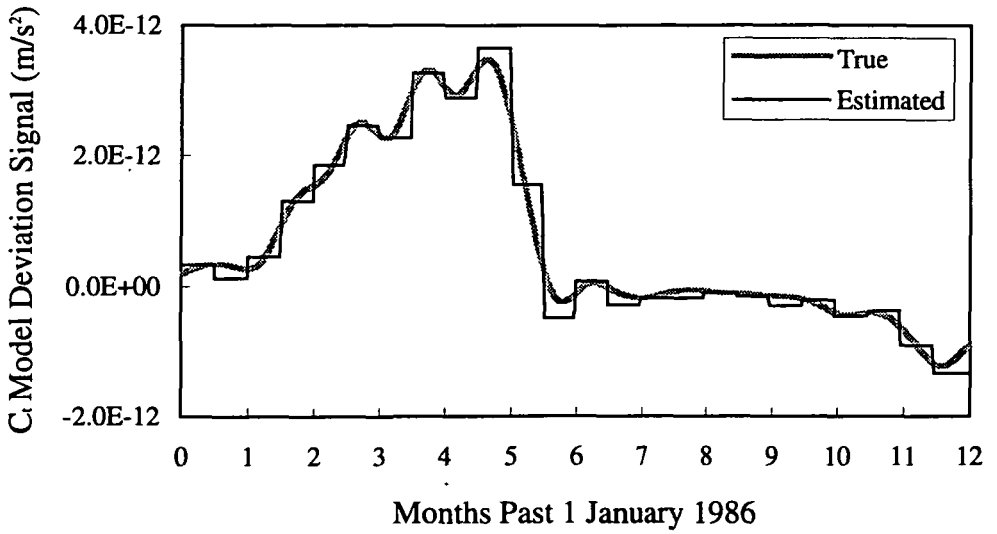

Figure 5.1. True C_t and Estimated C_t Using Boxcars.

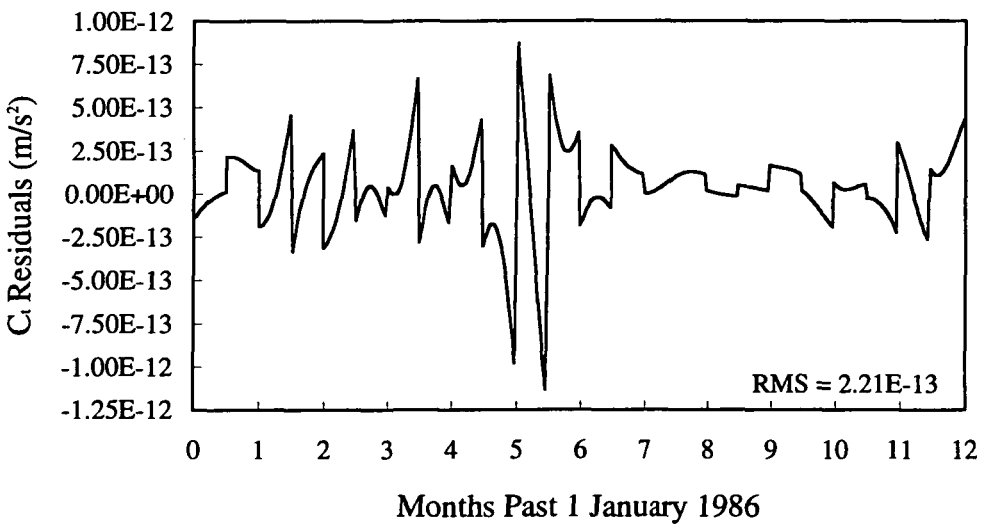

Figure 5.2. C_t Residuals Using Boxcars.

The boxcar estimates for C_t track the true signal quite well. This is consistent with the success that others have had using this approach to estimate C_t variations with actual LAGEOS data [*Tapley et al.*, 1993]. Figures 5.3 and 5.4 show the true J_2 and estimated J_2 and the J_2 residuals respectively.

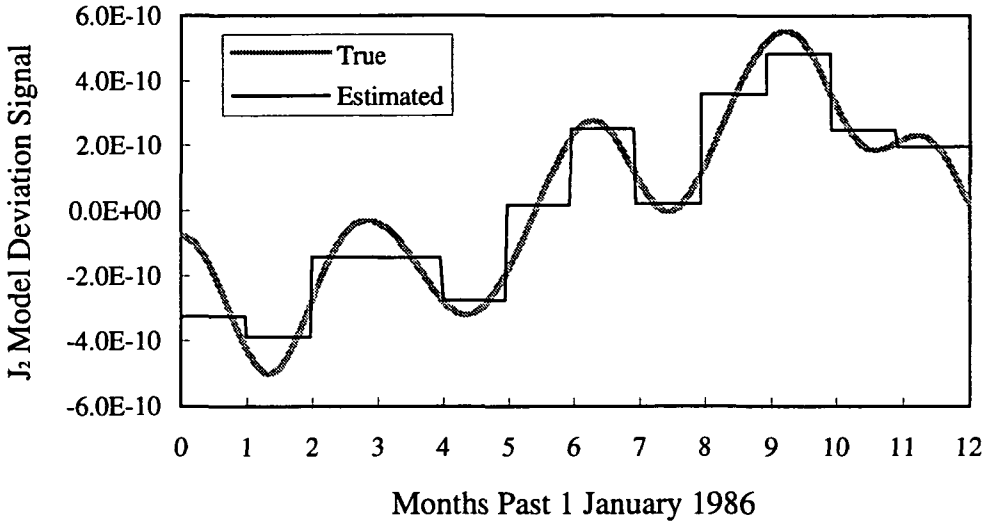

Figure 5.3. True J_2 and Estimated J_2 Using Boxcars.

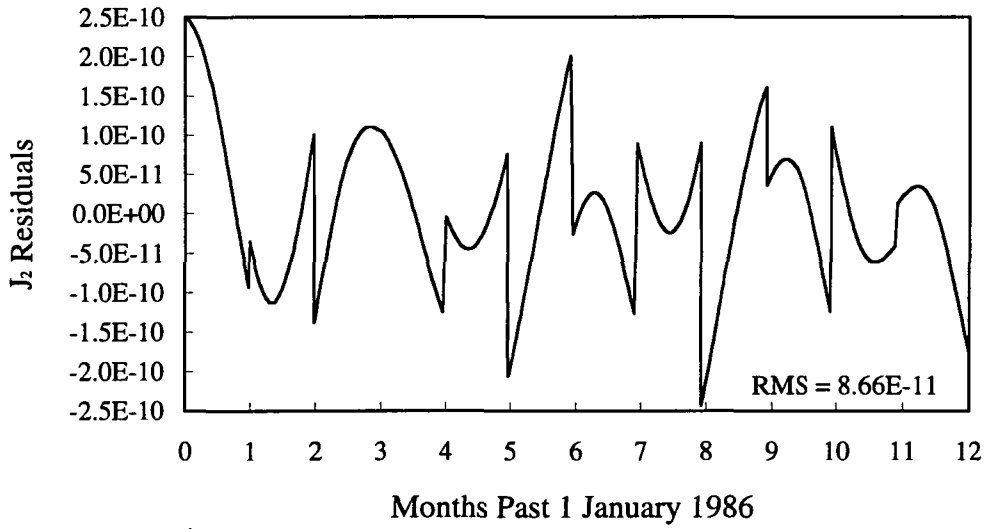

Figure 5.4. J_2 Residuals Using Boxcars.

Likewise, Figures 5.5 and 5.6 show the true J_3 and estimated J_3 and the J_3 residuals respectively.

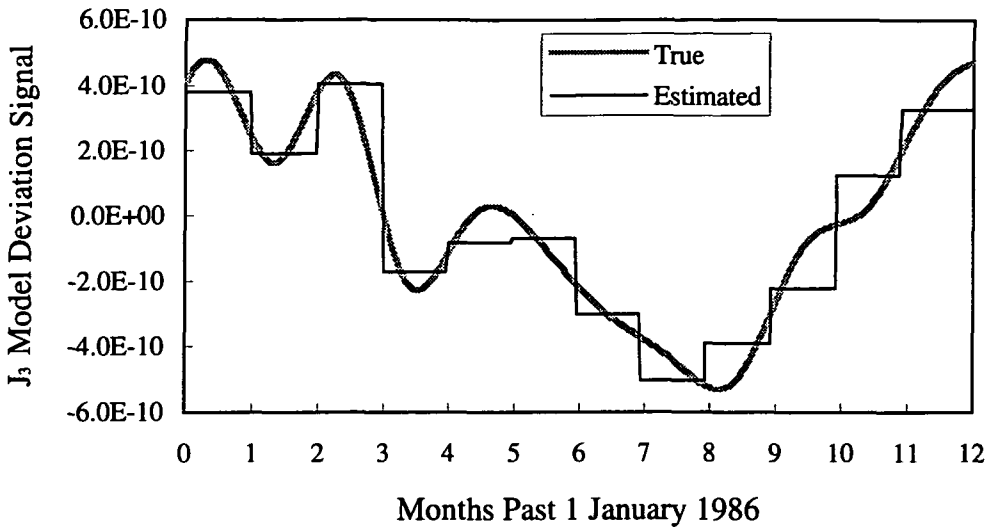

Figure 5.5. True J_3 and Estimated J_3 Using Boxcars.

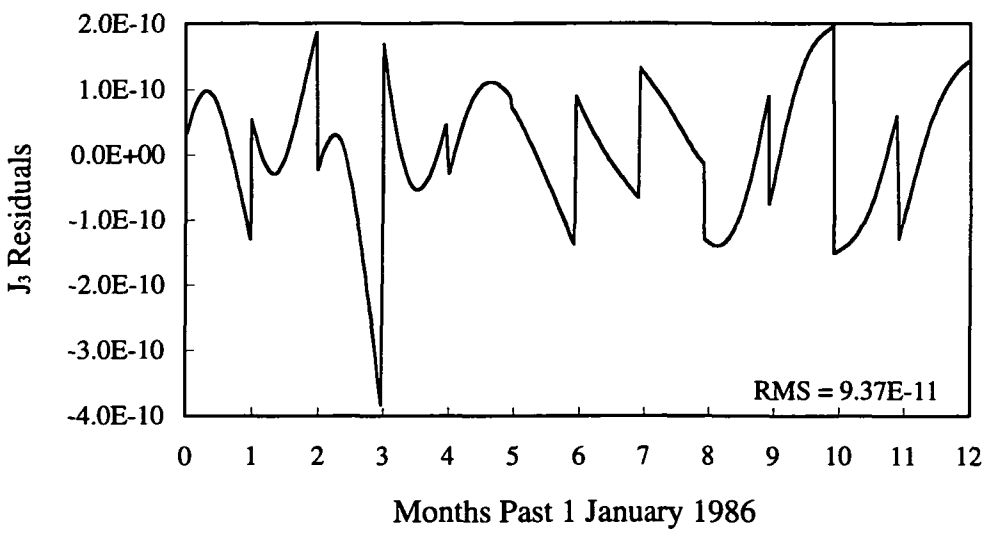

Figure 5.6. J_3 Residuals Using Boxcars.

Again, the boxcar estimates track the true signals quite well for both the J_2 and J_3 parameters. This too is consistent with the success that others have had using this approach to estimate J_2 and J_3 variations with actual LAGEOS data [*Nerem et al.*,

1993]. Table 5.1 summarizes the RMS statistics for the C_t, J_2, and J_3 residuals. The RMS statistics of the respective model deviation signals are also shown for reference.

Table 5.1. RMS for C_t, J_2, and J_3 Residuals Using Boxcars.

Parameter	Model Deviation Signal RMS	Residual RMS Using Boxcars
C_t	1.37×10^{-12} m/s^2	2.21×10^{-13} m/s^2
J_2	2.85×10^{-10}	8.66×10^{-11}
J_3	3.10×10^{-10}	9.37×10^{-11}

Next, the differences between the true orbit and the estimated orbit are analyzed from a positional standpoint. The radial, transverse, and normal (RTN) residuals are shown in Figures 5.7 to 5.9. These residuals represent the true position minus the estimated position in each direction respectively. The radial direction is the direction of the satellite position vector $\mathbf{r}$. The normal direction is the direction resulting from the matrix cross product of the satellite position vector $\mathbf{r}$ and the satellite velocity vector $\dot{\mathbf{r}}$ (the normal direction is perpendicular to the satellite's plane of motion). The transverse direction results from the matrix cross product of the normal and radial directions.

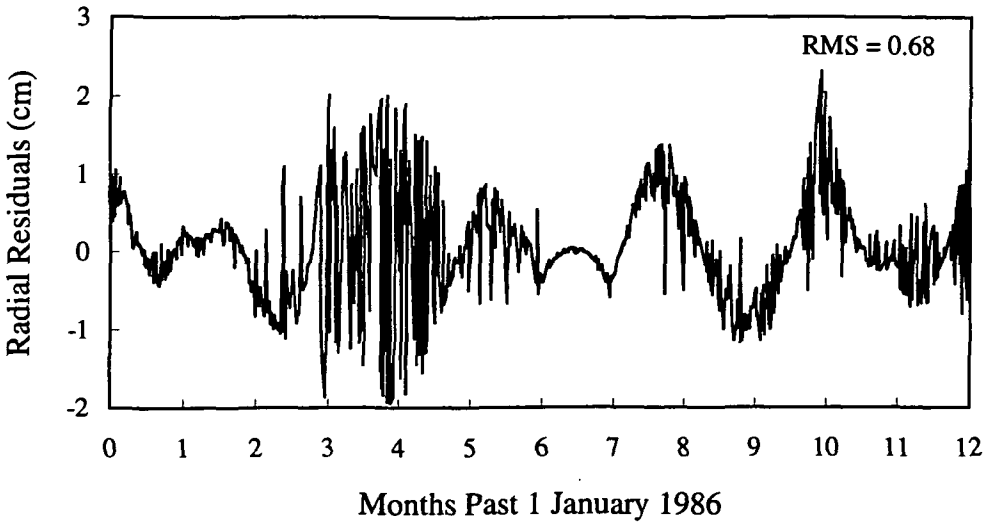

Figure 5.7. Radial Residuals Using Boxcars.

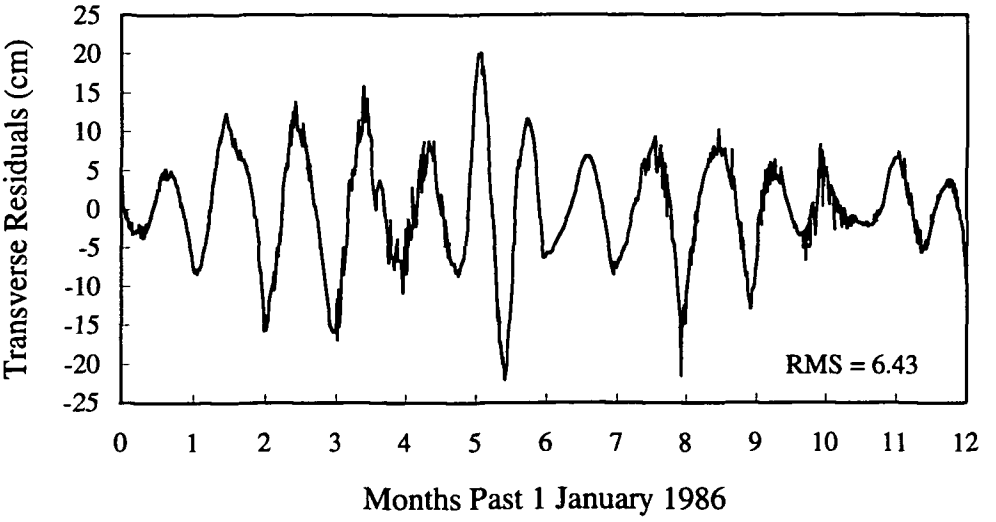

Figure 5.8. Transverse Residuals Using Boxcars.

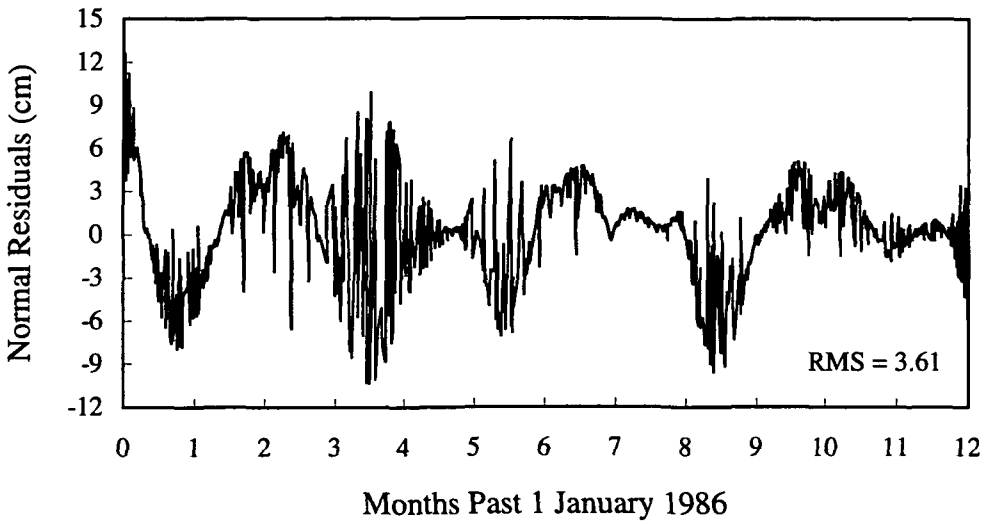

Figure 5.9. Normal Residuals Using Boxcars.

The total magnitude of the RTN residuals (3-d position residuals) are shown in Figure 5.10. This is simply the magnitude of the positional difference between the true position and the estimated position of the satellite at each time.

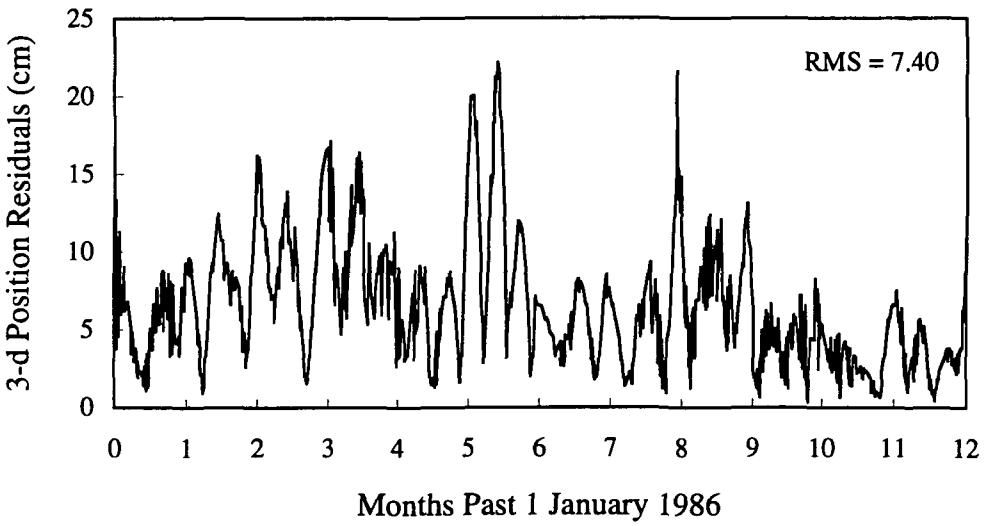

Figure 5.10. 3-d Position Residuals Using Boxcars.

Figures A.1 through A.6 in Appendix A show the orbit residuals in terms of the Keplerian elements (semi-major axis a, eccentricity e, inclination i, argument of periapse ω, longitude of ascending node Ω, and argument of latitude $\omega + f$, where f is true anomaly).

Finally, the range residuals (observed range minus computed range) are determined. Figure 5.11 shows the range residuals, and Table 5.2 summarizes the RMS statistics for the RTN, 3-d position, and range residuals. Since 1 cm RMS noise is present in the simulated observations, it is expected that the RMS of the range residuals will approach 1 cm as the estimated solution approaches the truth.

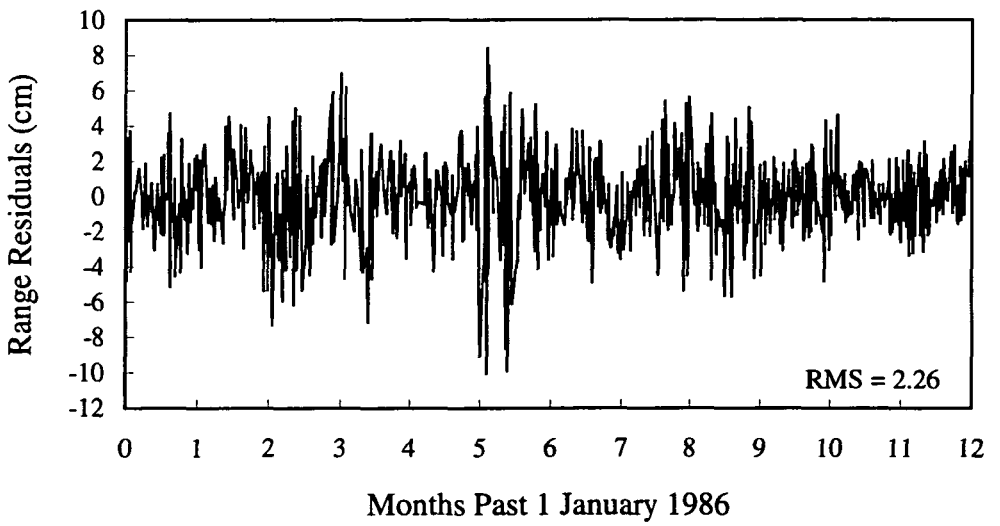

Figure 5.11. Range Residuals Using Boxcars.

Table 5.2. RMS for RTN and Range Residuals Using Boxcars.

Residual	RMS (cm)
Radial	0.68
Transverse	6.43
Normal	3.61
3-d Position	7.40
Range	2.26

These residuals, along with the individual C_t, J_2, and J_3 parameter residuals, form the basis for the statistical comparison of the standard SRIF boxcar solution to the process noise SRIF solution.

5.2.2 Process Noise SRIF

The process noise SRIF is implemented with stochastic estimates made for C_t, J_2, and J_3. Stochastic estimates of each parameter are made at every time that an observation exists. Specific values for τ and σ (as defined in chapter 2) are chosen for each parameter based on the expected time correlation and amplitude of the model deviation signal for that parameter. Table 5.3 summarizes the values used for each parameter.

Table 5.3. Values for the Time Correlation Constant τ, and Steady State Standard Deviation σ, for One Year Arc with C_t, J_2, and J_3 Model Deviation Signals.

Parameter	τ (years)	σ
C_t	$\frac{1}{12}$	3.5×10^{-12} m/s^2
J_2	$\frac{1}{4}$	1.5×10^{-9}
J_3	$\frac{1}{4}$	3.0×10^{-9}

The stochastic estimates for the C_t, J_2, and J_3 temporal variations are compared to the truth. Figure 5.12 shows the true C_t and the estimated C_t and Figure 5.13 shows the C_t residuals, or the true C_t minus the estimated C_t.

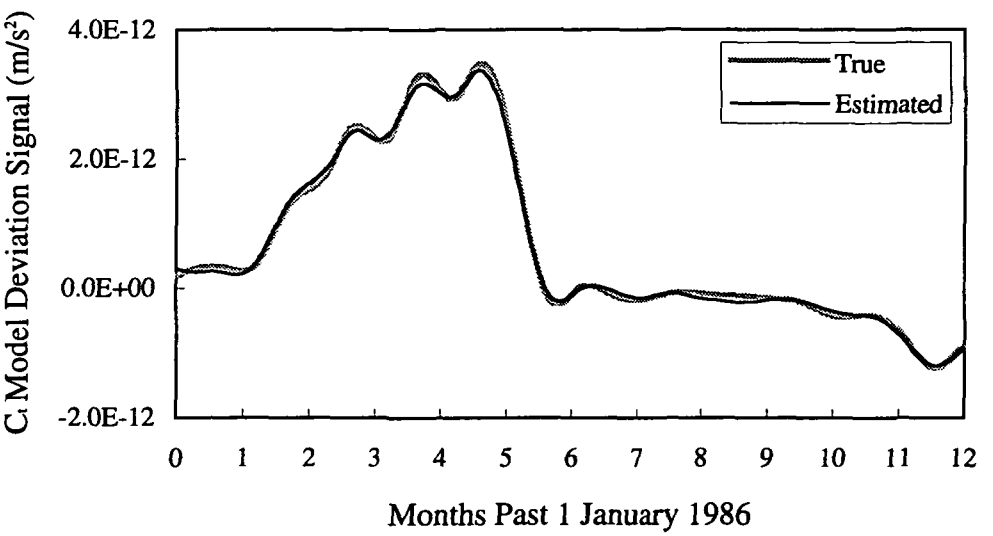

Figure 5.12. True C_t and Estimated C_t Using Process Noise.

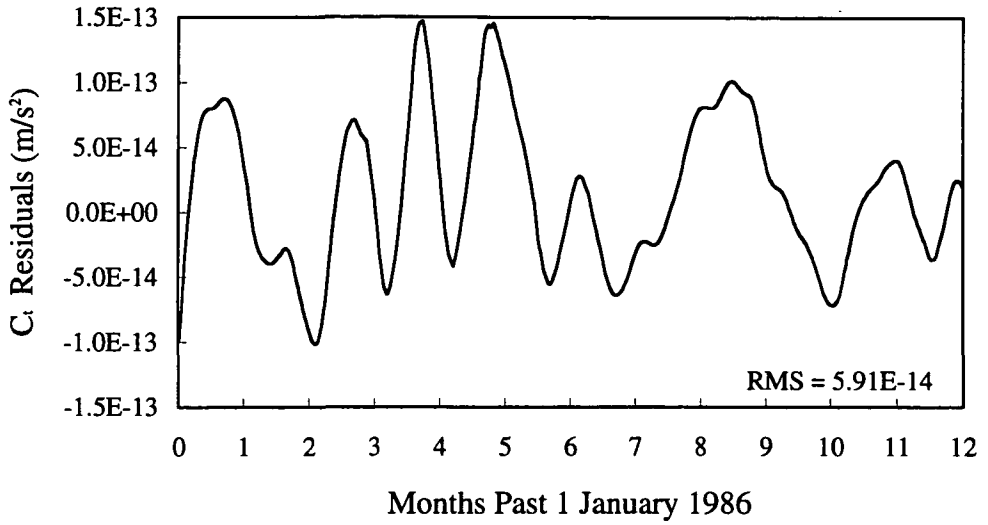

Figure 5.13. C_t Residuals Using Process Noise.

The stochastic estimate of C_t appears excellent. Relative to the previous boxcar estimate for C_t, the stochastic estimate appears to have much better temporal resolution and accuracy. Figures 5.14 and 5.15 show the true J_2 and estimated J_2 and the J_2 residuals respectively.

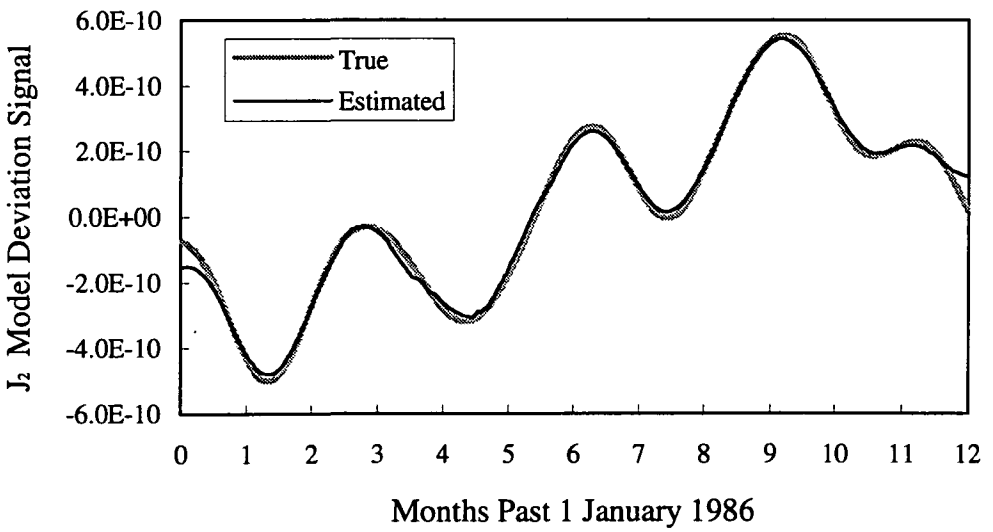

Figure 5.14. True J_2 and Estimated J_2 Using Process Noise.

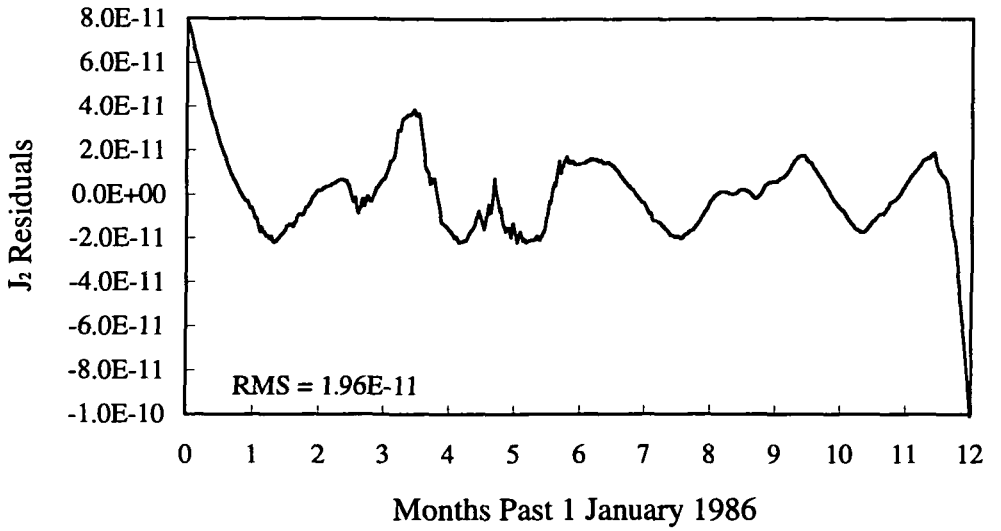

Figure 5.15. J_2 Residuals Using Process Noise.

Likewise, Figures 5.16 and 5.17 show the true J_3 and estimated J_3 and the J_3 residuals respectively.

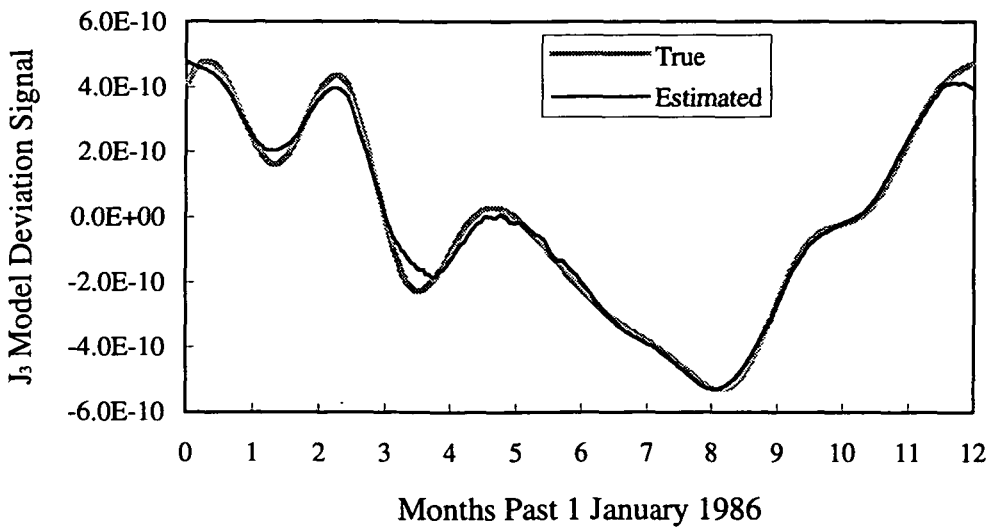

Figure 5.16. True J_3 and Estimated J_3 Using Process Noise.

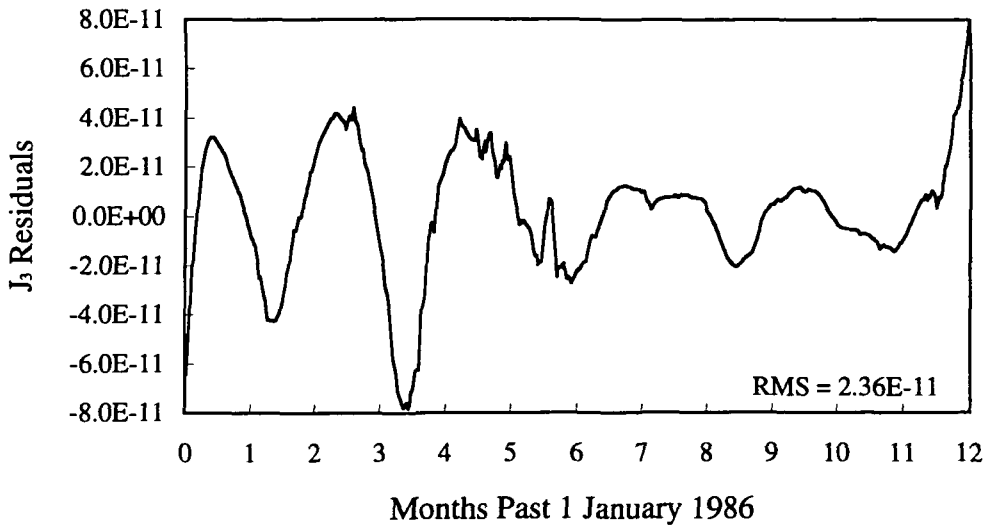

Figure 5.17. J_3 Residuals Using Process Noise.

The stochastic estimates of J_2 and J_3 are also excellent. Relative to the previous boxcar estimates for J_2 and J_3, the stochastic estimates appear to have much better temporal resolution and accuracy. Table 5.4 summarizes the RMS statistics for the C_t, J_2, and J_3 residuals with the respective RMS statistics from the previous boxcar solution shown for comparison (from Table 5.1). The RMS statistics of the respective model deviation signals are also shown for reference.

Table 5.4. RMS for C_t, J_2, and J_3 Residuals Using Process Noise and Boxcars.

Parameter	Model Deviation Signal RMS	Residual RMS Using Boxcars	Residual RMS Using Process Noise
C_t	1.37×10^{-12} m/s^2	2.21×10^{-13} m/s^2	5.91×10^{-14} m/s^2
J_2	2.85×10^{-10}	8.66×10^{-11}	1.96×10^{-11}
J_3	3.10×10^{-10}	9.37×10^{-11}	2.36×10^{-11}

The process noise residuals for C_t, J_2, and J_3 are noticeably improved relative to the respective boxcar residuals.

Next, the RTN positional residuals are shown in Figures 5.18 to 5.20. The total RTN, or 3-d position residuals are shown in Figure 5.21.

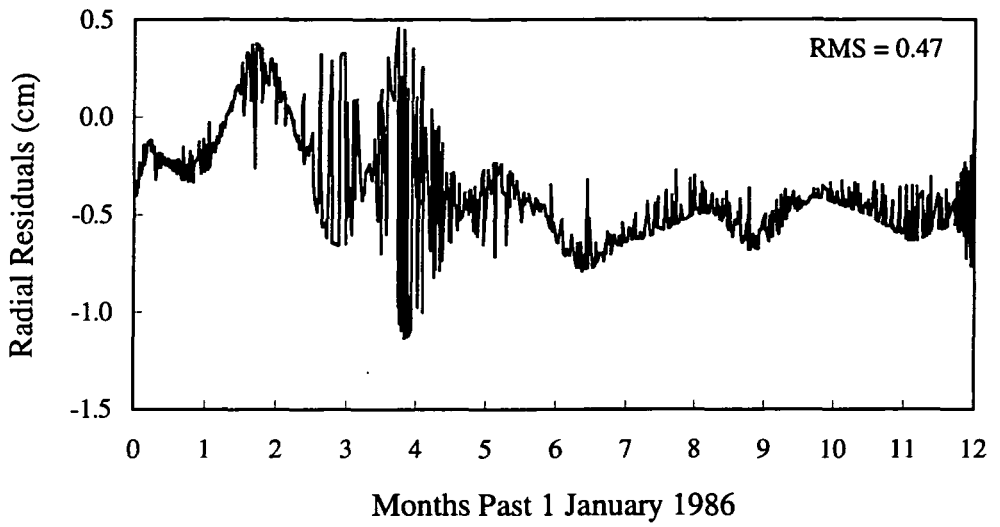

Figure 5.18. Radial Residuals Using Process Noise.

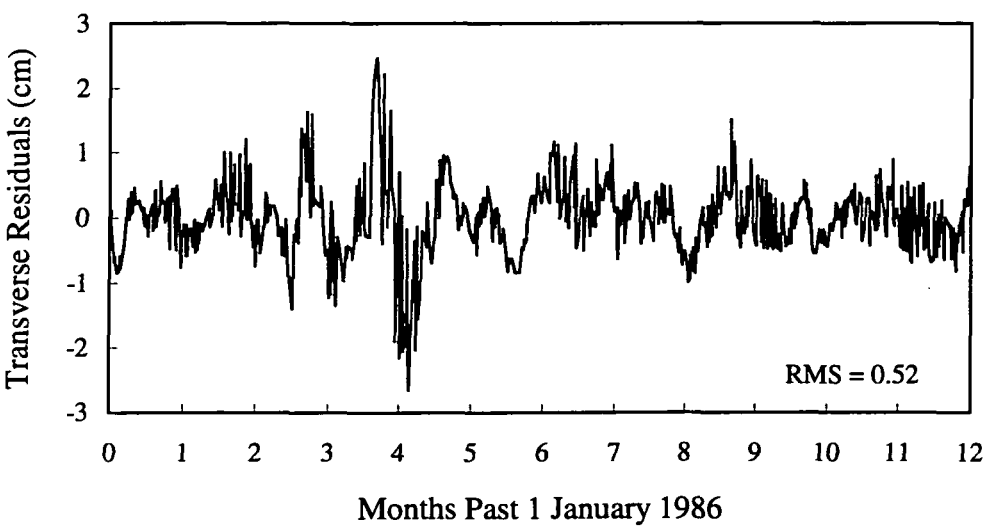

Figure 5.19. Transverse Residuals Using Process Noise.

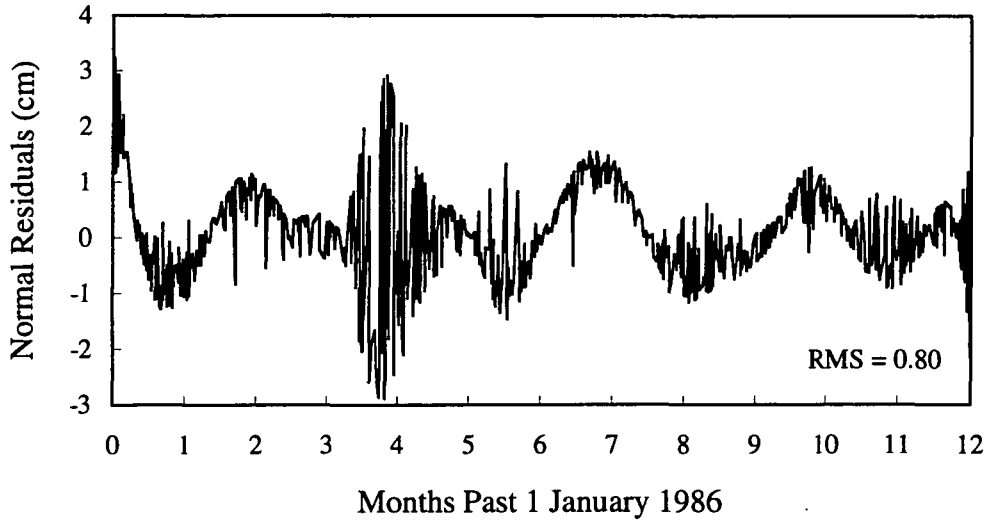

Figure 5.20. Normal Residuals Using Process Noise.

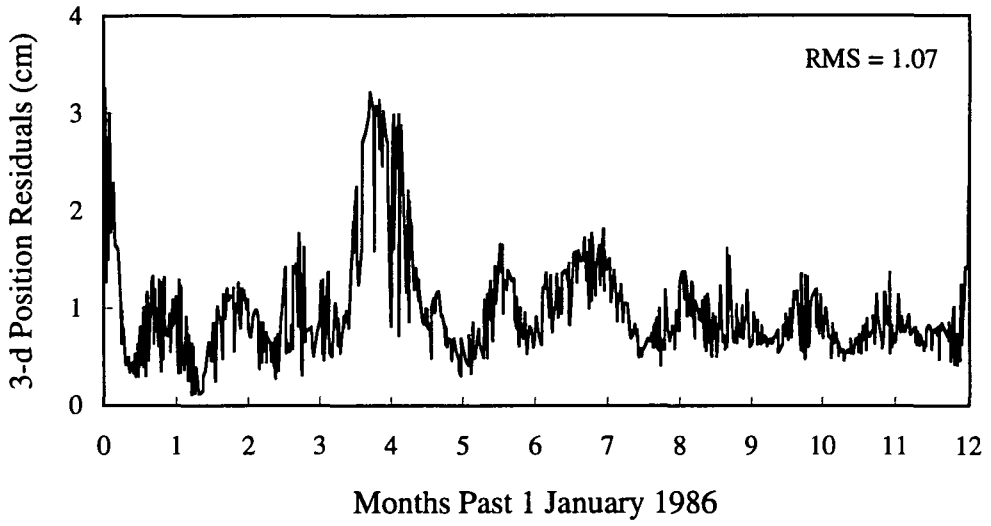

Figure 5.21. 3-d Position Residuals Using Process Noise.

Figures B.1 through B.6 in Appendix B show the orbit residuals in terms of the Keplerian elements (semi-major axis a, eccentricity e, inclination i, argument of

periapse ω, longitude of ascending node Ω, and argument of latitude $\omega + f$, where f is true anomaly).

Figure 5.22 shows the range residuals, and Table 5.5 summarizes the RMS statistics for the RTN, 3-d position, and range residuals (with comparison to the respective boxcar statistics from Table 5.2 for reference). Again, since 1 cm RMS noise is present in the simulated observations, it is expected that the RMS of the range residuals will approach 1 cm as the estimated solution approaches the truth.

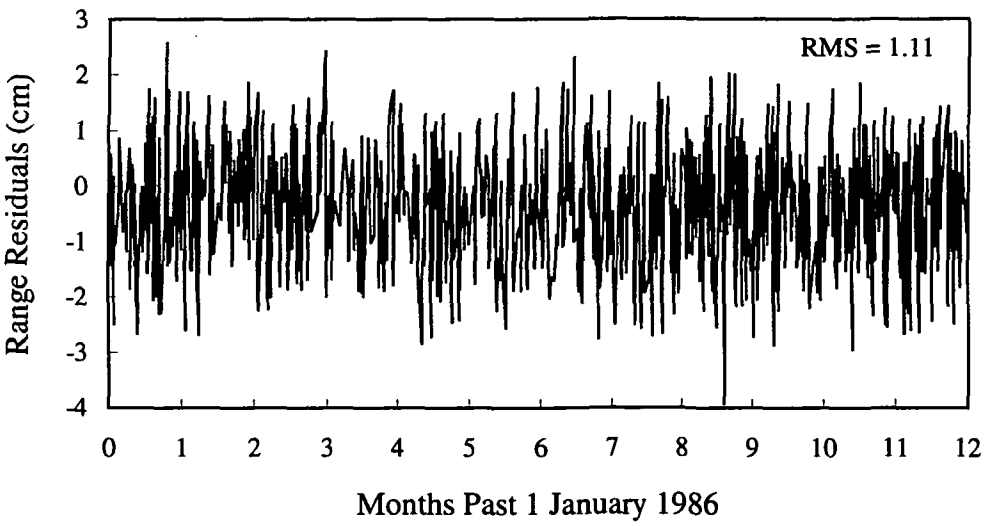

Figure 5.22. Range Residuals Using Process Noise.

Table 5.5. RMS for RTN and Range Residuals Using Process Noise and Boxcars.

Residual	RMS Using Boxcars (cm)	RMS Using Process Noise (cm)
Radial	0.68	0.47
Transverse	6.43	0.52
Normal	3.61	0.80
3-d Position	7.40	1.07
Range	2.26	1.11

Figures 5.23 to 5.27 show the RTN, 3-d position, and range residuals from both the standard boxcar SRIF and the process noise SRIF solutions side by side on the same scale for visual comparison.

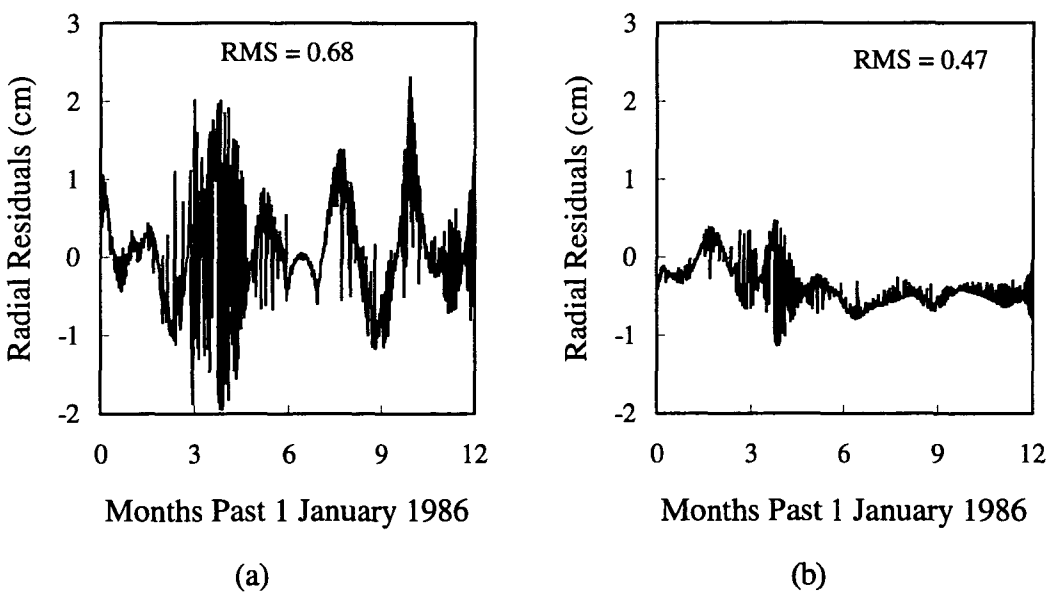

Figure 5.23. Radial Residuals Using Boxcars (a) and Process Noise (b).

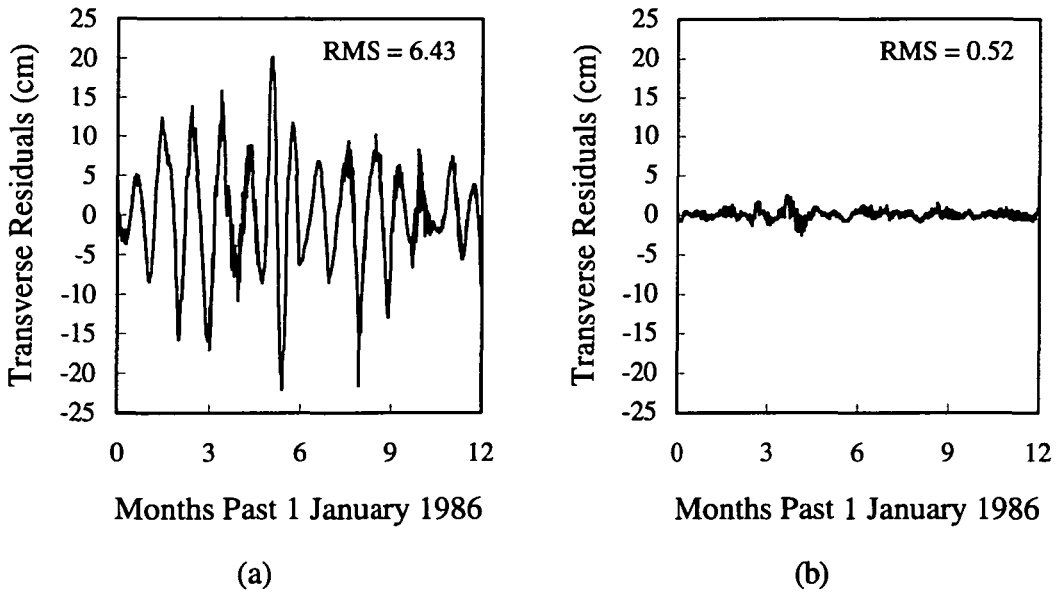

Figure 5.24. Transverse Residuals Using Boxcars (a) and Process Noise (b).

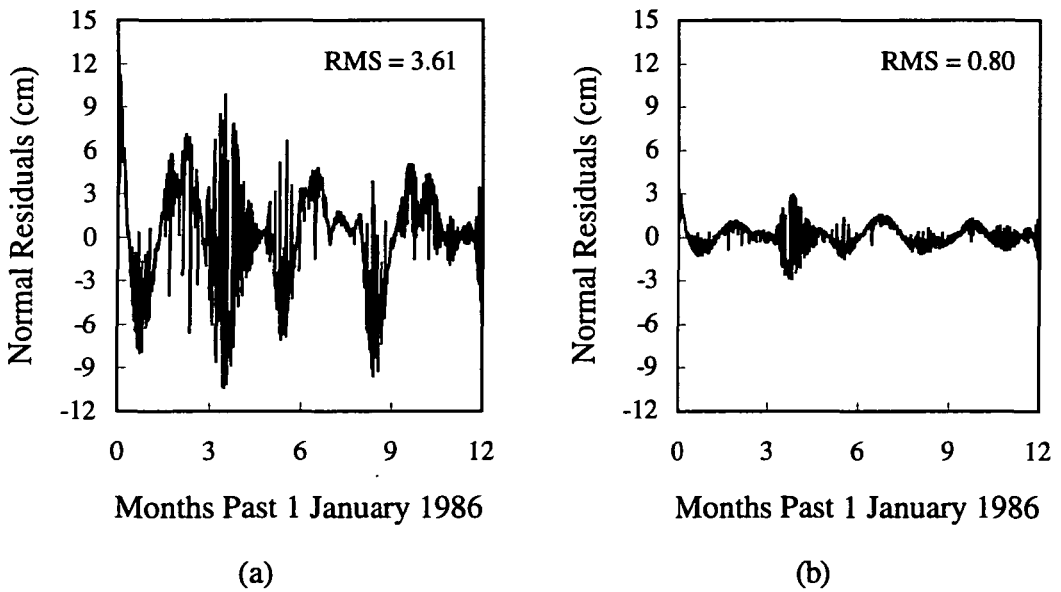

Figure 5.25. Normal Residuals Using Boxcars (a) and Process Noise (b).

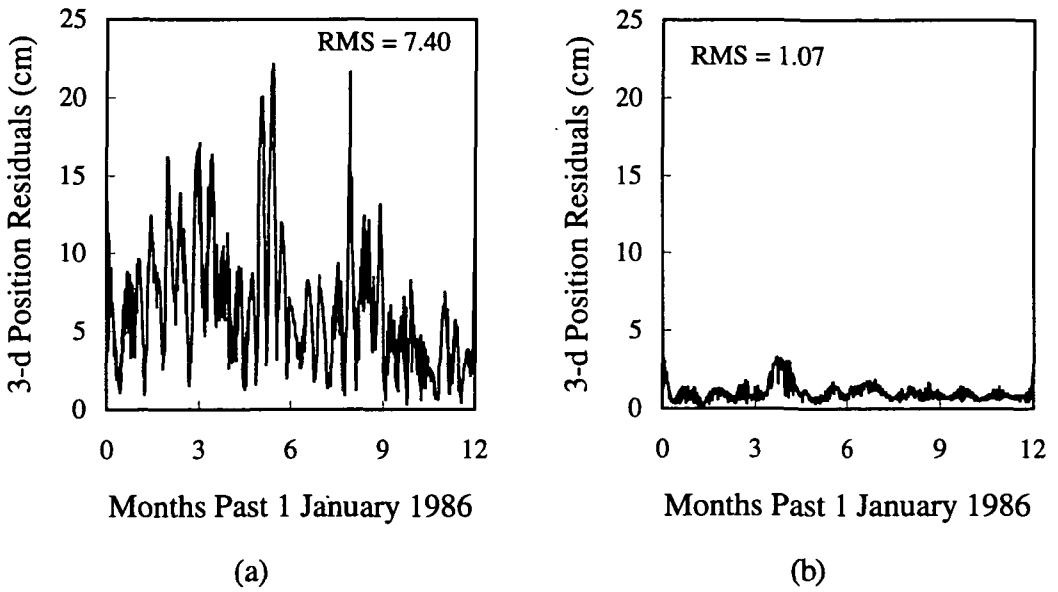

Figure 5.26. 3-d Position Residuals Using Boxcars (a) and Process Noise (b).

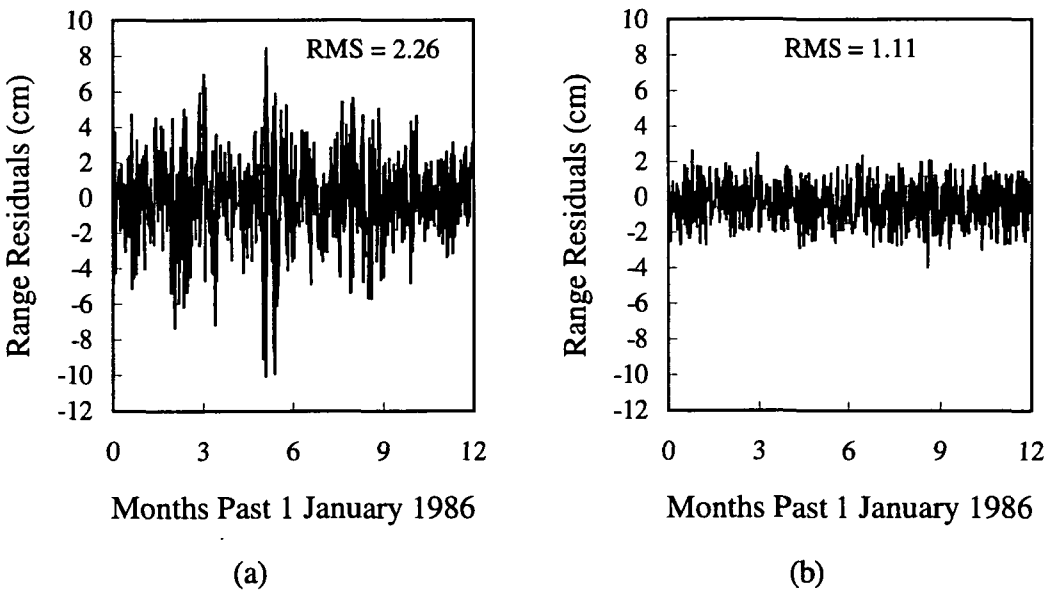

Figure 5.27. Range Residuals Using Boxcars (a) and Process Noise (b).

Clearly, the stochastic filtering method produces a temporal solution for C_t, J_2, and J_3 which is more accurate than the standard boxcar solution. The RMS for the C_t,

J_2, and J_3 residuals are reduced to approximately 25% of the respective residuals using the standard boxcar method (a 75% improvement). Similarly, by using the stochastic filtering method the total 3-d positional residual is reduced to approximately 15% of the 3-d positional residual resulting from the standard boxcar filtering method (an 85% improvement). The range residuals are reduced by about 50%.

5.3 One Year Arc: C_t, J_2, J_3, J_4, and J_5 Model Deviation Signals

Next, a simulated one year data arc with model deviation signals present for C_t, J_2, J_3, J_4, and J_5 is processed. Again, the one year data arc is processed with a single estimate made for the satellite state, and no estimate made for μ, J_4, or J_5, even though J_4 and J_5 model deviation signals are present in the data for this case. This configuration assesses the ability of each filter to resolve the C_t variation and the *effective* J_2 and J_3 temporal variations since J_4 and J_5 model deviation signals are present but not estimated (a discussion on the effective J_2 and J_3 temporal variations will follow shortly). This situation more closely parallels typical filtering scenarios which estimate temporal variations in particular parameters in the presence of other parameter variations/model deviation signals which are not estimated. Aside from the introduction of the J_4 and J_5 model deviation signal, the analysis parallels the previous scenario.

5.3.1 Standard SRIF Using Boxcars

The standard SRIF is implemented using 24 consecutive 15 day estimates for C_t and 12 consecutive one month estimates for J_2 and J_3 throughout the arc. First, the boxcar estimates for the C_t, J_2, and J_3 temporal variations are compared to the truth. Figure 5.28 shows the true C_t and the estimated C_t and Figure 5.29 shows the C_t residuals, or the true C_t minus the estimated C_t. The boxcar estimates for C_t appear to

be as accurate as in the previous boxcar case where no J_4 or J_5 model deviation signals are present.

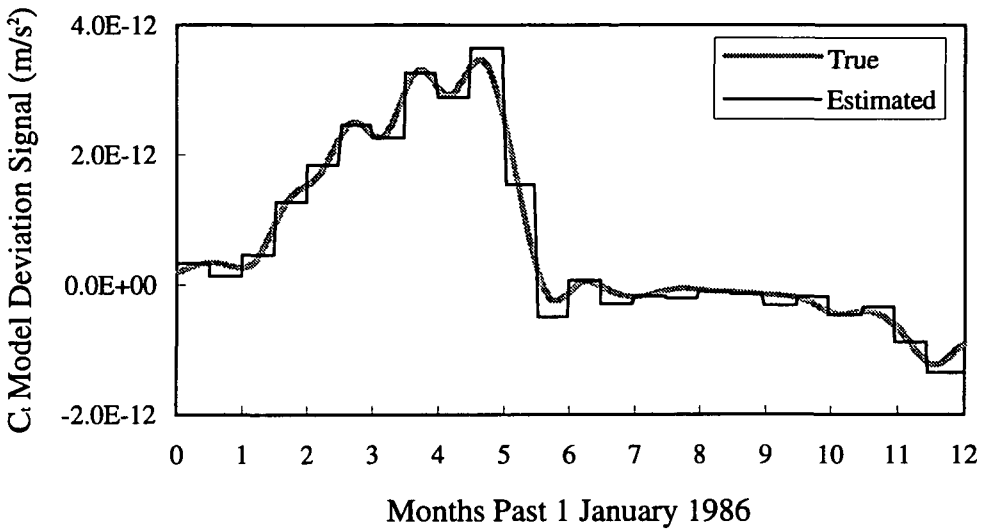

Figure 5.28. True C_t and Estimated C_t Using Boxcars with J_4 and J_5 Model Deviation Signals Present but not Estimated.

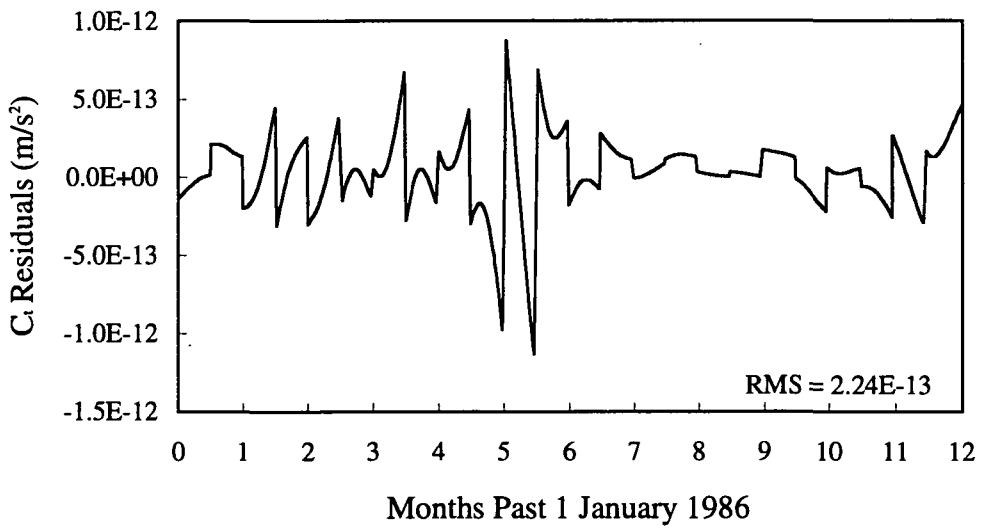

Figure 5.29. C_t Residuals Using Boxcars with J_4 and J_5 Model Deviation Signals Present but not Estimated.

Figures 5.30 and 5.31 show the true and estimated J_2 and true and estimated J_3 respectively.

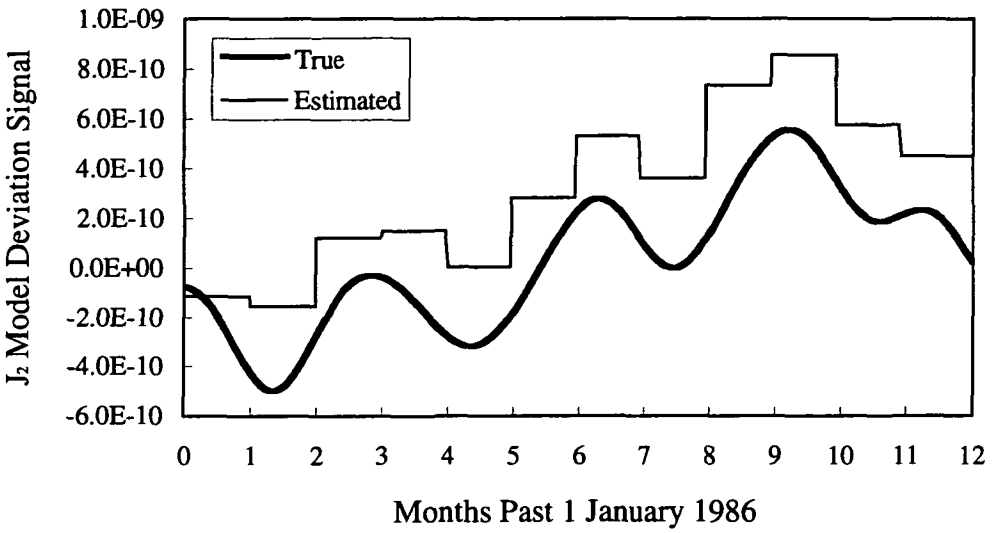

Figure 5.30. True J_2 and Estimated J_2 Using Boxcars with J_4 and J_5 Model Deviation Signals Present but not Estimated.

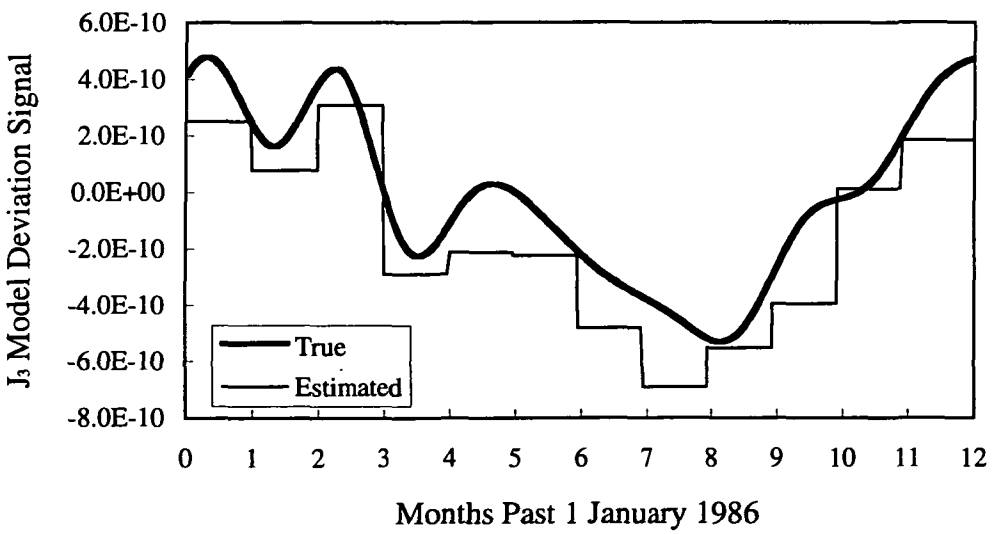

Figure 5.31. True J_3 and Estimated J_3 Using Boxcars with J_4 and J_5 Model Deviation Signals Present but not Estimated.

It is clear from Figures 5.30 and 5.31 that the estimates of the J_2 and J_3 variations with J_4 and J_5 model deviation signals present but not estimated do not correspond to the true J_2 and J_3 model deviation signals very well. A bias differentiates the two. This is a result of the fact that the estimates of the J_2 and J_3 variations are estimates of the "effective" J_2 and J_3 variations. A discussion of effective J_2 and J_3 signals now follows.

5.3.1.1 Effective J_2 and J_3 Model Deviation Signals

For this part of the analysis, J_4 and J_5 model deviation signals are present in the data, but not estimated. In this scenario, estimates of the J_2 and J_3 variations are estimates of the "effective" J_2 and J_3 variations. That is, the estimate of the J_2 variation is a value that alone would have the same effect (acceleration) on the satellite that the J_2 *and* J_4 variations cause. Put another way, the J_2 and J_4 variations in the data are combined into an single (effective) J_2 variation. This effective J_2 variation is estimated by the filter since no estimate is being made for the J_4 variations. Further, if the J_4 variations were estimated, the filter could not separate the J_2 and J_4 variations based on observations only from LAGEOS. The two variations are not separable without observations from other satellites. Likewise, the same relationship exists between J_3 and J_5. For the most part, when temporal variations of low degree zonal geopotential coefficients are estimated from single satellite data, they are effective estimates since variations in the higher degree zonals are not estimated separately. Thus, the effect of variations in all higher even degree zonals can be aliased into the variations of even low degree zonals that are estimated. Similarly, the effect of variations in all higher odd degree zonals can alias into the variations of odd low degree zonals that are estimated.

The "true" effective J_2 (and true effective J_2 variation) is determined as follows:

The secular variation in the longitude of node Ω, due to J_2 may be written

$$\frac{d\Omega}{dt} = -\frac{3}{2} n \left(\frac{a_e}{a}\right)^2 \frac{\cos i}{\left(1-e^2\right)^2} J_2 \tag{5.1}$$

where n is the satellite mean motion ($n^2 a^3 = \mu$), a_e is the semi-major axis of the central body's reference ellipsoid, i is the satellite inclination, and a is the satellite semi-major axis.

Likewise, the secular variation in Ω due to J_4 may be written

$$\frac{d\Omega}{dt} = -\frac{15}{4} n \left(\frac{a_e}{a}\right)^4 \frac{\cos i}{\left(1-e^2\right)^4} \left(1+\frac{3}{2}e^2\right)\left(\frac{7}{4}\sin^2 i - 1\right) J_4 \tag{5.2}$$

The expression for the secular variation in Ω due to both J_2 and J_4 may be equated with an expression for the secular variation in Ω due to an effective J_2:

$$\begin{aligned} -\frac{3}{2} n \left(\frac{a_e}{a}\right)^2 \frac{\cos i}{\left(1-e^2\right)^2} J_{2e} &= -\frac{3}{2} n \left(\frac{a_e}{a}\right)^2 \frac{\cos i}{\left(1-e^2\right)^2} J_2 \\ -\frac{15}{4} n \left(\frac{a_e}{a}\right)^4 \frac{\cos i}{\left(1-e^2\right)^4} \left(1+\frac{3}{2}e^2\right)\left(\frac{7}{4}\sin^2 i - 1\right) J_4 \end{aligned} \tag{5.3}$$

where J_{2e} is the effective J_2.

Thus, the effective J_2 (and effective J_2 variation) is simply a linear function of J_2 and J_4:

$$J_{2e} = J_2 + \frac{5}{2}\left(\frac{a_e}{a}\right)^2 \frac{1}{\left(1-e^2\right)^2} \left(1+\frac{3}{2}e^2\right)\left(\frac{7}{4}\sin^2 i - 1\right) J_4 \tag{5.4}$$

For LAGEOS, the expression for the secular variation in the longitude of node due to J_2 and J_4 (equations 5.1 and 5.2) is suitable for determining an effective J_2 since the LAGEOS orbit is very sensitive to secular changes in the longitude of node. For other

satellites, using expressions for the secular variation in argument of periapse, ω, or mean anomaly M, may be preferable if they are not suitably sensitive to the node rate.

The "true" effective J_3 (and true effective J_3 variation) is determined as follows: The long period variation in the eccentricity e, due to J_3 may be written

$$\frac{de}{dt} = -\frac{3}{2} n \left(\frac{a_e}{a}\right)^3 \frac{\sin i}{\left(1-e^2\right)^2}\left(1 - \frac{5}{4}\sin^2 i\right)\cos\omega J_3 \tag{5.5}$$

where a is the satellite semi-major axis, a_e is the semi-major axis of the central body's reference ellipsoid, i is the satellite inclination, n is the satellite mean motion, and ω is the satellite argument of periapse.

Likewise, the long period variation in eccentricity due to J_5 may be written

$$\frac{de}{dt} = -n\left(\frac{a_e}{a}\right)^5 \left(\frac{4+3e^2}{\left(1-e^2\right)^4}\right)\left(-\frac{15}{16}\sin i + \frac{105}{32}\sin^3 i - \frac{315}{128}\sin^5 i\right)\cos\omega J_5 \tag{5.6}$$

The expression for the long period variation in eccentricity due to both J_3 and J_5 may be equated with an expression for the long period variation in eccentricity due to an effective J_3:

$$-\frac{3}{2} n \left(\frac{a_e}{a}\right)^3 \frac{\sin i}{\left(1-e^2\right)^2}\left(1 - \frac{5}{4}\sin^2 i\right)\cos\omega J_{3e} = -\frac{3}{2} n \left(\frac{a_e}{a}\right)^3 \frac{\sin i}{\left(1-e^2\right)^2}\left(1 - \frac{5}{4}\sin^2 i\right)\cos\omega J_3$$

$$-n\left(\frac{a_e}{a}\right)^5 \left(\frac{4+3e^2}{\left(1-e^2\right)^4}\right)\left(-\frac{15}{16}\sin i + \frac{105}{32}\sin^3 i - \frac{315}{128}\sin^5 i\right)\cos\omega J_5 \tag{5.7}$$

where J_{3e} is the effective J_3.

Thus, the effective J_3 (and effective J_3 variation) for a particular satellite is simply a linear function of J_3 and J_5:

$$J_{3e} = J_3 + \frac{\left(\frac{a_e}{a}\right)^2 \left(\frac{4+3e^2}{\left(1-e^2\right)^2}\right)\left(-\frac{15}{16} + \frac{105}{32}\sin^2 i - \frac{315}{128}\sin^4 i\right)}{-\frac{3}{2}\left(1 - \frac{5}{4}\sin^2 i\right)} J_5 \tag{5.8}$$

Again, for LAGEOS, the expression for the long period variation in eccentricity due to J_3 and J_5 (equations 5.5 and 5.6) is suitable for determining an effective J_3 since the LAGEOS orbit is sensitive to long period changes in eccentricity. For other satellites, using expressions for the long period variation in a different element may be preferable if they are not suitably sensitive to variations in eccentricity.

Figure 5.32 shows the effective J_2 model deviation signal based on the actual J_2 and J_4 model deviation signals shown in Figures 4.5 and 4.7. It is shown with the actual J_2 model deviation signal for reference. Thus, the actual J_2 model deviation signal combined with the actual J_4 model deviation signal produces the same acceleration to LAGEOS as the effective J_2 model deviation signal combined with no J_4 model deviation signal (just a constant reference J_4).

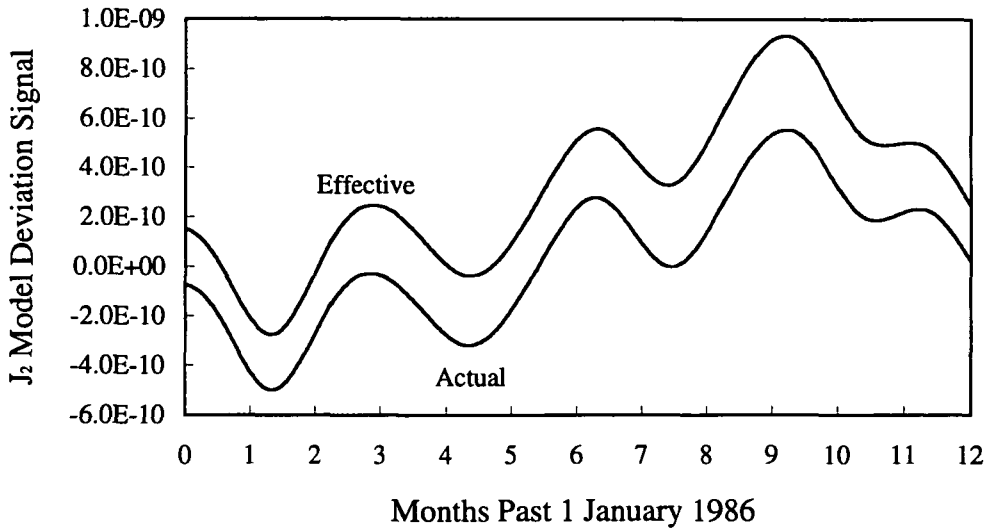

Figure 5.32. Effective and Actual J_2 Model Deviation Signals.

Figure 5.33 shows the effective J_3 model deviation signal based on the actual J_3 and J_5 model deviation signals shown in Figures 4.6 and 4.8. It is plotted with the actual J_3 model deviation signal for reference.

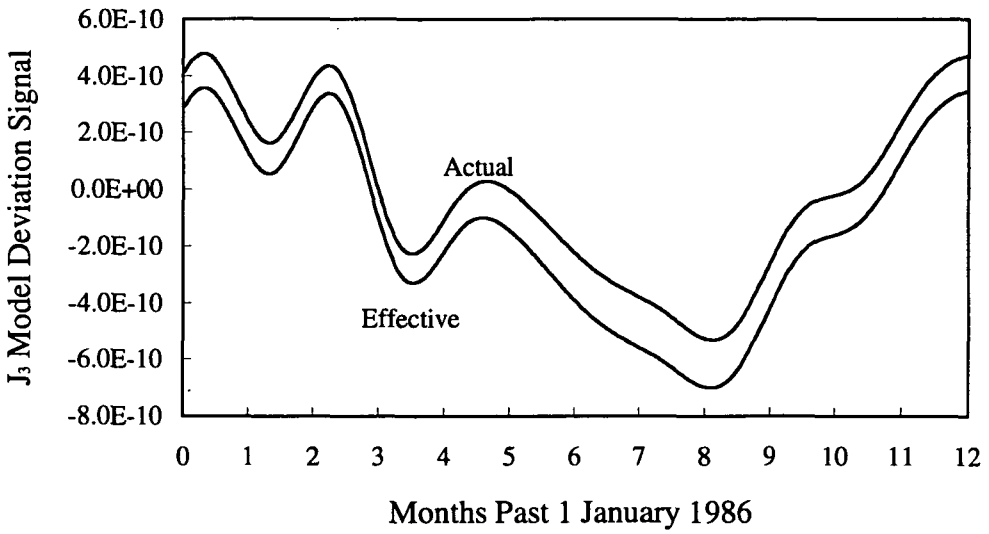

Figure 5.33. Effective and Actual J_3 Model Deviation Signals.

Thus, the comparisons of interest are between the true effective J_2 and J_3 variations and the estimated J_2 and J_3 variations. Continuing with the results for the previous boxcar case, Figures 5.34 and 5.35 show the true effective and estimated J_2 and the effective J_2 residuals respectively.

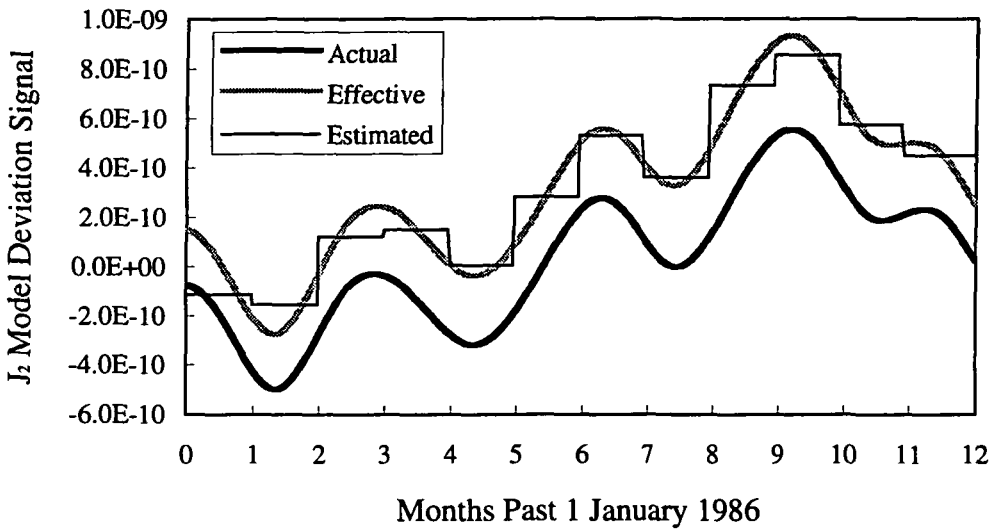

Figure 5.34. True Effective J_2 and Estimated J_2 Using Boxcars with J_4 and J_5 Model Deviation Signals Present but not Estimated.

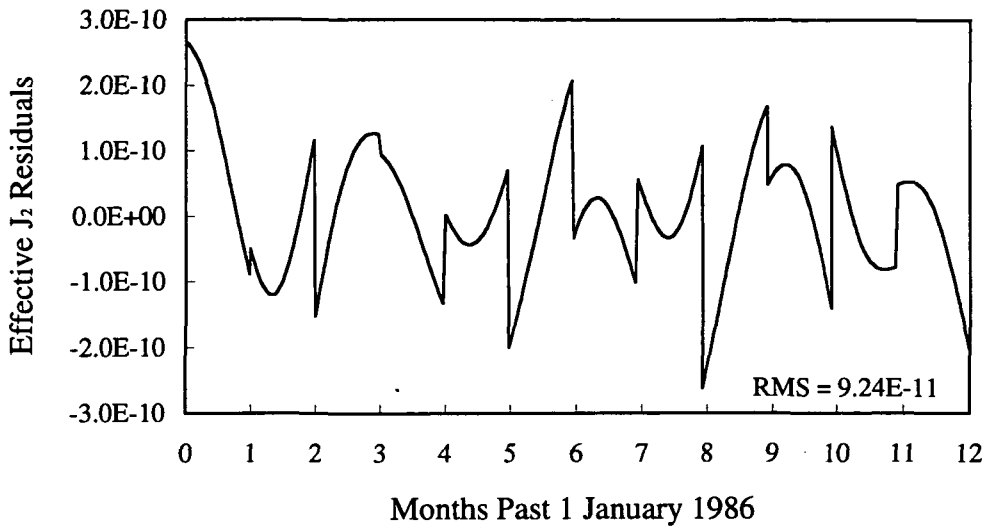

Figure 5.35. Effective J_2 Residuals Using Boxcars with J_4 and J_5 Model Deviation Signals Present but not Estimated.

Clearly, the boxcar estimates for J_2 agree quite well with the effective values as expected. Figures 5.36 and 5.37 show the true effective and estimated J_3 and the effective J_3 residuals respectively.

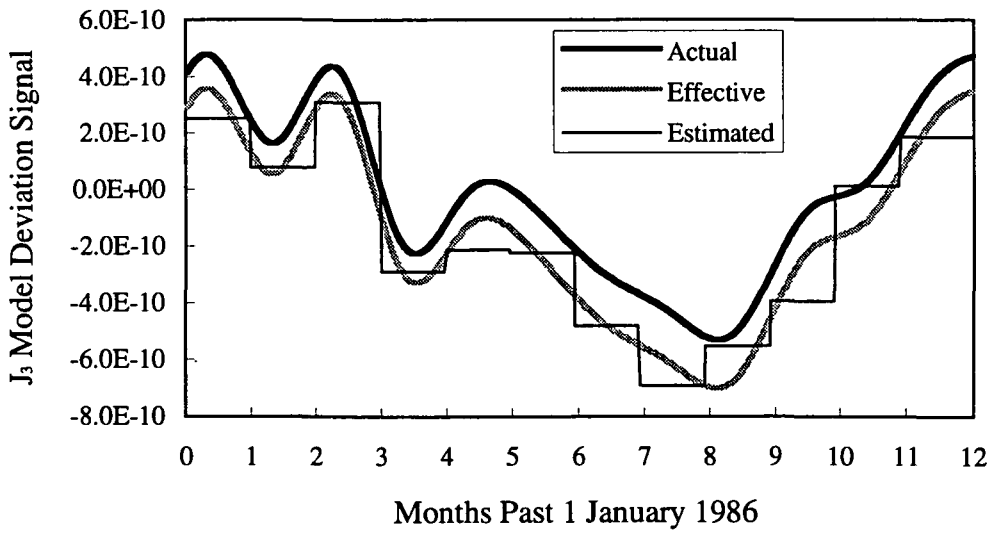

Figure 5.36. True Effective J_3 and Estimated J_3 Using Boxcars with J_4 and J_5 Model Deviation Signals Present but not Estimated.

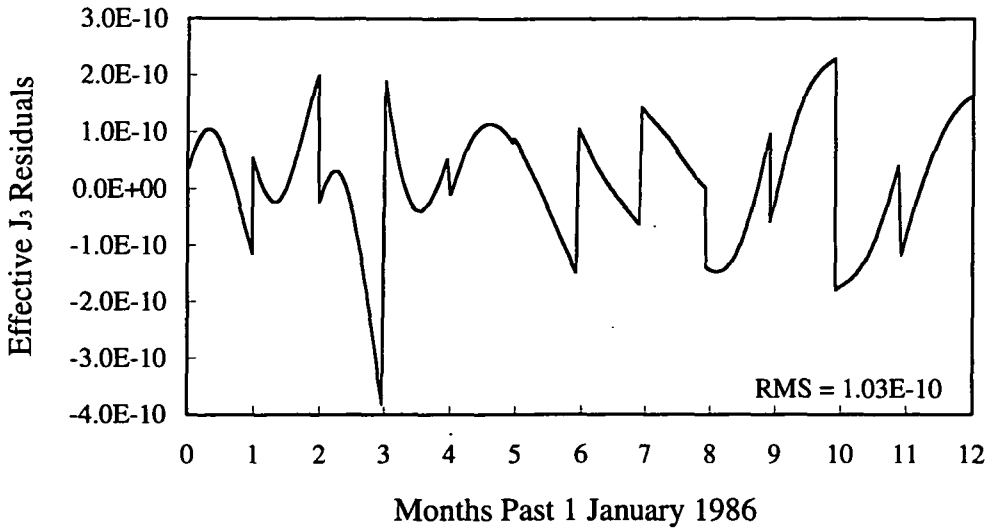

Figure 5.37. Effective J_3 Residuals Using Boxcars with J_4 and J_5 Model Deviation Signals Present but not Estimated.

The results for J_3 also agree quite well with the effective values. Table 5.6 summarizes the RMS statistics for the C_t, J_2, and J_3 residuals. The RMS statistics of the respective model deviation signals are also shown for reference.

Table 5.6. RMS for C_t, J_2, and J_3 Residuals Using Boxcars with J_4 and J_5 Model Deviation Signals Present but not Estimated.

Parameter	Model Deviation Signal RMS	Residual RMS Using Boxcars
C_t	1.37×10^{-12} m/s^2	2.24×10^{-13} m/s^2
J_2	2.85×10^{-10}	9.24×10^{-11}
J_3	3.10×10^{-10}	1.03×10^{-10}

Figures 5.38 to 5.40 show the RTN respective residuals.

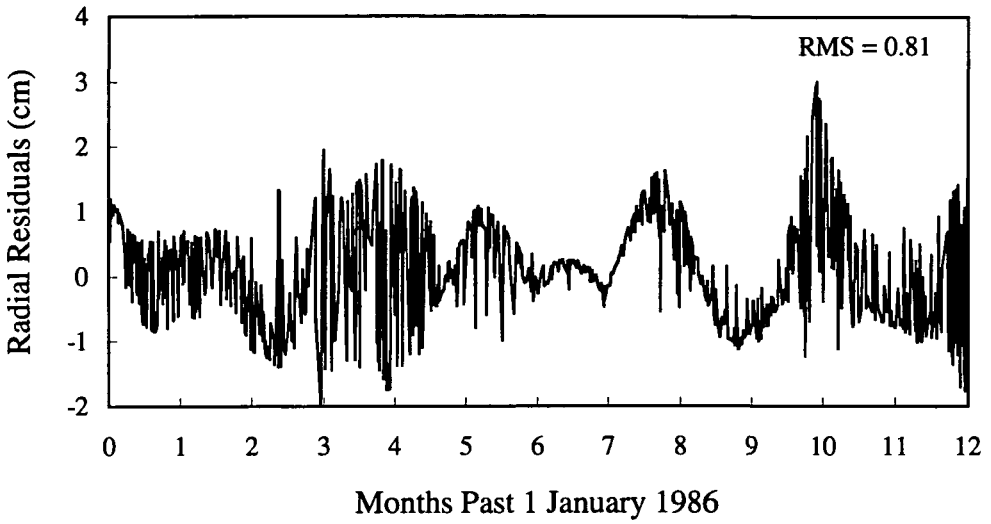

Figure 5.38. Radial Residuals Using Boxcars with J_4 and J_5 Model Deviation Signals Present but not Estimated.

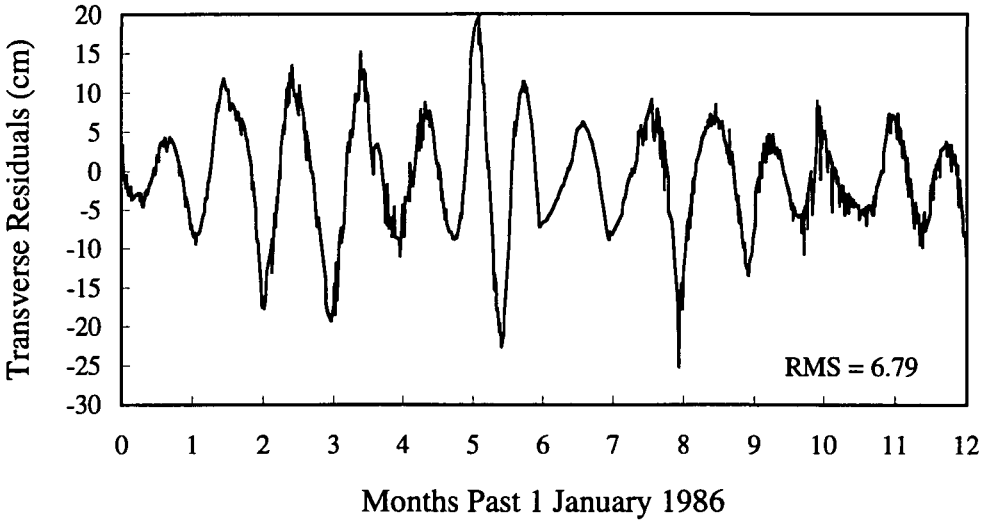

Figure 5.39. Transverse Residuals Using Boxcars with J_4 and J_5 Model Deviation Signals Present but not Estimated.

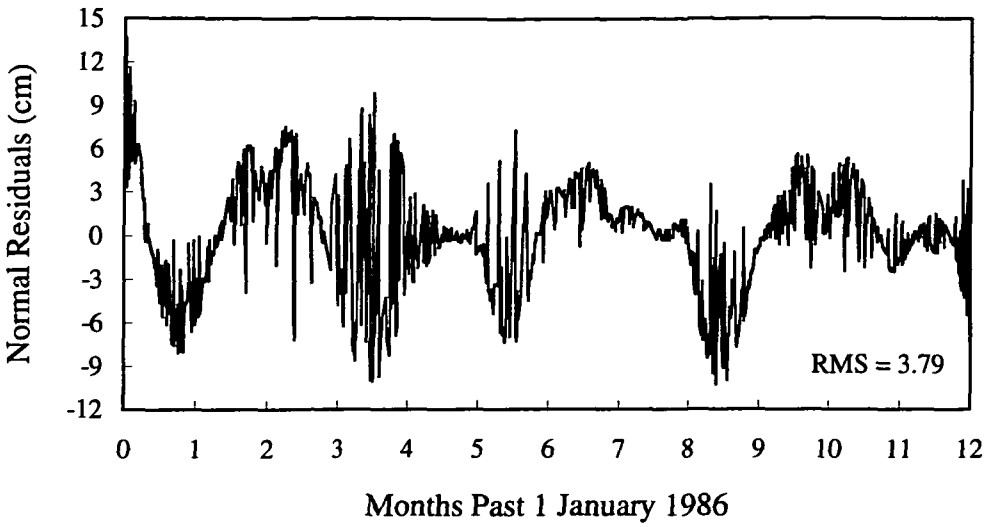

Figure 5.40. Normal Residuals Using Boxcars with J_4 and J_5 Model Deviation Signals Present but not Estimated.

The total 3-d position residuals are shown in Figure 5.41.

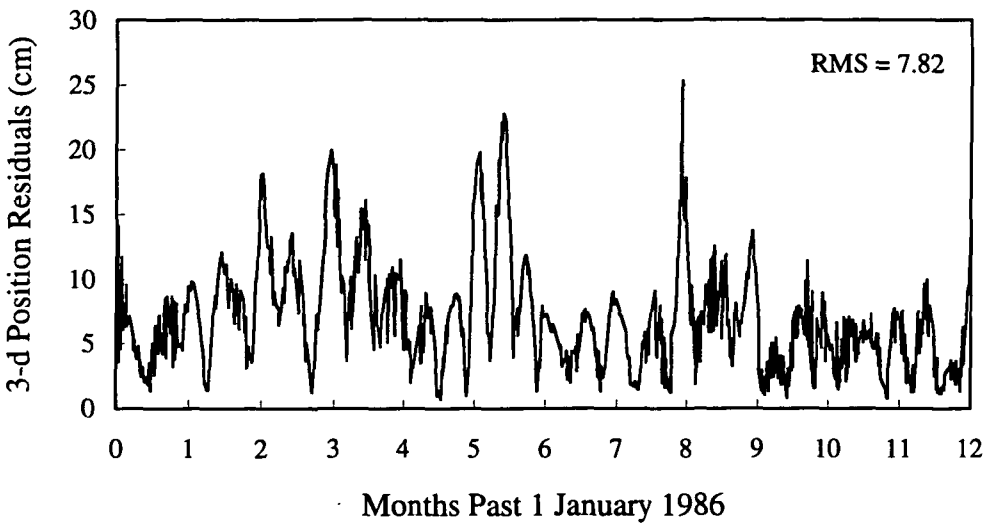

Figure 5.41. 3-d Position Residuals Using Boxcars with J_4 and J_5 Model Deviation Signals Present but not Estimated.

Figures C.1 through C.6 in Appendix C show the orbit residuals in terms of the Keplerian elements (semi-major axis a, eccentricity e, inclination i, argument of

periapse ω, longitude of ascending node Ω, and argument of latitude $\omega + f$, where f is true anomaly).

Finally, the range residuals are determined. Figure 5.42 shows the range residuals, and Table 5.7 summarizes the RMS statistics for the RTN, 3-d position, and range residuals for the boxcar mode.

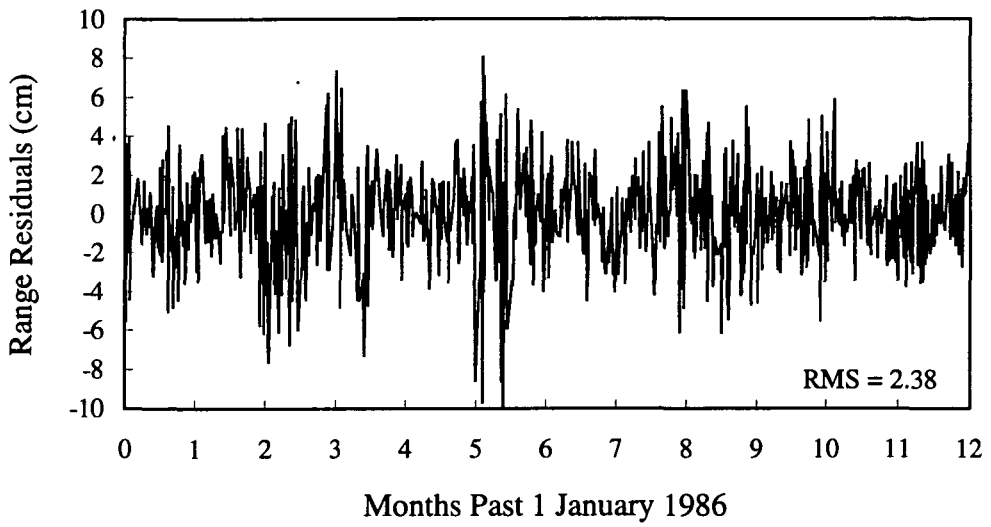

Figure 5.42. Range Residuals Using Boxcars with J_4 and J_5 Model Deviation Signals Present but not Estimated.

Table 5.7. RMS for RTN and Range Residuals Using Boxcars with J_4 and J_5 Model Deviation Signals Present but not Estimated.

Residual	RMS (cm)
Radial	0.81
Transverse	6.79
Normal	3.79
3-d Position	7.82
Range	2.38

These positional residuals and range residuals are slightly larger but statistically similar to those obtained from the boxcar solution where no J_4 or J_5 model deviation signal is present in the data (refer to Table 5.2). These slightly larger residuals indicate that the model deviation signals in the J_4 and J_5 parameters have not been completely removed. These residuals, along with the individual C_t, J_2, and J_3 parameter residuals, are now compared to the process noise SRIF solution.

5.3.2 Process Noise SRIF

The process noise SRIF is implemented with stochastic estimates made for C_t, J_2, and J_3, but not for J_4 or J_5 even though model deviation signals exist for J_4 and J_5. Stochastic estimates of each parameter, based on specific values of τ and σ, are made at every time that an observation exists. The values of τ and σ used for each parameter are the same as those that were used in the previous process noise case where no J_4 or J_5 model deviation signal is present in the data (refer to Table 5.3).

The stochastic estimates for the C_t, J_2, and J_3 temporal variations are compared to the true variations. Figure 5.43 shows the true C_t and the estimated C_t and Figure 5.44 shows the C_t residuals.

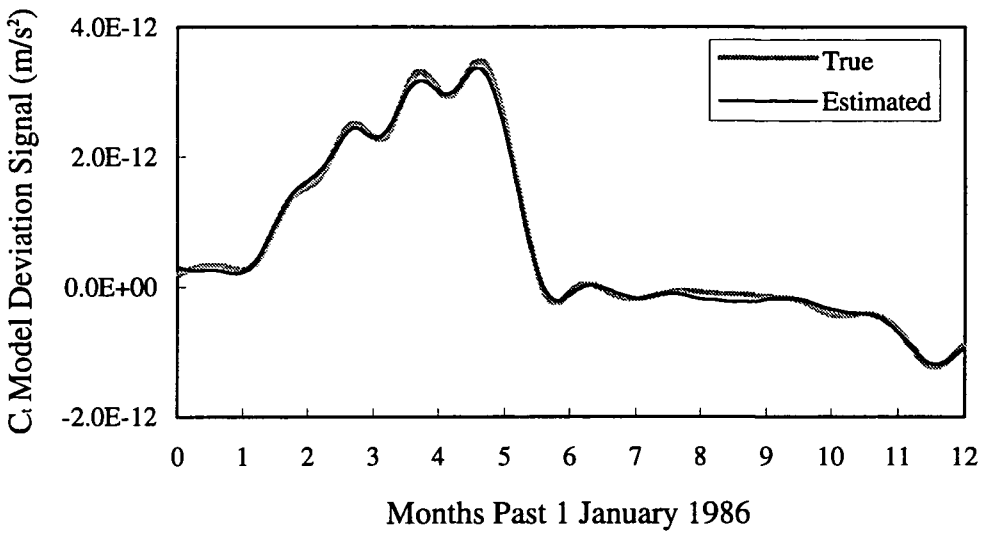

Figure 5.43. True C_t and Estimated C_t Using Process Noise with J_4 and J_5 Model Deviation Signals Present but not Estimated.

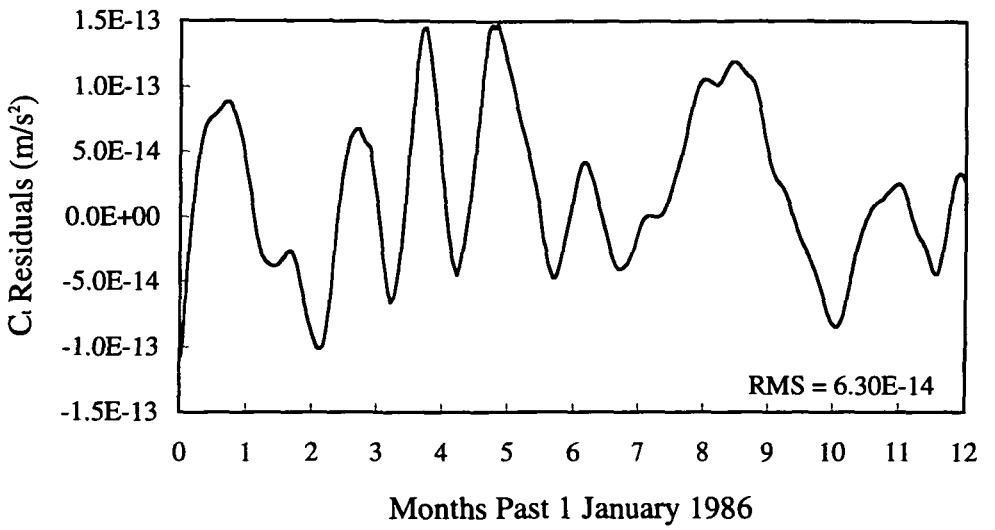

Figure 5.44. C_t Residuals Using Process Noise with J_4 and J_5 Model Deviation Signals Present but not Estimated.

The stochastic estimates of C_t appear just as superb as in the previous stochastic case where no J_4 or J_5 model deviation signals are present. Figures 5.45 and 5.46 show the true effective and estimated J_2 and the effective J_2 residuals respectively.

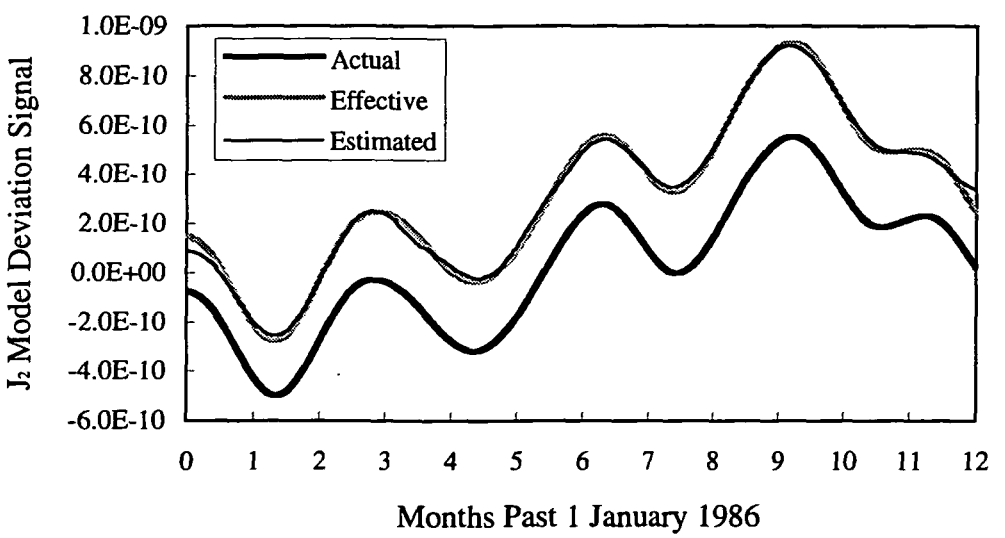

Figure 5.45. True Effective J_2 and Estimated J_2 Using Process Noise with J_4 and J_5 Model Deviation Signals Present but not Estimated.

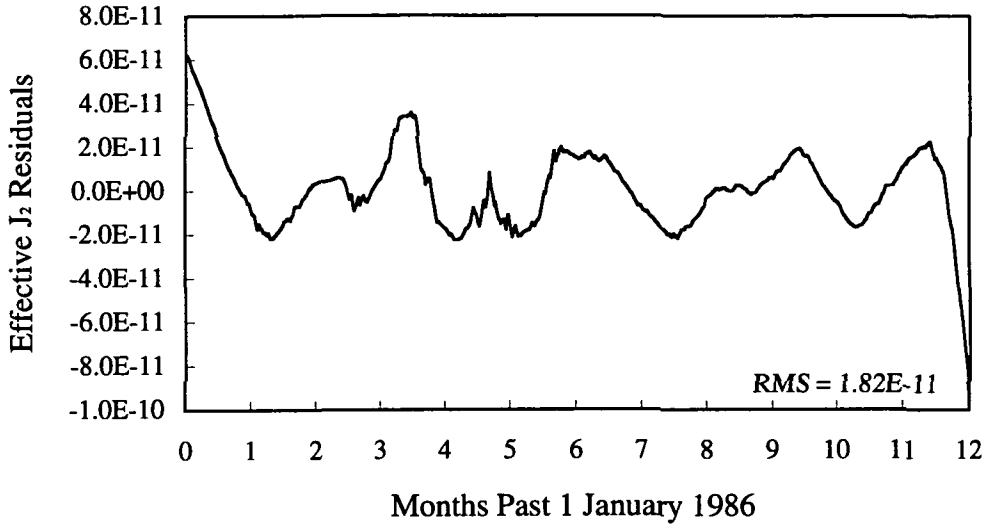

Figure 5.46. Effective J_2 Residuals Using Process Noise with J_4 and J_5 Model Deviation Signals Present but not Estimated.

Figures 5.46 and 5.48 show the true effective and estimated J_3 and the effective J_3 residuals respectively.

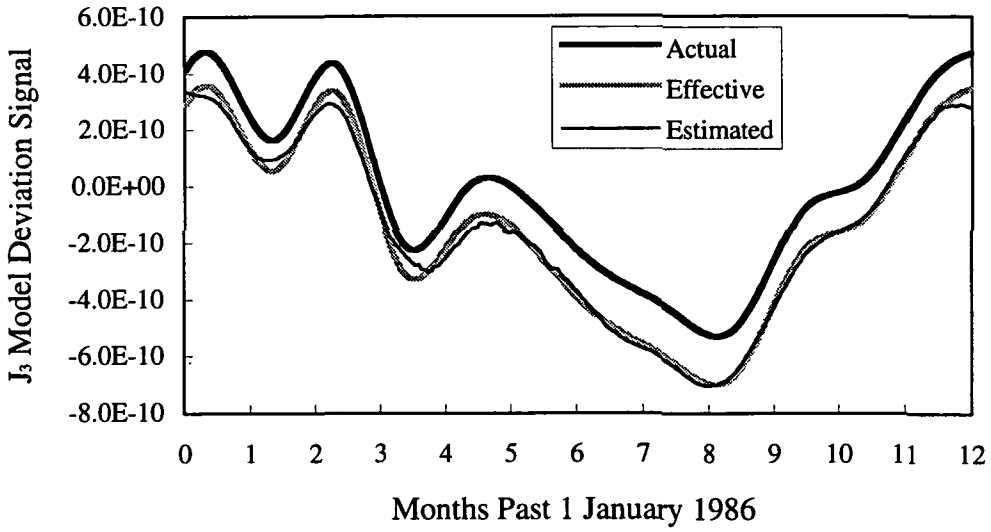

Figure 5.47. True Effective J_3 and Estimated J_3 Using Process Noise with J_4 and J_5 Model Deviation Signals Present but not Estimated.

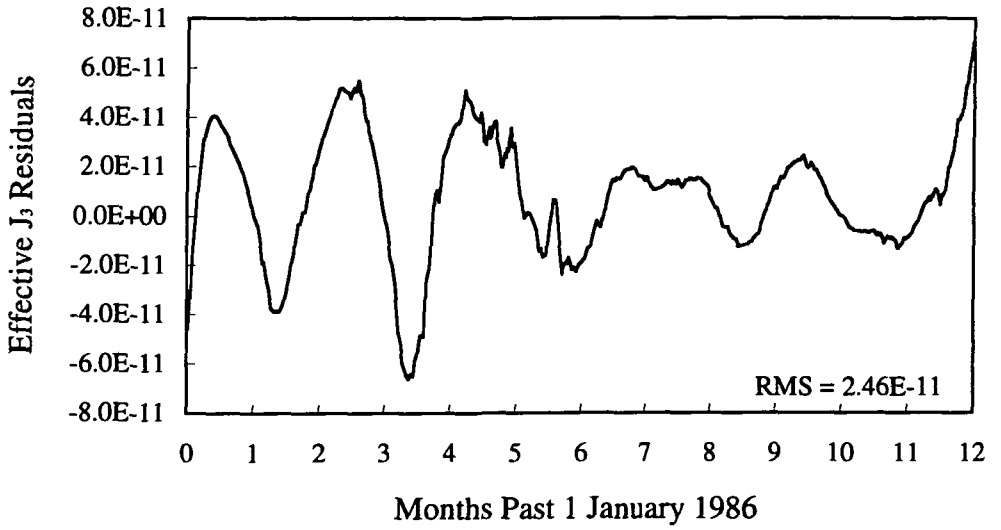

Figure 5.48. Effective J_3 Residuals Using Process Noise with J_4 and J_5 Model Deviation Signals Present but not Estimated.

Table 5.9 summarizes the RMS statistics for the C_t, J_2, and J_3 residuals using process noise. The respective residuals from the boxcar solution are shown for reference (from Table 5.6). The RMS statistics of the respective model deviation signals are also shown for reference.

Table 5.8. RMS for C_t, J_2, and J_3 Residuals Using Process Noise and Boxcars with J_4 and J_5 Model Deviation Signals Present but not Estimated.

Parameter	Model Deviation Signal RMS	Residual RMS Using Boxcars	Residual RMS Using Process Noise
C_t	1.37×10^{-12} m/s^2	2.24×10^{-13} m/s^2	6.30×10^{-14} m/s^2
J_2	2.85×10^{-10}	9.24×10^{-11}	1.82×10^{-11}
J_3	3.10×10^{-10}	1.03×10^{-10}	2.46×10^{-11}

Again, the process noise residuals for C_t, J_2, and J_3 are noticeably improved relative to the respective boxcar residuals.

Next, the RTN residuals are shown in Figures 5.49 to 5.51. The 3-d position residuals are shown in Figure 5.52.

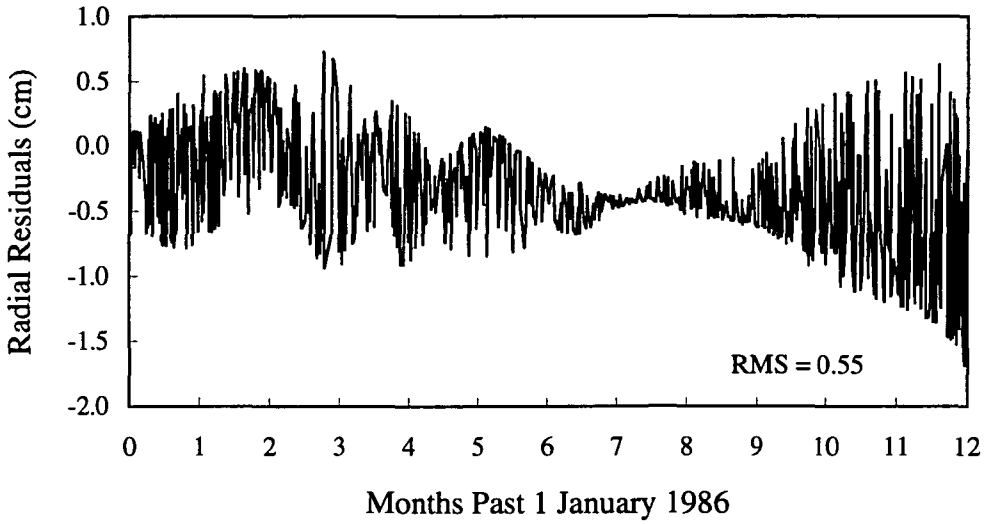

Figure 5.49. Radial Residuals Using Process Noise with J_4 and J_5 Model Deviation Signals Present but not Estimated.

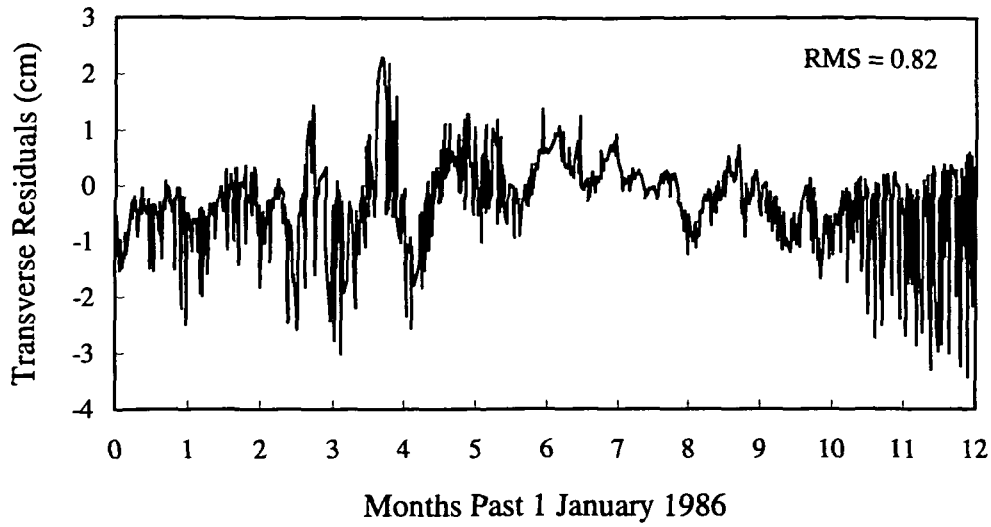

Figure 5.50. Transverse Residuals Using Process Noise with J_4 and J_5 Model Deviation Signals Present but not Estimated.

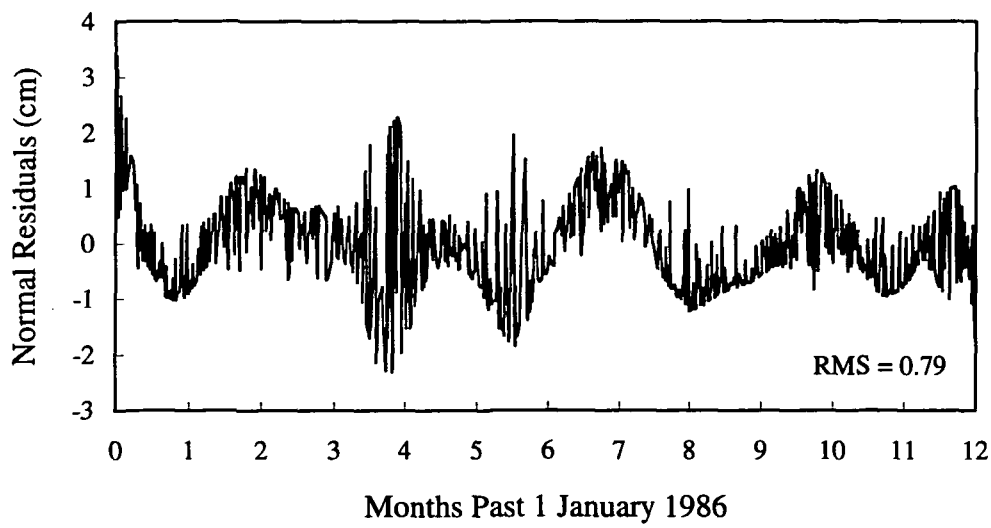

Figure 5.51. Normal Residuals Using Process Noise with J_4 and J_5 Model Deviation Signals Present but not Estimated.

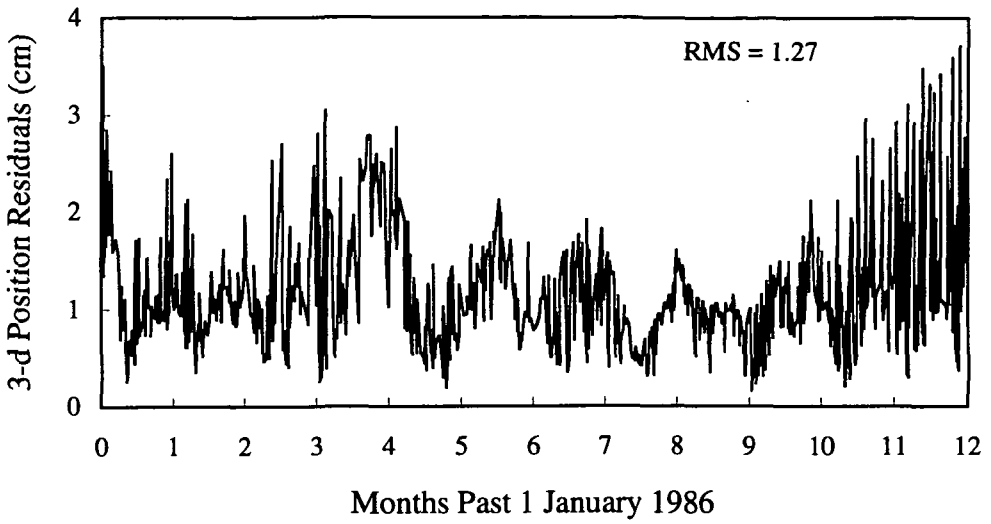

Figure 5.52. 3-d Position Residuals Using Process Noise with J_4 and J_5 Model Deviation Signals Present but not Estimated.

Figures D.1 through D.6 in Appendix D show the orbit residuals in terms of the Keplerian elements (semi-major axis a, eccentricity e, inclination i, argument of periapse ω, longitude of ascending node Ω, and argument of latitude $\omega + f$, where f is true anomaly).

Figure 5.53 shows the range residuals, and Table 5.10 summarizes the RMS statistics for the RTN, 3-d position, and range residuals (with comparison to the respective boxcar statistics from Table 5.7 for reference).

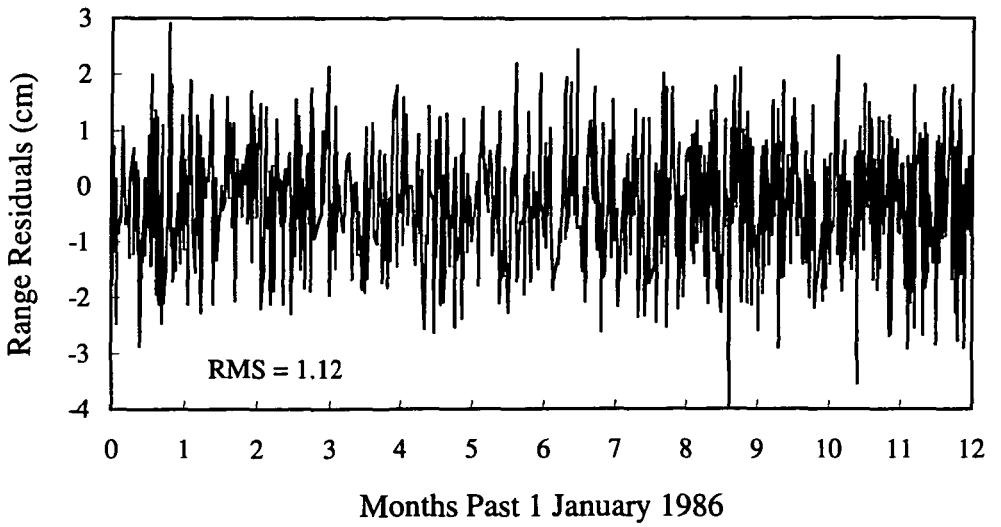

Figure 5.53. Range Residuals Using Process Noise with J_4 and J_5 Model Deviation Signals Present but not Estimated.

Table 5.9. RMS for RTN and Range Residuals Using Process Noise and Boxcars with J_4 and J_5 Model Deviation Signals Present but not Estimated.

Residual	RMS Using Boxcars (cm)	RMS Using Process Noise (cm)
Radial	0.81	0.55
Transverse	6.79	0.82
Normal	3.79	0.79
3-d Position	7.82	1.27
Range	2.38	1.12

Again, relative to the process noise results shown in Table 5.5 where no J_4 or J_5 model deviation signal exists in the data, these process noise results show slightly larger residuals. These slightly larger residuals indicate that the model deviation signals in the

J_4 and J_5 parameters have not been completely removed. It is also clear that these process noise residuals are much better than the corresponding boxcar residuals.

Figures 5.54 to 5.58 show the RTN, 3-d position, and range residuals from both the standard boxcar SRIF and the process noise SRIF solutions side by side on the same scale for visual comparison.

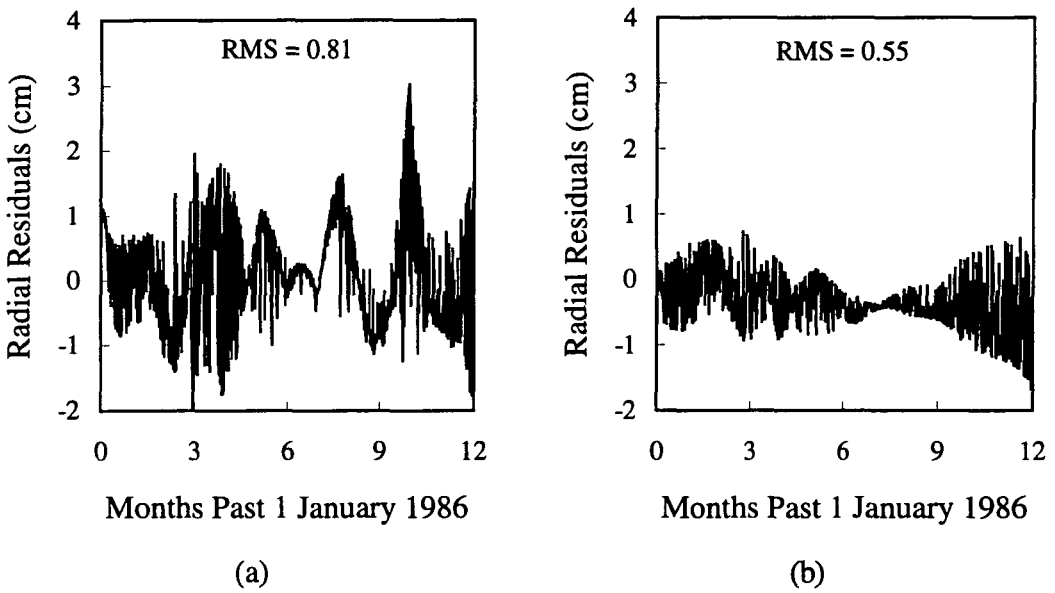

Figure 5.54. Radial Residuals Using Boxcars (a) and Process Noise (b) with J_4 and J_5 Model Deviation Signals Present but not Estimated.

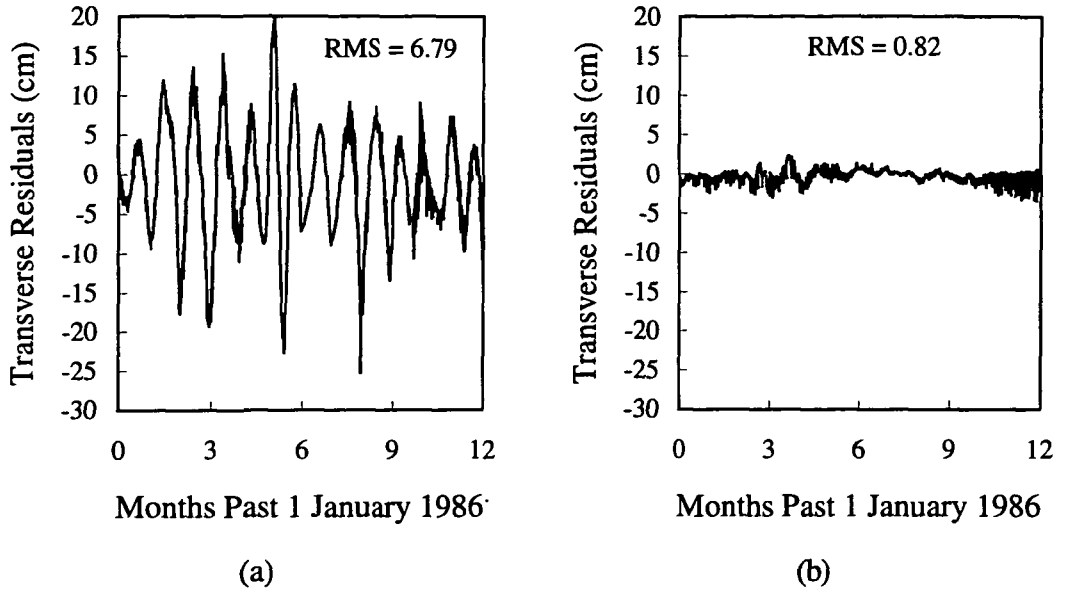

Figure 5.55. Transverse Residuals Using Boxcars (a) and Process Noise (b) with J_4 and J_5 Model Deviation Signals Present but not Estimated.

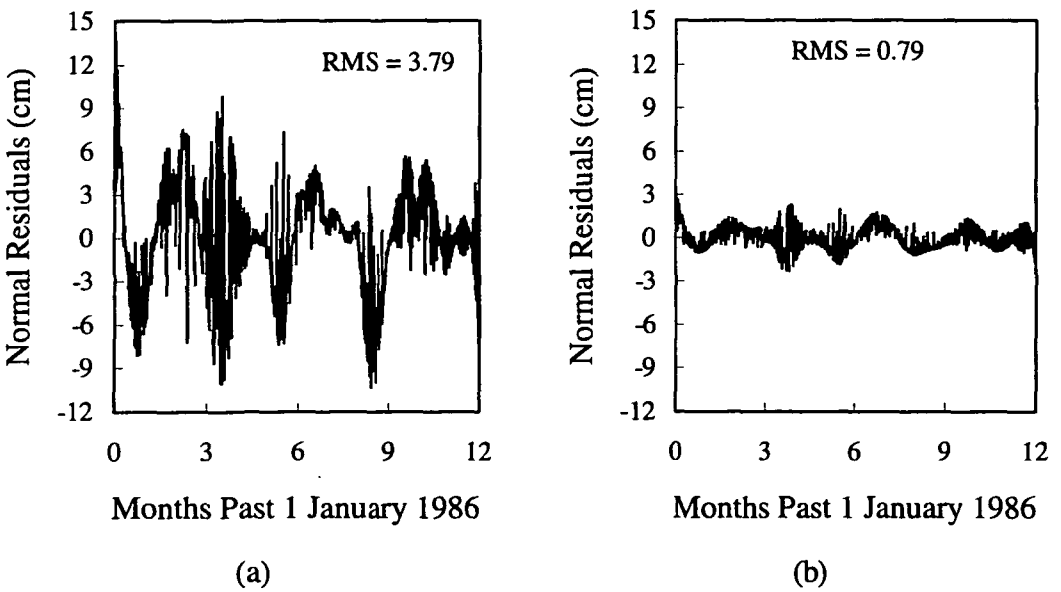

Figure 5.56. Normal Residuals Using Boxcars (a) and Process Noise (b) with J_4 and J_5 Model Deviation Signals Present but not Estimated.

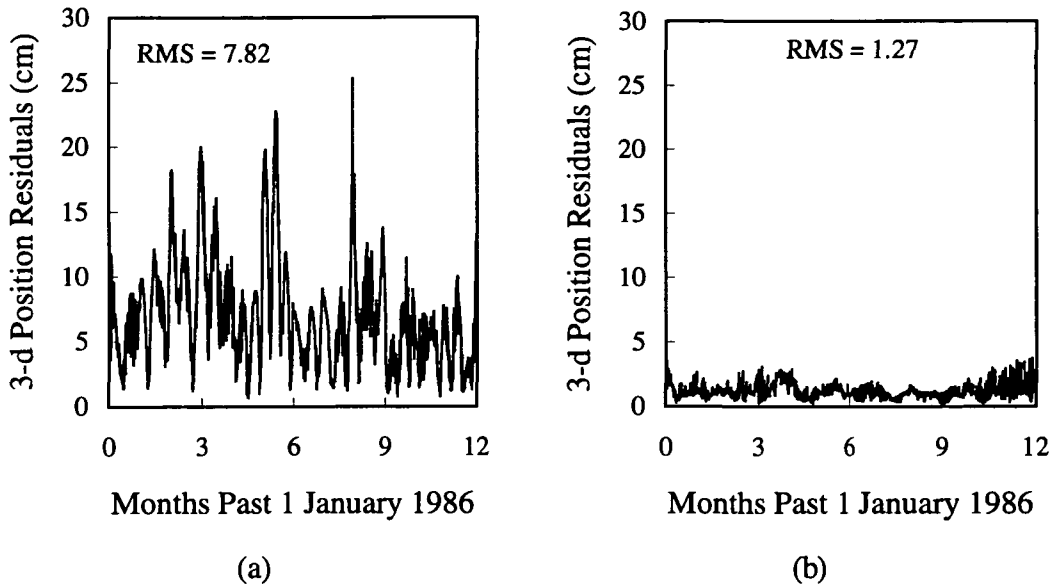

Figure 5.57. 3-d Position Residuals Using Boxcars (a) and Process Noise (b) with J_4 and J_5 Model Deviation Signals Present but not Estimated.

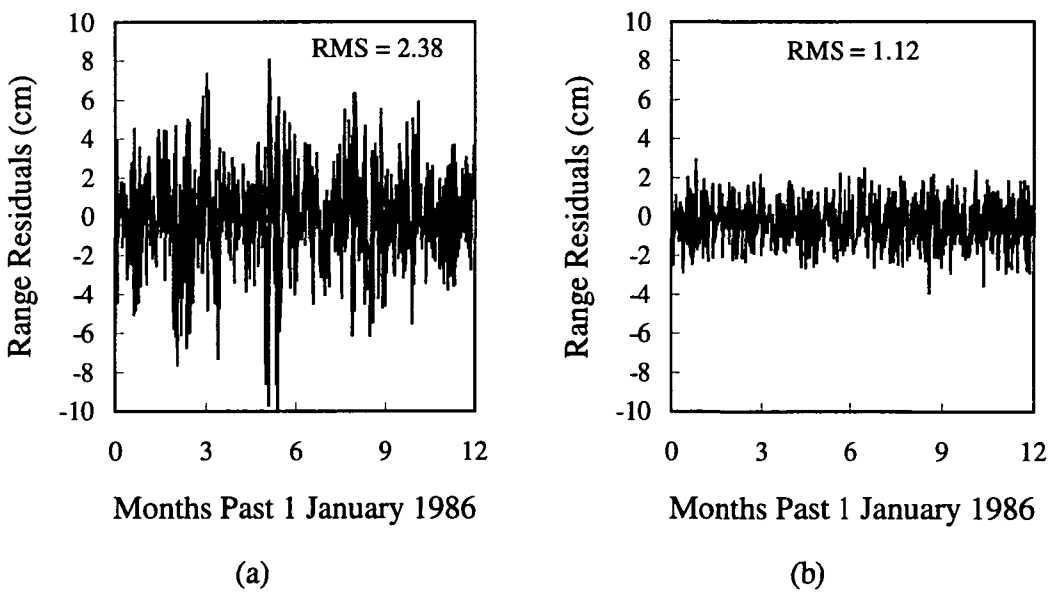

Figure 5.58. Range Residuals Using Boxcars (a) and Process Noise (b) with J_4 and J_5 Model Deviation Signals Present but not Estimated.

Again, the stochastic filtering method produces a temporal solution for C_t, effective J_2, and effective J_3 which is more accurate than the standard boxcar solution. The RMS for the C_t, J_2, and J_3 residuals are reduced to approximately 25% of the respective residuals using the standard boxcar method (a 75% improvement). Similarly, by using the stochastic filtering method the total 3-d positional residual is reduced to approximately 15% of the 3-d positional residual resulting from the standard boxcar filtering method (an 85% improvement). Once again, the range residuals are reduced by about 50%. The improvement in the orbit accuracy and temporal resolution of the model deviation signals is clearly noticeable when using stochastic process noise parameters to estimate the model deviation signals.

5.4 Three Year Arc: C_t, J_2, and J_3 Model Deviation Signals

A simulated three year data arc with model deviation signals present in C_t, J_2, and J_3 and no model deviation signals present in J_4 or J_5 is processed. The three year arc is only processed using the stochastic process noise filtering method. A non-stochastic solution for the three year data arc requires substantially more time computationally due to the significantly larger satellite state, and is not determined in this study. Thus, the three year stochastic solution is presented alone without comparison to a standard non-stochastic solution. The three year data arc is processed with a single estimate made for the satellite state ($\mathbf{r}$ and $\dot{\mathbf{r}}$), and no correction made for μ, J_4, or J_5 (since no model deviation signal is present in the μ, J_4, or J_5 parameters, no correction is needed). For this three year process noise SRIF solution, two preliminary corrections are made to the satellite state ($\mathbf{r}$ and $\dot{\mathbf{r}}$) while fixing all other parameters. This gives a reference orbit that is sufficiently close to the true orbit over the entire three year arc, thus minimizing linearization errors. A third and final iteration is performed

using the process noise mode once these preliminary, non-stochastic corrections are made to the initial conditions of the satellite.

5.4.1 True Model Deviation Signals for the Three Year Arc

As detailed in section 4.4, specific model deviation signals are introduced into the model parameters as the simulated SLR measurements are generated. For the three year arc, model deviation signals are introduced into the C_t, J_2, and J_3 parameters. No model deviation signal is present in J_4 or J_5 for the three year arc. The model deviation signals for the three year arc are derived in the same manner that those from the one year arc are derived (refer to section 4.4). The only difference is that the model deviation signals for the three year arc are based on C_t, J_2, and J_3 estimates from the three year period from January 1, 1986 to December 31, 1988. The true model deviation signals introduced into the three year simulated data arc are now detailed.

5.4.1.1 Drag Model Deviation Signal

For the along track drag parameter C_t, the model deviation signal shown in Figure 5.59 is added to the nominal C_t value of -3.5 picometer/s^2 during the simulation of the observations.

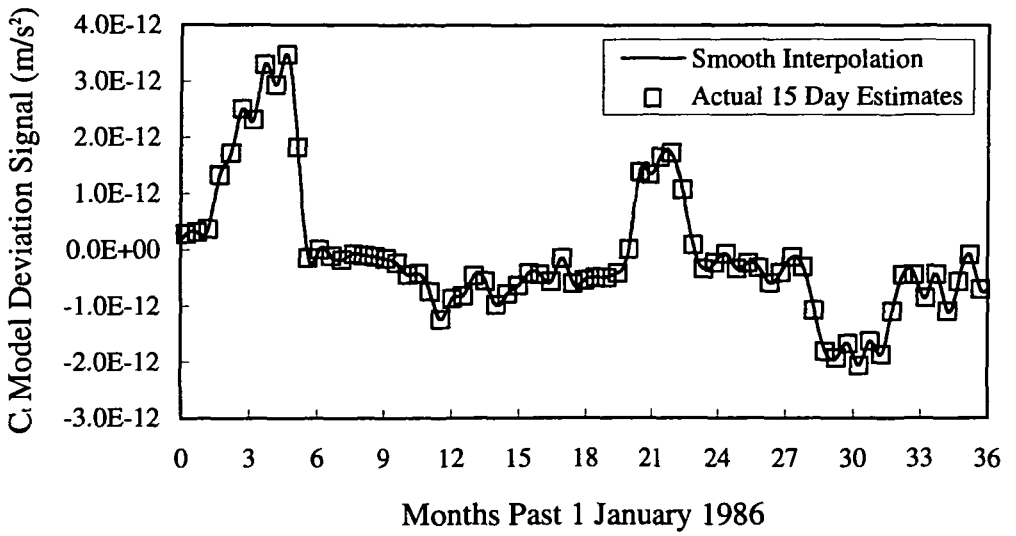

Figure 5.59. True Model Deviation Signal for the C_t Parameter Based on Current Best Estimates.

This model deviation signal is again taken from *Tapley et al.* [1993] which gives 15 day estimates for the observed along track drag for LAGEOS over a 14 year period. The 15 day estimates falling between January 1, 1986 and December 31, 1988 are also shown in Figure 5.59 for reference. This three years of interpolated along track drag variation, with the average value subtracted out, is what is shown in Figure 5.59.

5.4.1.2 J_2 and J_3 Model Deviation Signal

As was the case for the one year arc, the model deviation signal for the J_2 coefficient consists of a secular and nonsecular term. The model deviation signal for the J_3 coefficient is purely nonsecular. The nonsecular part of the J_2 and J_3 model deviation signal is again taken from *Nerem et al.* [1993] which gives monthly estimates for the nonsecular variations of J_2 and J_3 over the time period from 1980 to 1989. Their monthly estimates for the nonsecular variations from January, 1986 to December, 1988 are interpolated with a natural cubic spline. This three years of interpolated J_2 and J_3 nonsecular variation, with the secular variation for J_2 added back, is what is shown in

Figures 5.60 and 5.61 with the monthly estimates they are based on shown for reference (unnormalized). This is the total model deviation signal (total temporal variation) added to the nominal JGM-2 J_2 and J_3 values.

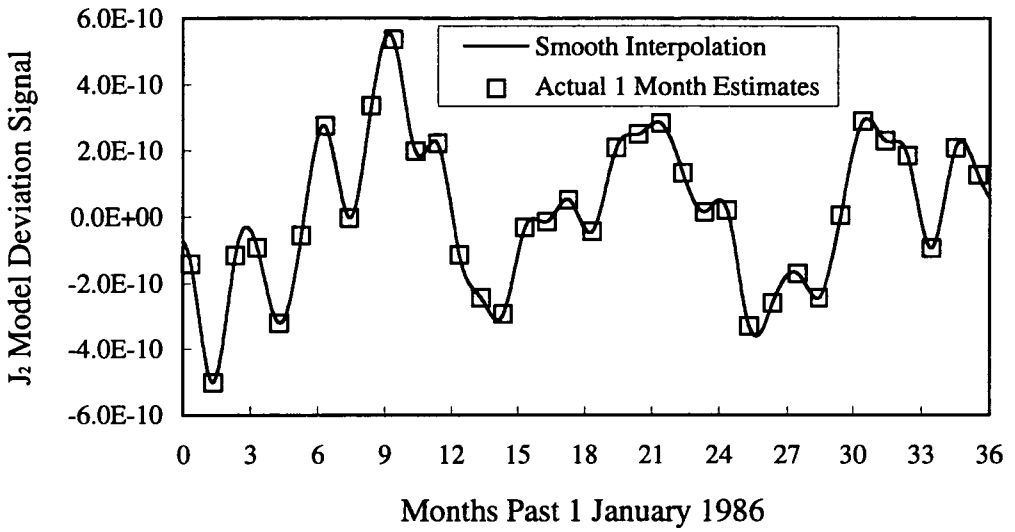

Figure 5.60. True Model Deviation Signal for the J_2 Parameter Based on Current Best Estimates.

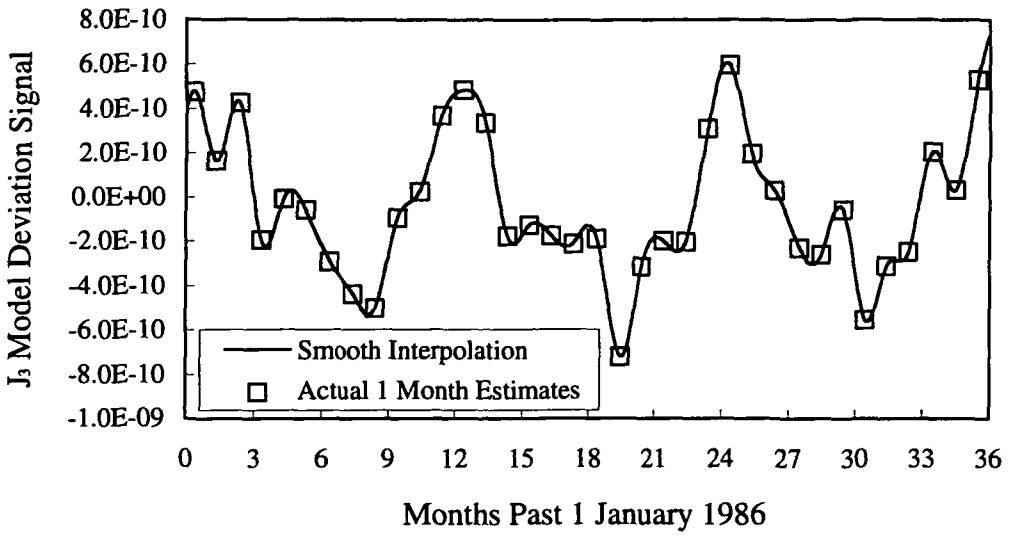

Figure 5.61. True Model Deviation Signal for the J_3 Parameter Based on Current Best Estimates.

5.4.2 Process Noise SRIF

The process noise SRIF is implemented with stochastic estimates made for C_t, J_2, and J_3. Stochastic estimates of each parameter are made at every time that an observation exists during the three year arc. The values of τ and σ used for each parameter are the same as those that were used for the one year arc stochastic solutions (refer to Table 5.3).

The stochastic estimates for the C_t, J_2, and J_3 temporal variations are compared to the truth. Figure 5.62 shows the true C_t and the estimated C_t and Figure 5.63 shows the C_t residuals, or the true C_t minus the estimated C_t.

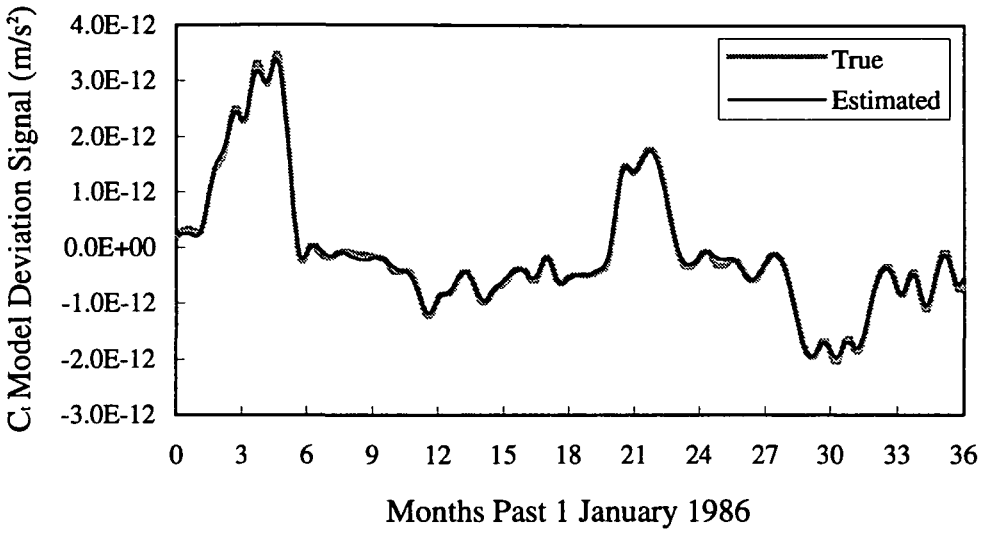

Figure 5.62. True C_t and Estimated C_t Using Process Noise.

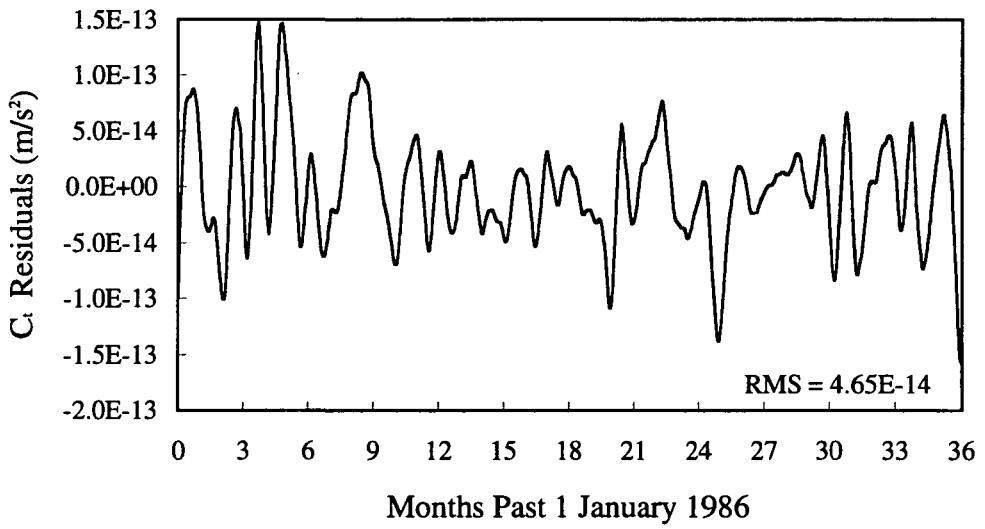

Figure 5.63. C_t Residuals Using Process Noise.

The three year stochastic estimate of C_t appears excellent. No noticeable degradation in the solution is observed relative to the previous stochastic estimate for C_t from the one year arc. Figures 5.64 and 5.65 show the true J_2 and estimated J_2 and the J_2 residuals respectively.

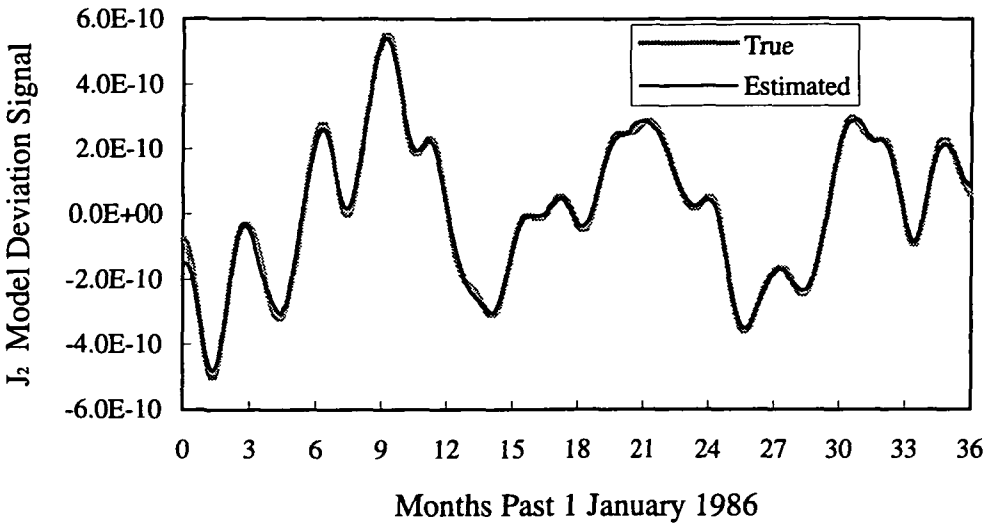

Figure 5.64. True J_2 and Estimated J_2 Using Process Noise.

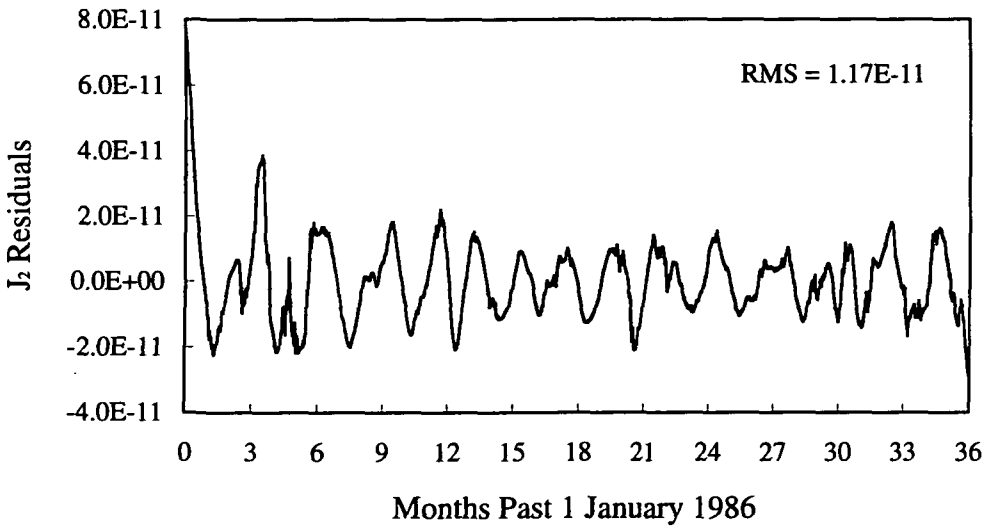

Figure 5.65. J_2 Residuals Using Process Noise.

Likewise, Figures 5.66 and 5.67 show the true J_3 and estimated J_3 and the J_3 residuals respectively.

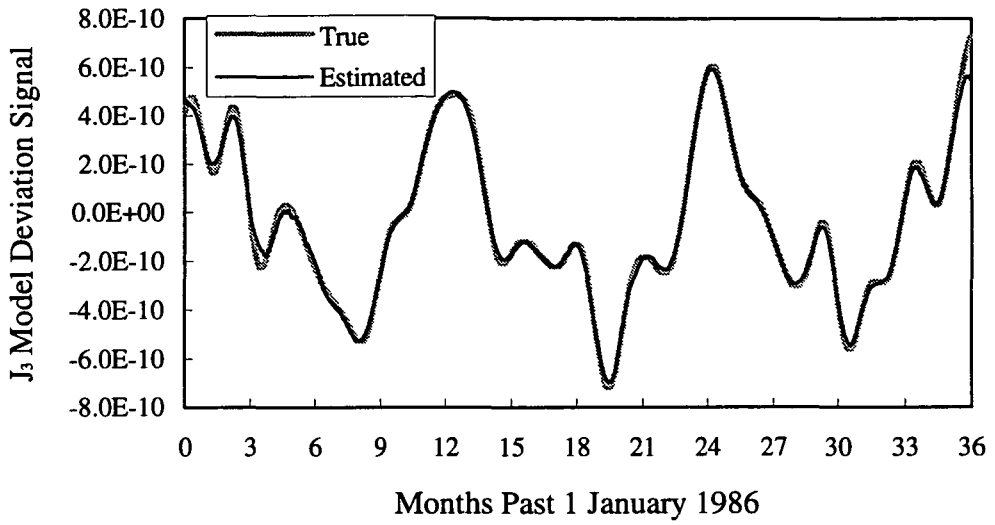

Figure 5.66. True J_3 and Estimated J_3 Using Process Noise.

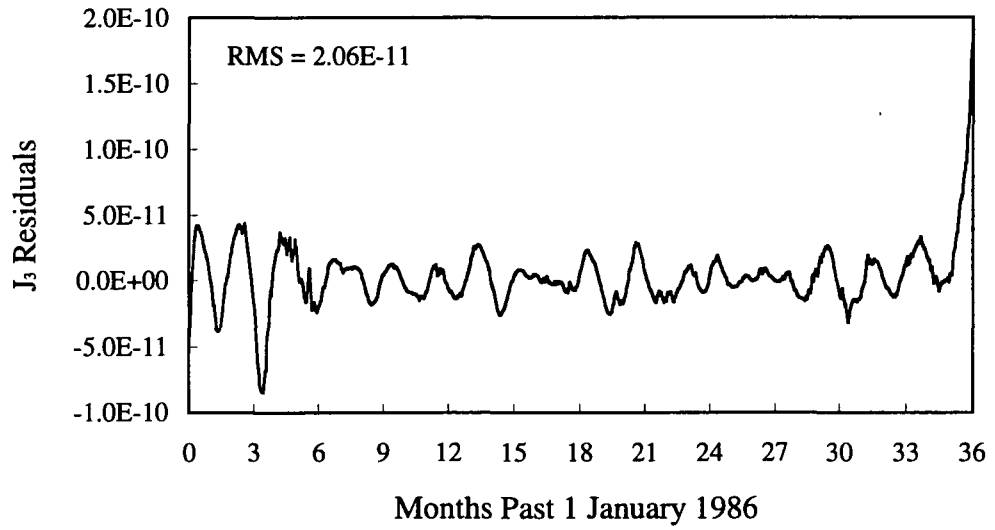

Figure 5.67. J_3 Residuals Using Process Noise.

The stochastic estimates of J_2 and J_3 are also excellent. Relative to the previous stochastic estimates for J_2 and J_3 from the one year arc, the three year stochastic estimates appear to have similar temporal resolution and accuracy. Table 5.10

summarizes the RMS statistics for the C_t, J_2, and J_3 residuals. The RMS statistics of the respective model deviation signals are shown for reference.

Table 5.10. RMS for C_t, J_2, and J_3 Residuals Using Process Noise.

Parameter	Model Deviation Signal RMS	Residual RMS Using Process Noise
C_t	1.10×10^{-12} m/s^2	4.65×10^{-14} m/s^2
J_2	2.22×10^{-10}	1.17×10^{-11}
J_3	3.14×10^{-10}	2.06×10^{-11}

The three year process noise residuals for C_t, J_2, and J_3 are slightly improved relative to the respective one year process noise residuals (refer to Table 5.4).

Next, the RTN positional residuals are shown in Figures 5.68 to 5.70. The total RTN, or 3-d position residuals are shown in Figure 5.71. Figures 5.68 to 5.71 indicate the presence of numerical integration errors at the end of the three year arc. This can be dealt with by using integration methods which minimize the accumulation of this type of error.

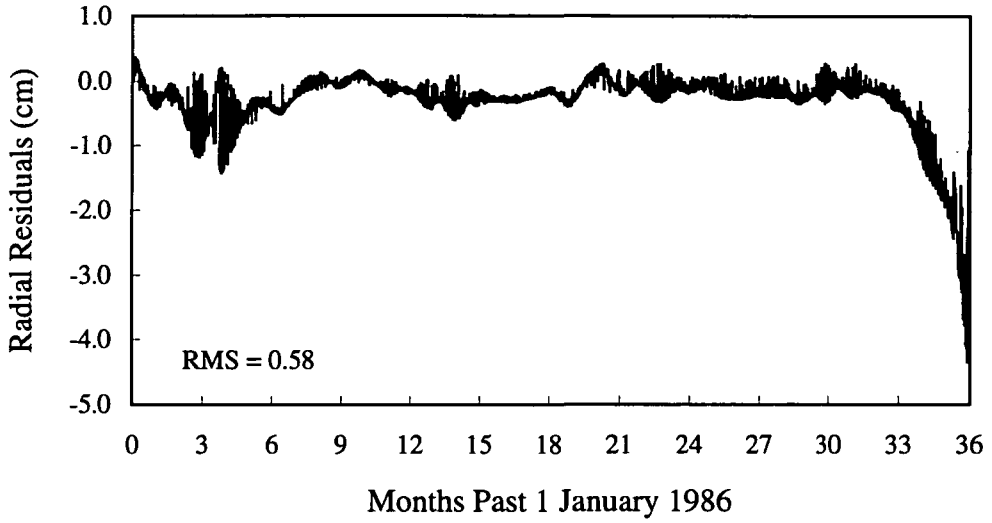

Figure 5.68. Radial Residuals Using Process Noise.

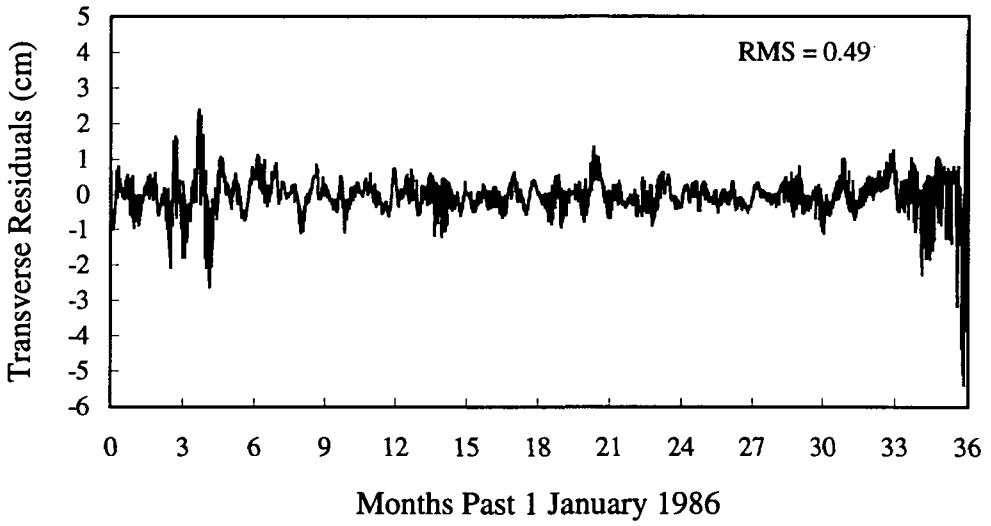

Figure 5.69. Transverse Residuals Using Process Noise.

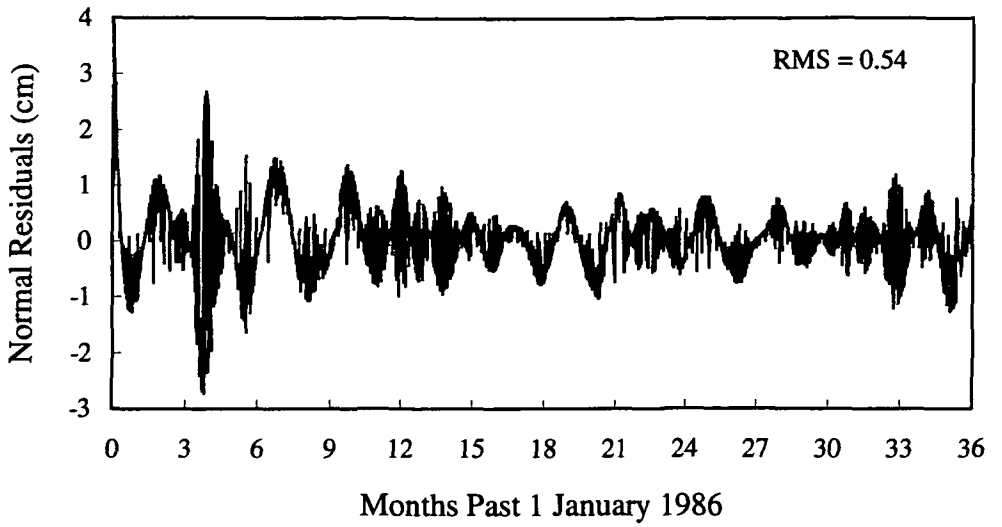

Figure 5.70. Normal Residuals Using Process Noise.

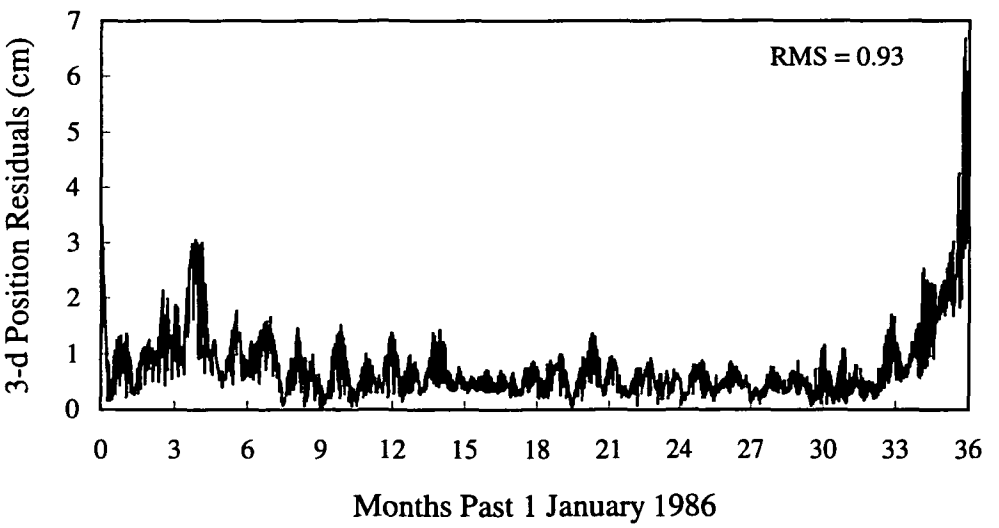

Figure 5.71. 3-d Position Residuals Using Process Noise.

Figure 5.72 shows the range residuals, and Table 5.11 summarizes the RMS statistics for the RTN, 3-d position, and range residuals. Again, since 1 cm RMS noise is present in the simulated observations, it is expected that the RMS of the range residuals will approach 1 cm as the estimated solution approaches the truth.

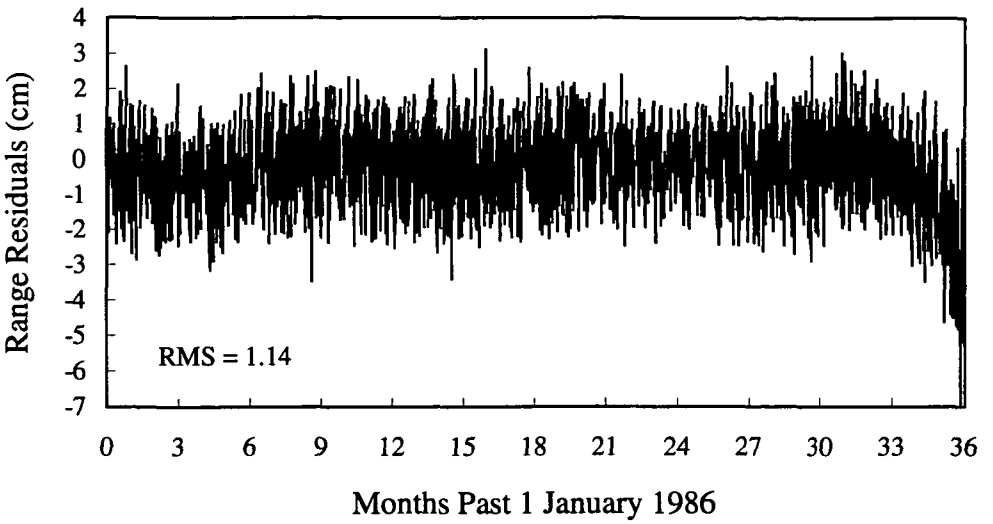

Figure 5.72. Range Residuals Using Process Noise.

Table 5.11. RMS for RTN and Range Residuals Using Process Noise.

Residual	RMS Using Process Noise (cm)
Radial	0.58
Transverse	0.49
Normal	0.54
3-d Position	0.93
Range	1.14

The stochastic filtering method produces a three year temporal solution for C_t, J_2, and J_3 which is comparable to the one year stochastic solution. The RMS for the stochastic C_t, J_2, and J_3 residuals are slightly less for the three year arc than the one year

arc. The orbit position and range residuals are similar for both the three year and one year stochastic solutions as well (refer to Table 5.5). Reducing the errors associated with numerically integrating the orbit for three years may lead to improved orbit position and range residuals for the three year solution.

CHAPTER 6

CONCLUSIONS

6.1 Summary and Discussion

The feasibility of determining the temporal variations in geodynamically interesting parameters, such as the low degree coefficients of the Earth's gravity field, through the use of LAGEOS SLR tracking data has been analyzed. A simulation that included realistic variations in J_2 and J_3, and also the LAGEOS along track drag effect, was carried out to evaluate the capability of a stochastic filter to track these variations using the relatively sparse SLR data.

Various conclusions can be drawn in assessing the results of this analysis. Overall, the filtering results have shown that a stochastic filter can accurately track the temporal variations in LAGEOS along track drag, as well as in the J_2 and J_3 gravity field coefficients. And the accuracy of these estimates is such that the expected variations in these parameters are readily observable.

In addition, these (stochastic) filtering results are found to provide much better accuracy and much better temporal resolution as compared to the conventional (boxcar) estimation procedure. These improvements are with respect to results obtained from a standard, non-stochastic filter making semi-monthly estimates for C_t and monthly estimates for J_2 and J_3. Similarly, the positional accuracy of the orbit is improved by using the process noise filter. These improvements are observed both when estimating the parameters with and without J_4 and J_5 variations present. Generally, by using the process noise filtering approach, the residual RMS errors for the variations in C_t, J_2, and J_3 are reduced to approximately 25% of the residual RMS errors obtained using the

standard non-stochastic filtering approach. This demonstrates that it is potentially feasible to use process noise filtering techniques to improve the temporal resolutions and accuracies of LAGEOS along track drag variations and second and third degree zonal harmonic coefficient variations. It is also feasible to improve the orbit positional accuracy by using multiple stochastic parameters which estimate specific geophysical parameters as opposed to simply estimating additional accelerations with these parameters. By using the process noise filter, the residual RMS errors for the total 3-d orbit position are reduced to approximately 15% of the residual RMS errors obtained using the standard filter. Thus, both the orbit positional accuracy *and* the temporal resolution of geodynamic parameters can be improved simultaneously. These improvements in the estimates of the C_t, J_2, and J_3 parameters and the orbit itself translate into a 50% reduction in the RMS error in the range residuals.

In addition, the stochastic results from the three year arc show that these improvements are possible for longer arcs. While no comparisons to a non-stochastic solution for the three year arc are made, the accuracies of the estimates for the model parameters and the orbit position are similar to those from the one year stochastic solution. This suggests that the ability of the stochastic filter to improve the orbit position and temporal resolution of geodynamic parameters simultaneously may be possible for longer arcs (such as three years or more) as well. In fact, the accuracies of the stochastic estimates for the C_t, J_2, and J_3 parameters were slightly better for the three year arc than those from the one year arc. However, other factors such as numerical integration errors do become more important for the three year arc, as evidenced by the orbit position and range residuals near the end of the three year simulation case. Nevertheless, this type of error can be handled effectively, and the accuracies of the three year stochastic estimates for the C_t, J_2, and J_3 parameters are very encouraging.

It seems reasonable to conclude that improving the temporal resolution of similar parameters is possible. Examples would be solar radiation pressure coefficient variations, higher degree effective geopotential coefficient variations, and nonconservative force coefficients in general. Most variations in Earth orientation parameters can be estimated with constants at a daily resolution (daily boxcars). The strength in determining these parameters geometrically allows estimates to be made at a much higher frequency. However, resolution may still be improved with stochastic filtering methods.

It also seems feasible to extend this stochastic filtering approach to other satellites. Satellites whose orbits are reasonably predictable and known and whose observations are highly accurate with noise levels which are suitably low would be appropriate candidates. If the noise level associated with the observations is too high, it may mask the temporal variations of interest. Depending on the particular satellite and the impact of specific geodynamic parameters on its dynamics, the feasibility of estimating these parameters stochastically with any degree of accuracy may or may not be possible.

6.1.1 Benefits of Stochastic Filtering

Some general benefits of process noise filtering are discussed as they relate to this research and possibly other applications. It is clear that stochastic filters have the potential to be used to improve orbit accuracies *and* temporal resolutions of specific geophysical parameters. In addition to improving orbit accuracies along with temporal estimates of geophysical parameters, another major benefit is computational in nature. In using a standard filter to estimate multiple boxcar estimates over a long arc, additional columns of a portion of the state transition matrix must be integrated since the state vector requires an additional parameter for each boxcar. As the length of the data

arc increases, the number of boxcars required for each parameter increases in order to maintain a given temporal resolution for each parameter. For example, in estimating 12 monthly boxcar estimates for a particular parameter throughout a one year arc rather than a single year long estimate adds 11 columns to the partition of the state transition matrix which corresponds to the satellite accelerations (velocity rows of the state vector). For this study, estimating 15 day boxcars for along track drag and monthly estimates for J_2 and J_3 over the one year arc requires 48 such columns as opposed to three columns if a single year long estimate is made. With the stochastic filter, however, no additional columns of the state transition matrix need to be integrated since the size of the satellite state vector remains fixed. Only one parameter is required to estimate a specific temporal variation over any arc length since independent estimates are possible at each observation time. For arcs that are one year or longer, this results in a truly significant time savings computationally. Due to this computational disadvantage for the standard non-stochastic approach, a boxcar solution for the three year arc was not computed for comparison to the stochastic solution. In order to estimate a single dynamically consistent orbit for a three year boxcar solution, 72 parameters for C_t, 36 parameters for J_2, and 36 parameters for J_3 would need to be estimated simultaneously. Compared to the stochastic method, the computational cost is extraordinary. Moreover, the temporal resolution of the model parameters and accuracy of the orbit position is likely to be no better than those from the one year boxcar solution.

Further, for variations which are observable in the presence of the measurement noise and temporally resolved equally by both filtering approaches, the stochastic approach is simply a more elegant way of estimating those variations that the standard approach must estimate with boxcars. By using process noise parameters to estimate

unpredictable variations in geodynamic parameters stochastically, no increase in the size of the satellite state vector is required. By specifying the time correlation window for the variation, controlled by τ, and the amplitude of the variation, controlled by σ, the need to split up the arc into multiple boxcars is eliminated. While some innovative algorithms may minimize the computational hindrances associated with the standard boxcar filter to some extent, the process noise approach is inherently computationally advantageous with respect to maintaining a smaller state vector and state transition matrix while providing higher temporal resolution. In addition, with respect to boxcar estimates, a very high temporal resolution may be achieved through the definition of τ and σ since separate estimates are made at every time an observation is accumulated.

6.1.2 Drawbacks of Stochastic Filtering

One drawback related to stochastic filtering observed in this study relates to iterating in order to improve the reference trajectory. Improving the initial reference trajectory by iterating and producing an improved reference trajectory with stochastic solutions of specific state parameters through the use of a process noise filter is generally not desirable. If a stochastic solution were to be used for the new reference trajectory, then new σ parameters would need to be used for each iteration since corrections to the stochastic solution would likely be a different order of magnitude than the previous correction. While quite straightforward theoretically, the determination of successive values for σ for each process noise parameter that produce a meaningful improved stochastic solution may not be practical. In addition, the use of a stochastic solution for a reference trajectory may complicate the filtering depending on the robustness of the filter in propagating a reference trajectory and the particular application. This approach is definitely possible, but not likely to be advantageous.

This minor drawback is quite trivial since determining a suitable reference trajectory without using stochastics is generally not a problem.

Another drawback is the use of stochastics to estimate completely unknown variations in a parameter. Not knowing some basic trends regarding the amplitude and frequency of the variations' deviation from an average or reference value is unfavorable, particularly if multiple parameters are involved. While estimates can be made with no such insight, they may not be reasonable until a proper τ and σ are chosen. It is possible, however, to estimate a parameter with a random walk process by simply choosing an appropriate variance q for the parameter (assuming the variation is expected to be continuous). In this study, random walk solutions, with accuracies comparable to the colored noise solutions previously presented, were generated using a variance which was on the order of magnitude of the square of the amplitude of the model deviation signal for the parameter. Based on a random walk solution, additional insights into a proper τ and σ are likely, since information regarding the amplitude and frequency of the unknown model deviation signal is gained. The practical significance of this drawback is minor since a preliminary standard boxcar solution for a given variation will likely provide adequate insights into the temporal behavior of the variation.

Finally, the possibilities of using stochastic filtering to improve orbit accuracies and temporal resolutions of geodynamic parameters should be kept in perspective. While this study has shown that it is feasible to make such improvements, it does not suggest that applying process noise filtering to all satellite solutions will improve every aspect of each solution. Although it is very encouraging to verify via simulated LAGEOS SLR data that variations in parameters such as along track drag, J_2, and J_3 can be recovered and estimated more accurately with process noise parameters while

improving the orbit position accuracy, overly optimistic extensions of these findings without similar verification is improper.

6.2 Recommendations for Future Work

Some recommendations for future studies are now summarized. A similar simulation using a different satellite state may be of interest. By using a satellite state composed of Keplerian elements, variations from a reference secularly precessing ellipse might be estimated with or instead of the actual geodynamic variations. This would lead to direct comparisons of those variations to temporal variations in the geopotential or other model variations. Further insights as to the relationships between these variations may be gained.

Another study which assesses the advantages of a hybrid standard-stochastic filter may prove valuable. Filters using both boxcars and stochastic parameters to estimate particular variations would be more robust. Estimating some parameters, such as daily polar motion parameters or tracking station positions and movements, with boxcars, and other parameters, such as gravity or non-conservative force variations, stochastically would be interesting. Also, by incorporating data from multiple satellites, the determination of true variations in higher degree geopotential coefficients might be possible since aliasing could be reduced. This multi-satellite study might use a simulation to assess the feasibility of determining multiple variations of geopotential coefficients. This type of study would contribute to improvements in the modeling of the static geopotential field by better accommodating the temporal variations in gravity. Since many of the long-wavelength gravity coefficients are only known to the same level as their observed temporal variations [*Nerem et al.*, 1993], improvements in the estimates of these coefficients must involve dealing with the temporal variations in an

appropriate manner. A similar study addressing the estimation of temporal variations in the Mars gravity field is also recommended.

Finally, a study using actual data, perhaps LAGEOS, to compare a stochastic filtering solution to a standard boxcar solution over a multi-year arc is recommended. Knowing that it is feasible to estimate parameters such as C_t, J_2, and J_3 stochastically, such a study would seem productive. The dynamical model would need to be more complex, such as that used in actual LAGEOS filtering. The stochastic estimates could then be compared to the existing boxcar estimates of the corresponding parameters.

BIBLIOGRAPHY

Andrews, A., "A Square Root Formulation of the Kalman Covariance Equations," *AIAA Journal*, Vol. 6, pp. 1165-1166, 1968.

Bate, R. R., D. D. Mueller, and J. E. White, *Fundamentals of Astrodynamics*, Dover Publications, New York, 1971.

Battin, R. H., *Astronautical Guidance*, McGraw-Hill, New York, 1964.

Battin, R. H., *An Introduction to the Mathematics and Methods of Astrodynamics*, American Institute of Aeronautics and Astronautics, New York, 1987.

Biancale, R., A. Cazenave, and K. Dominh, "Tectonic Plate Motions Derived from LAGEOS," *Earth and Planetary Science Letters*, Vol. 103, pp. 379-394, 1991.

Bierman, G. J., *Factorization Methods for Discrete Sequential Estimation*, Academic Press, New York, 1977.

Born, G. H., B. D. Tapley, and B. E. Schutz, "Satellite Orbit Determination: Fundamentals and Applications," Class Notes, University of Colorado, 1990.

Caporali, A., A. Cenci, and M. Fermi, "Study of the High Frequency Structure of Polar Motion Derived from LAGEOS Ranging Data," *Journal of Geophysical Research*, Vol. 95, No. B7, pp. 10965-10972, 1990.

Chao, B. F., W. P. O'Connor, A. T. C. Chang, D. K. Hall, and J. L. Foster, "Snow Load Effect on the Earth's Rotation and Gravitational Field, 1979-1985," *Journal of Geophysical Research*, Vol. 92, No. B9, pp. 9415-9422, 1987.

Chao, B. F., and W. P. O'Connor, "Global Surface-Water-Induced Seasonal Variations in the Earth's Rotation and Gravitational Field," *Geophys. J.*, Vol. 94, pp. 263-270, 1988.

Chao, B. F., and A. Y. Au, "Temporal Variation of the Earth's Low-Degree Zonal Gravitational Field Caused by Atmospheric Mass Redistribution: 1980-1988," *Journal of Geophysical Research*, Vol. 96, No. B4, pp. 6569-6575, 1991.

Chao, B. F., "Excitation of Earth's Polar Motion by Atmospheric Angular Momentum Variations, 1980-1990," *Geophysical Research Letters*, Vol. 20, No. 2, pp. 253-256, 1993.

Cheng, M. K., R. J. Eanes, C. K. Shum, B. E. Schutz, and B. D. Tapley, "Temporal Variations in Low Degree Zonal Harmonics from Starlette Orbit Analysis," *Geophysical Research Letters*, Vol. 16, No. 5, pp. 393-396, 1989.

Cheng, M. K., B. E. Schutz, and B. D. Tapley, "Seasonal Variations in the Earth's Gravity Field form 15-Year Starlette Orbit Analysis," *EOS Trans. AGU*, Vol. 71, p. 481, 1990.

Christodoulidis, D. C., D. E. Smith, R. Kolenkiewicz, S. M. Klosko, M. H. Torrence, and P. J. Dunn, "Observing Tectonic Plate Motions and Deformations from Satellite Laser Ranging," *Journal of Geophysical Research*, Vol. 90, No. B11, pp. 9249-9263, 1985.

Christodoulidis, D. C., D. E. Smith, S. M. Klosko, and P. J. Dunn, "Solid Earth and Ocean Tide Parameters from LAGEOS," *Proceedings of the Tenth International Symposium of Earth Tides*, ed. by R. Vieira, pp. 953-961, 1986.

Cohen, S. C., and D. E. Smith, "LAGEOS Scientific Results: Introduction," *Journal of Geophysical Research*, Vol. 90, No. B11, pp. 9217-9220, 1985.

Degnan, J. J., "Satellite Laser Ranging: Current Status and Future Prospects 1985," *IEEE Trans. Geosci. and Rem. Sens.*, Vol. GE-23, pp. 398-413, 1985.

Degnan, J. J., "Millimeter Accuracy Satellite Laser Ranging: A Review," *Contributions of Space Geodesy to Geodynamics: Technology*, Geodynamics Series Vol. 25, pp. 133-162, 1993.

Degnan, J. J. (ed.), *Satellite Laser Ranging in the 1990's, Report of the 1994 Belmont Workshop*, NASA Conference Publication 3283, 1994.

Dickey, J. O., "Atmospheric Excitation of the Earth's Rotation: Progress and Prospects Via Space Geodesy," *Contributions of Space Geodesy to Geodynamics: Earth Dynamics*, Geodynamics Series Vol. 24, pp. 55-70, 1993.

Dow, J. M., P. Duque, and M. R. Merino, "Global Geodynamics from LAGEOS and Starlette Combination Solutions," *Advances in Space Research*, Vol. 11, No. 6, pp. (6)119-(6)124, 1991.

Dyer, P., and S. McReynolds, "Extension of Square Root Filtering to Include Process Noise," *J. of Opt. Theory, Appl.*, Vol. 3, No. 6, pp. 444-459, 1969.

Escobal, P. R., *Methods of Orbit Determination*, Krieger Publishing Company, Malabar, Florida, 1965.

Fitzmaurice, M. W., P. O. Minott, J. B. Abshire, and H. E. Rowe, "Prelaunch Testing of the Laser Geodynamic Satellite (LAGEOS) ," NASA Technical Paper 1062, October, 1977.

Garland, G. D., *Introduction to Geophysics (Mantle, Core, and Crust)*, W. B. Saunders Company, Philadelphia, 1979.

Gegout, P., and A. Cazenave, "Geodynamic Parameters Derived from 7 Years of Laser Data on LAGEOS," *Geophysical Research Letters*, Vol. 18, No. 9, pp. 1739-1742, 1991.

Givens, J. W., "The Linear Equations Problem," Applied Mathematics and Statistics Laboratories, Stanford University, Technical Report 3, 1959.

Gold, K. L., "GPS Orbit Determination for the Extreme Ultraviolet Explorer," *Ph. D. Dissertation*, The University of Colorado, 1994.

Golub, G. H., "Numerical Methods for Solving Linear Least Squares Problems," *Num. Math.*, Vol. 7, pp. 206-216, 1965.

Himwich, W. E., M. M. Watkins, C. Ma, D. S. MacMillan, T. A. Clark, R. J. Eanes, J. W. Ryan, B. E. Schutz, and B. D. Tapley, "The Consistency of the Scale of the Terrestrial Reference Frames Estimated from SLR and VLBI Data," *Contributions of Space Geodesy to Geodynamics: Earth Dynamics*, Geodynamics Series, Vol. 24 , pp. 113-120, 1993.

Householder, A. S., *The Theory of Matrices in Numerical Analysis*, Blaisdell Publishing Company, Waltham, Massachusetts, 1964.

Jazwinski, A. H., *Stochastic Processes and Filtering Theory*, Academic Press, New York, 1970.

Kaminski, P. G., "Square Root Filtering and Smoothing for Discrete Processes," *Ph. D. Dissertation*, Department of Aeronautics and Astronautics, Stanford University, Stanford, California, 1971.

Kaula, W. M., *Theory of Satellite Geodesy*, Blaisdell Publishing Company, Waltham, Massachusetts, 1966.

Kolenkiewicz, R., J. W. Ryan, and M. H. Torrence, "A Comparison Between LAGEOS Laser Ranging and Very Long Baseline Interferometry Determined Baseline Lengths," *Journal of Geophysical Research*, Vol. 90, No. B11, pp. 9265-9274, 1985.

Kolenkiewicz, R., D. E. Smith, P. J. Dunn, M. H. Torrence, J. W. Robbins, S. M. Klosko, R. G. Williamson, E. C. Pavlis, N. B. Douglas, and S. K. Fricke, "The Role of Laser Determined Orbits in Geodesy and Geophysics," *Advances in Space Research*, Vol. 11, No. 6, pp. (6)111-(6)118, 1991.

Lambeck, K., *Geophysical Geodesy: The Slow Deformations of the Earth*, Clarendon Press, Oxford, 1988.

Lawson, C. L., and R. J. Hanson, "Extensions and Applications of the Householder Algorithm for Solving Linear Least Squares Problems," *Math. Comp.*, Vol. 23, No. 108, pp. 787-812, 1969.

Lawson, C. L., and R. J. Hanson, *Solving Least Squares Problems*, Prentice-Hall, Englewood Cliffs, New Jersey, 1974.

Lerch, F. J., S. M. Klosko, G. B. Patel, and C. A. Wagner, "A Gravity Model for Crustal Dynamics (GEM-L2) ," *Journal of Geophysical Research*, Vol. 90, No. B11, pp. 9301-9311, 1985.

Lichten, S. M., "Towards GPS Orbit Accuracy of Tens of Centimeters," *Geophysical Research Letters*, Vol. 17, pp. 215-218, 1990a.

Lichten, S. M., "Estimation and Filtering for High-Precision GPS Positioning Applications," *Manuscripta Geodaetica*, Vol. 15, pp. 159-176, 1990b.

Lichten, S. M., S. L. Marcus, and J. O. Dickey, "Sub-Daily Resolution of Earth Rotation Variations with Global Positioning System Measurements," *Geophysical Research Letters*, Vol. 19, No. 6, 1992.

Marsh, J. G., F. J. Lerch, B. H. Putney, D. C. Christodoulidis, D. E. Smith, T. L. Felsentreger, B. V. Sanchez, S. M. Klosko, E. C. Pavlis, T. V. Martin, J. W. Robbins, R. G. Williamson, O. L. Colombo, D. D. Rowlands, W. F. Eddy, N. L. Chandler, K. E. Rachlin, G. B. Patel, S. Bhati, and D. S. Chinn, "A New Gravitational Model for the Earth from Satellite Tracking Data: GEM-T1," *Journal of Geophysical Research*, Vol. 93, pp. 6169-6215, 1988.

Marsh, J. G., F. J. Lerch, B. H. Putney, T. L. Felsentreger, B. V. Sanchez, S. M. Klosko, G. B. Patel, J. W. Robbins, R. G. Williamson, T. L. Engelis, W. F. Eddy, N. L. Chandler, D. S. Chinn, S. Kapoor, K. E. Rachlin, L. E. Braatz, and E. C. Pavlis, "The GEM-T2 Gravitational Model," *Journal of Geophysical Research*, Vol. 95, pp. 22043-22071, 1990.

McCarthy, D. D., "The Use of Crustal Dynamics Project Data to Predict the Orientation of the Earth," *Contributions of Space Geodesy to Geodynamics: Earth Dynamics*, Geodynamics Series, Vol. 24 , pp. 71-76, 1993.

McGarty, T. P., *Stochastic Systems and State Estimation*, John Wiley & Sons, New York, 1974.

McMillan, J. D., "Mathematical Specifications of the University of Texas Orbit Processor and Application to the Laser Observations of the Beacon Explorer-C Satellite," *M. S. Thesis*, University of Texas at Austin, 1973.

Mitrovica, J. X., and W. R. Peltier, "Present-Day Secular Variations in the Zonal Harmonics of Earth's Geopotential," *Journal of Geophysical Research*, Vol. 98, No. B3, pp. 4509-4526, 1993.

Munk, W. H., and G. J. F. MacDonald, *The Rotation of the Earth: A Geophysical Discussion*, Cambridge University Press, London, 1960.

Nerem, R. S., B. F. Chao, A. Y. Au, J. C. Chan, S. M. Klosko, N. K. Pavlis, and R. G. Williamson, "Temporal Variations of the Earth's Gravitational Field from Satellite Laser Ranging to LAGEOS," *Geophysical Research Letters*, Vol. 20, No. 7, pp. 595-598, 1993.

Nerem, R. S., F. J. Lerch, J. A. Marshall, E. C. Pavlis, B. H. Putney, B. D. Tapley, R. J. Eanes, J. C. Ries, B. E. Schutz, C. K. Shum, M. M. Watkins, S. M. Klosko, J. C. Chan, S. B. Luthcke, G. B. Patel, N. K. Pavlis, R. G. Williamson, R. H. Rapp, R. Biancale, and F. Nouel, "Gravity Model Development for TOPEX/POSEIDON: Joint Gravity Models 1 and 2," *Journal of Geophysical Research*, Vol. 99, No. C12, pp. 24421-24447, 1994.

Noble, B., *Applied Linear Algebra*, Prentice Hall, Englewood Cliffs, New Jersey, 1969.

Pavlis, E. C., R. G. Williamson, and D. E. Smith, "High Resolution Polar Motion from the LAGEOS Tracking," *EOS Trans. AGU*, Vol. 69, p. 1154, 1988.

Pond, S., and G. L. Pickard, *Introductory Dynamical Oceanography*, Pergamon Press, Oxford, 1983.

Press, W. H., B. P. Flannery, S. A. Teukolsky, and W. T. Vetterling, *Numerical Recipes: The Art of Scientific Computing (Fortran Version)*, Cambridge University Press, Cambridge, 1989.

Ries, J. C., R. J. Eanes, C. Huang, B. E. Schutz, C. K. Shum, B. D. Tapley, M. M. Watkins, and D. N. Yuan, "Determination of the Gravitational Coefficient of the Earth from Near-Earth Satellites," *Geophysical Research Letters*, Vol. 16, No. 4, pp. 271-274, 1989.

Ries, J. C., "Simulation of an Experiment to Measure the Lense-Thirring Precession Using a Second LAGEOS Satellite," *Ph. D. Dissertation*, The University of Texas at Austin, 1989.

Ries, J. C., R. J. Eanes, C. K. Shum, and M. M. Watkins, "Progress in the Determination of the Gravitational Coefficient of the Earth," *Geophysical Research Letters*, Vol. 19, No. 6, pp. 529-531, 1992.

Roy, A. E., *Orbital Motion*, Adam Hilger, New York, 1988.

Rubincam, D. P., "On the Secular Decrease in the Semimajor Axis of LAGEOS' Orbit," *Celest. Mech.*, Vol. 26, No. 4, p. 361, 1982.

Rubincam, D. P., "Postglacial Rebound observed by LAGEOS and the effective viscosity of the lower mantle," *Journal of Geophysical Research*, Vol. 89, pp. 1077-1087, 1984.

Rubincam, D. P., "LAGEOS Orbit Decay due to Infrared Radiation from the Earth," *Journal of Geophysical Research*, Vol. 92, No. B2, p. 1287, 1987.

Rubincam, D. P., "Yarkovsky Thermal Drag on LAGEOS," *Journal of Geophysical Research*, Vol. 93, No. B11, pp. 13805-13810, 1988.

Rubincam, D. P., "Drag on the LAGEOS Satellite," *Journal of Geophysical Research*, Vol. 95, No. B4, pp. 4881-4886, 1990.

Schmidt, S. F., "Estimation of State with Acceptable Accuracy Constraints," Analytical Mechanics Associated, Palo Alto, California, Technical Report 67-16, 1967.

Shum, C. K., B. E. Schutz, M. K. Cheng, R. J. Eanes, and B. D. Tapley, "Geophysical Parameters from the Analysis of Laser Ranging to Starlette," *EOS Trans. AGU*, Vol. 68, p. 281, 1987.

Smith, G. L., S. F. Schmidt, and L. A. McGee, "Application of Statistical Filtering to the Optimal Estimation of Position and Velocity On-Board a Circumlunar Vehicle," NASA Ames Research Center Report No. NASA TND-1205, 1962.

Smith, D. E., D. C. Christodoulidis, R. Kolenkiewicz, P. J. Dunn, S. M. Klosko, M. H. Torrence, S. Fricke, and S. Blackwell, "A Global Geodetic Reference Frame from LAGEOS Ranging (SL5.1AP)," *Journal of Geophysical Research*, Vol. 90, No. B11, pp. 9221-9233, 1985.

Smith, D. E., R. Kolenkiewicz, P. J. Dunn, J. W. Robbins, M. H. Torrence, S. M. Klosko, R. G. Williamson, E. C. Pavlis, N. B. Douglas, and S. K. Fricke, "Tectonic Motion and Deformation From Satellite Laser Ranging to LAGEOS," *Journal of Geophysical Research*, Vol. 95, No. B13, pp. 22013-22041, 1990.

Smith, D. E., R. Kolenkiewicz, P. J. Dunn, S. M. Klosko, J. W. Robbins, M. H. Torrence, R. G. Williamson, E. C. Pavlis, N. B. Douglas, and S. K. Fricke, "LAGEOS Geodetic Analysis--SL7.1," NASA Technical Memorandum 104549, September, 1991.

Stolz, A., M. A. Vincent, P. L. Bender, R. J. Eanes, M. M. Watkins, and B. D. Tapley, "Rate of Change of the Quincy-Monument Peak Baseline from a Translocation Analysis of LAGEOS Laser Range Data," *Geophysical Research Letters*, Vol. 16, No. 6, pp. 539-542, 1989.

Tapley, B. D., B. E. Schutz, and R. J. Eanes, "Station Coordinates, Baselines, and Earth Rotation from LAGEOS Laser Ranging: 1976-1984," *Journal of Geophysical Research*, Vol. 90, No. B11, pp. 9235-9248, 1985.

Tapley, B. D., R. J. Eanes, B. E. Schutz, and M. M. Watkins, "Contribution of Satellite Laser Ranging to Geodesy and Geodynamics," *Advances in Space Research*, Vol. 11, No. 6, pp. (6)103-(6)109, 1991.

Tapley, B. D., B. E. Schutz, R. J. Eanes, J. C. Ries, and M. M. Watkins, "Lageos Laser Ranging Contributions to Geodynamics, Geodesy, and Orbital Dynamics," *Contributions of Space Geodesy to Geodynamics: Earth Dynamics*, Geodynamics Series, Vol. 24 , pp. 147-173, 1993.

Thornton, C. L., "Triangular Covariance Factorizations for Kalman Filtering," *Ph. D. Dissertation*, UCLA School of Engineering, Department of Systems Science, 1976.

Watkins, M. M., and R. J. Eanes, "Diurnal and Semidiurnal Variations in Earth Orientation Determined From LAGEOS Laser Ranging," *Journal of Geophysical Research*, Vol. 99, No. B9, pp. 18073-18079, 1994.

Wertz, J. R. (ed.), *Spacecraft Attitude Determination and Control*, Kluwer Academic Publishers, Dordrecht, 1978.

Wilkinson, J. H., *The Algebraic Eigenvalue Problem*, Oxford University Press, London, 1965.

Wu, S. C., T. P. Yunck, and C. L. Thornton, "Reduced-Dynamic Technique for Precise Orbit Determination of Low Earth Satellites," *Journal of Guidance, Control, and Dynamics*, Vol. 14, No. 1, pp. 24-30, 1991.

Yoder, C. F., J. G. Williams, J. O. Dickey, B. E. Schutz, R. J. Eanes, and B. D. Tapley, "Secular Variations of Earth's Gravitational Harmonic J_2 Coefficient from LAGEOS and the Nontidal Acceleration of Earth Rotation," *Nature*, Vol. 303, pp. 757-762, 1983.

Yunck, T. P., S. C. Wu, J. T. Wu, and C. L. Thornton, "Precise Tracking of Remote Sensing Satellites With the Global Positioning System," *IEEE Transactions on Geoscience and Remote Sensing*, Vol. 28, No. 1, pp. 108-116, 1990.

Yunck, T. P., W. I. Bertiger, S. C. Wu, Y. E. Bar-Sever, E. J. Christensen, B. J. Haines, S. M. Lichten, R. J. Muellerschoen, Y. Vigue, and P. Willis, "First Assessment of GPS-based Reduced Dynamic Orbit Determination on TOPEX/Poseidon," *Geophysical Research Letters*, Vol. 21, No. 7, pp. 541-544, 1994.

APPENDIX A

KEPLERIAN RESIDUALS FOR ONE YEAR BOXCAR ARC WITH C_t, J_2, AND J_3 MODEL DEVIATION SIGNALS

The following Figures are orbit differences (with respect to the truth) resulting from the one year arc with C_t, J_2, and J_3 model deviation signals present using the standard boxcar method. They are shown in terms of the Keplerian elements (semi-major axis a, eccentricity e, inclination i, argument of periapse ω, longitude of ascending node Ω, and argument of latitude $\omega + f$, where f is true anomaly).

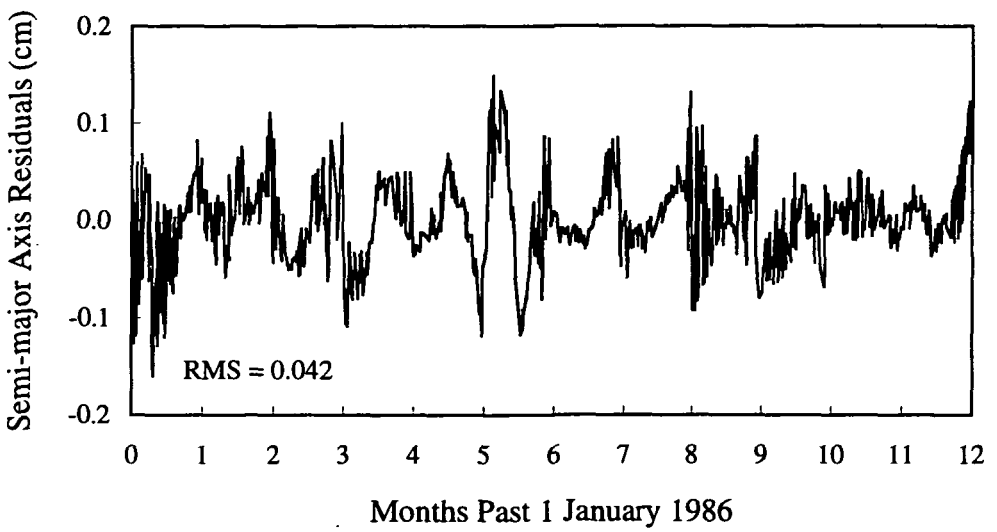

Figure A.1. Semi-Major Axis Residuals Using Boxcars.

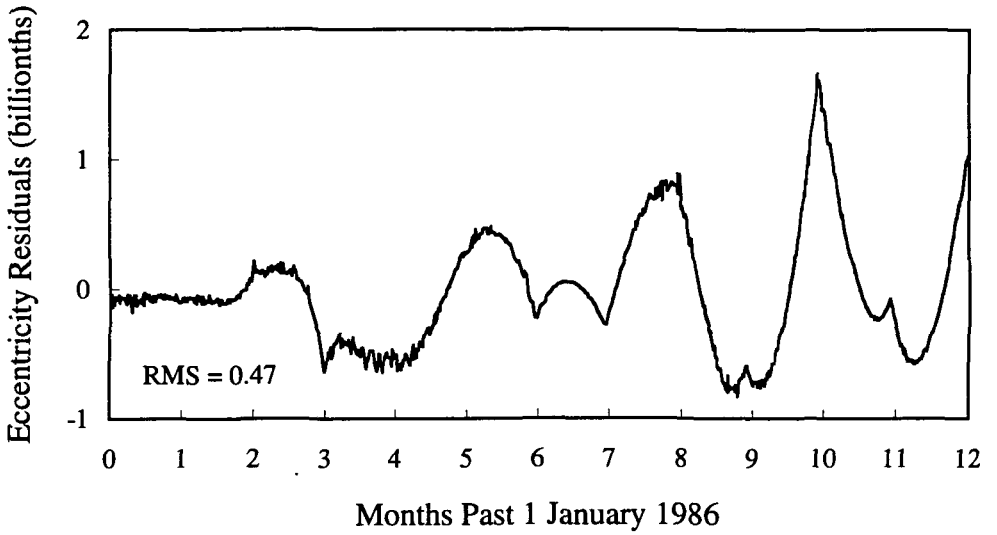

Figure A.2. Eccentricity Residuals Using Boxcars.

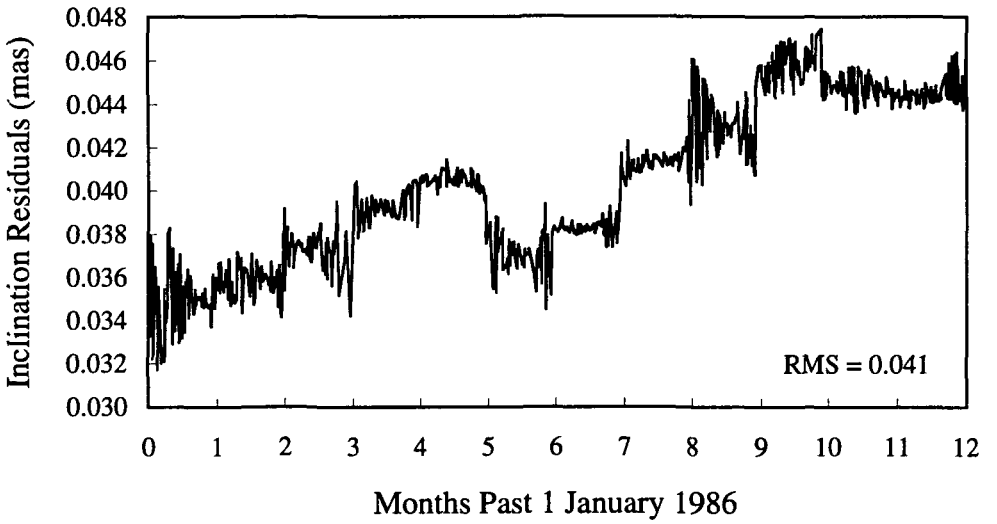

Figure A.3. Inclination Residuals Using Boxcars.

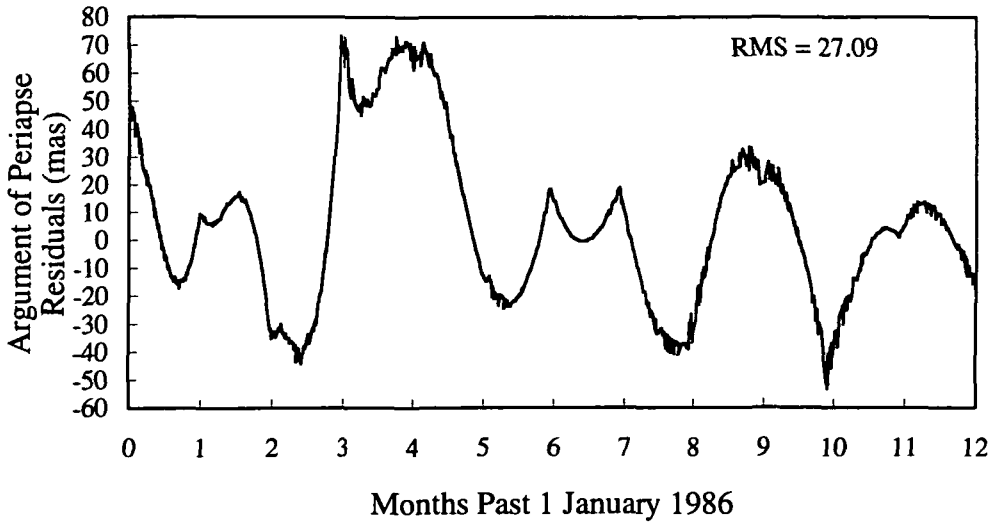

Figure A.4. Argument of Periapse Residuals Using Boxcars.

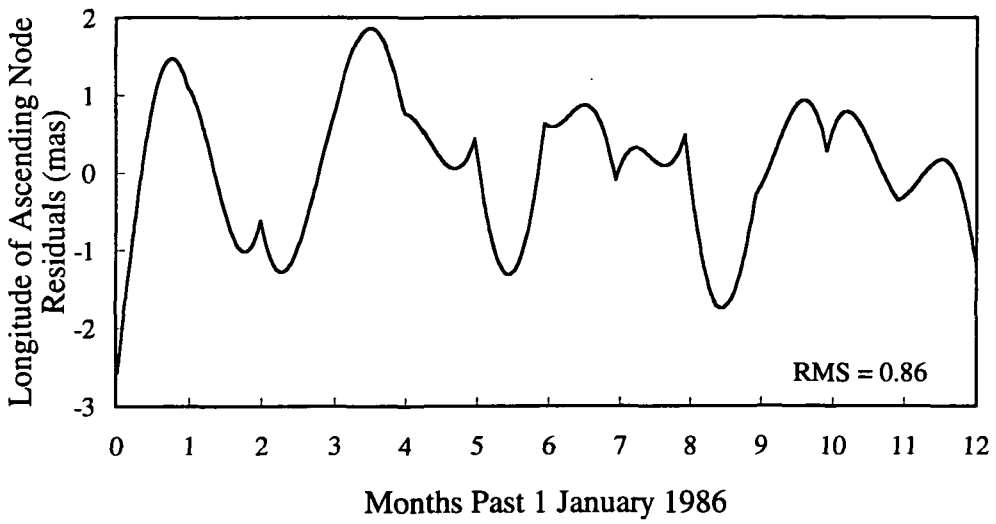

Figure A.5. Longitude of Ascending Node Residuals Using Boxcars.

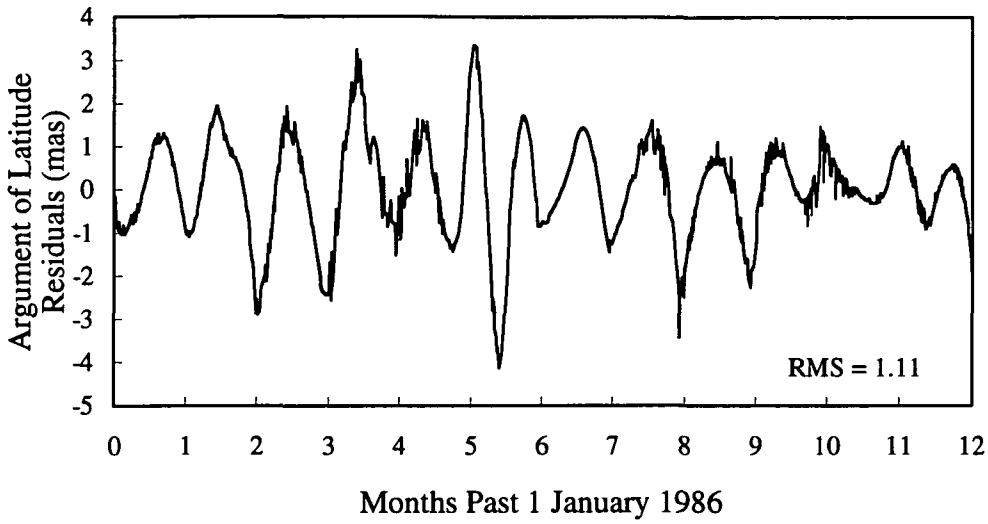

Figure A.6. Argument of Latitude Residuals Using Boxcars.

APPENDIX B

KEPLERIAN RESIDUALS FOR ONE YEAR PROCESS NOISE ARC WITH C_t, J_2, AND J_3 MODEL DEVIATION SIGNALS

The following Figures are orbit differences (with respect to the truth) resulting from the one year arc with C_t, J_2, and J_3 model deviation signals present using the process noise method. They are shown in terms of the Keplerian elements (semi-major axis a, eccentricity e, inclination i, argument of periapse ω, longitude of ascending node Ω, and argument of latitude $\omega + f$, where f is true anomaly).

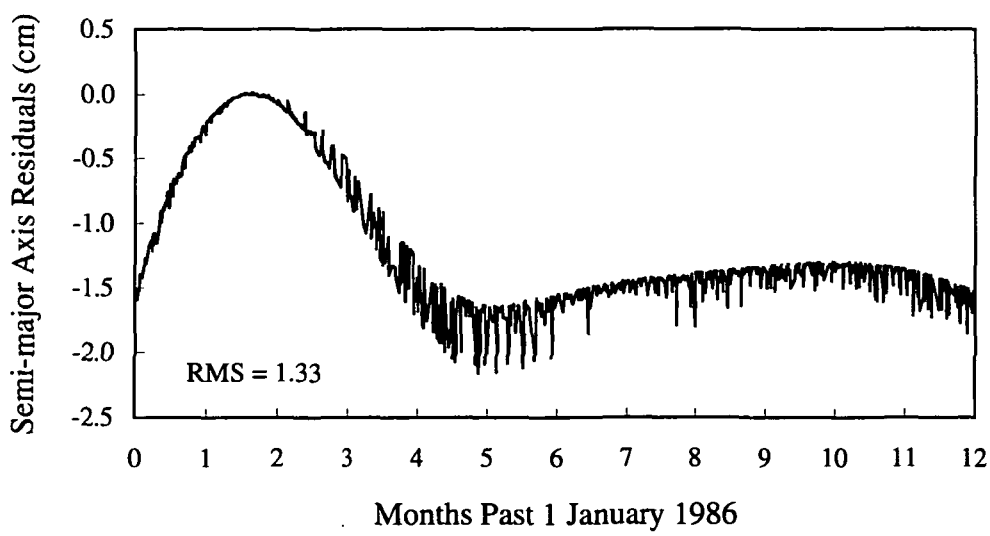

Figure B.1. Semi-Major Axis Residuals Using Process Noise.

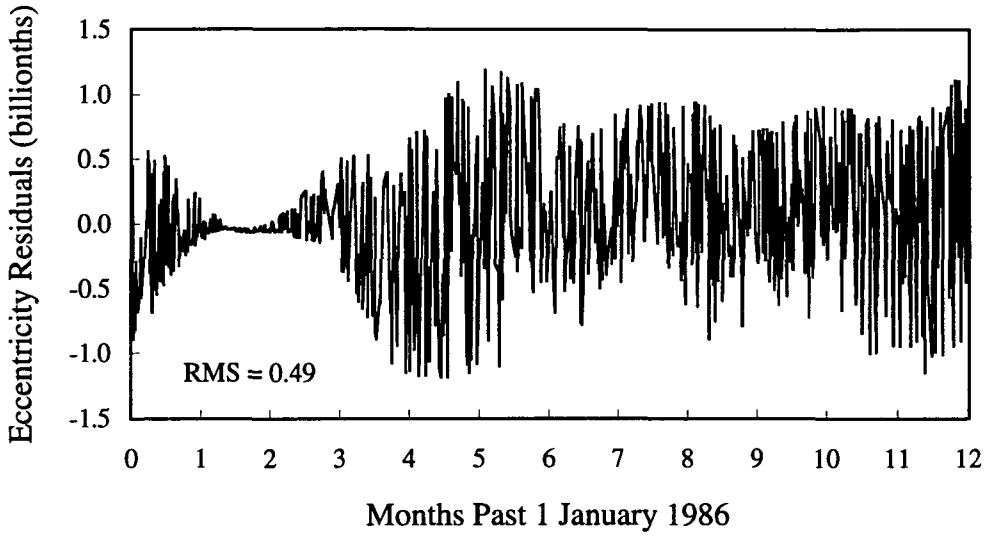

Figure B.2. Eccentricity Residuals Using Process Noise.

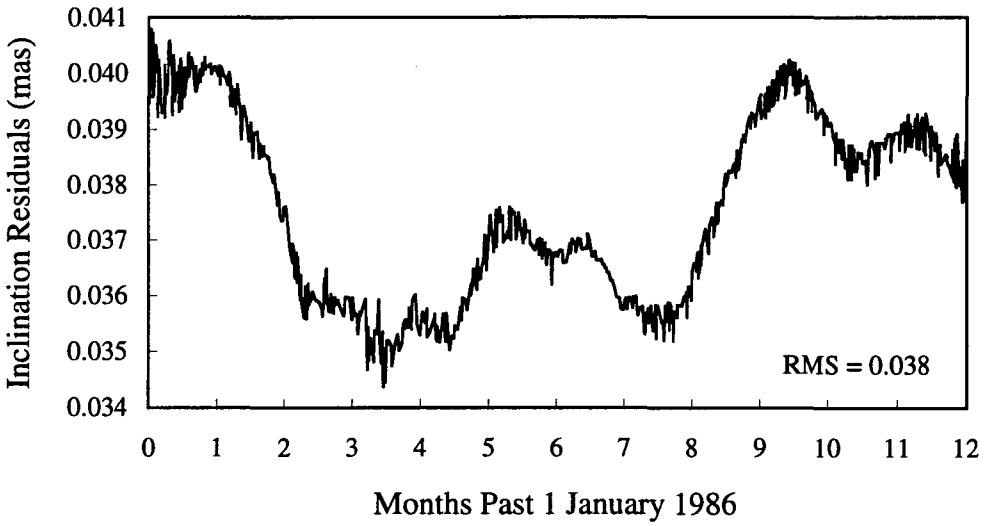

Figure B.3. Inclination Residuals Using Process Noise.

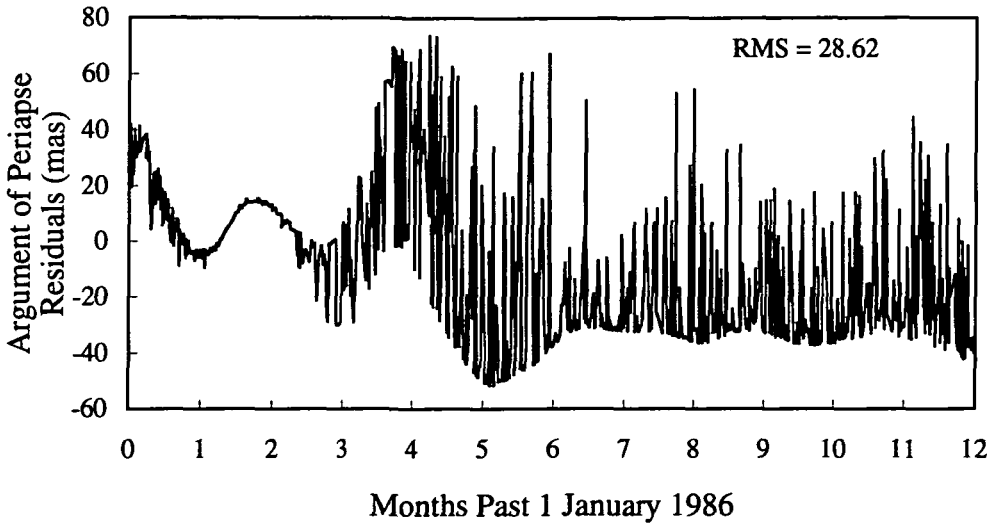

Figure B.4. Argument of Periapse Residuals Using Process Noise.

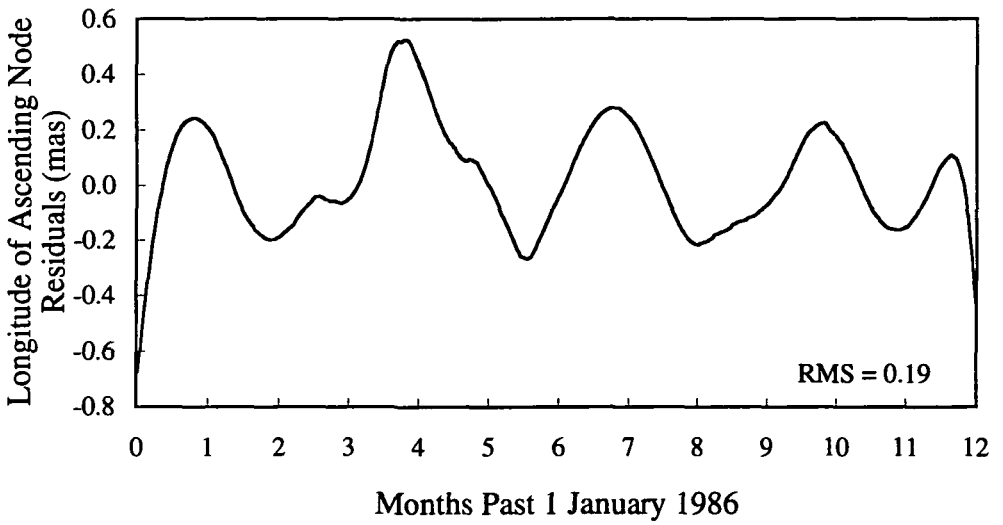

Figure B.5. Longitude of Ascending Node Residuals Using Process Noise.

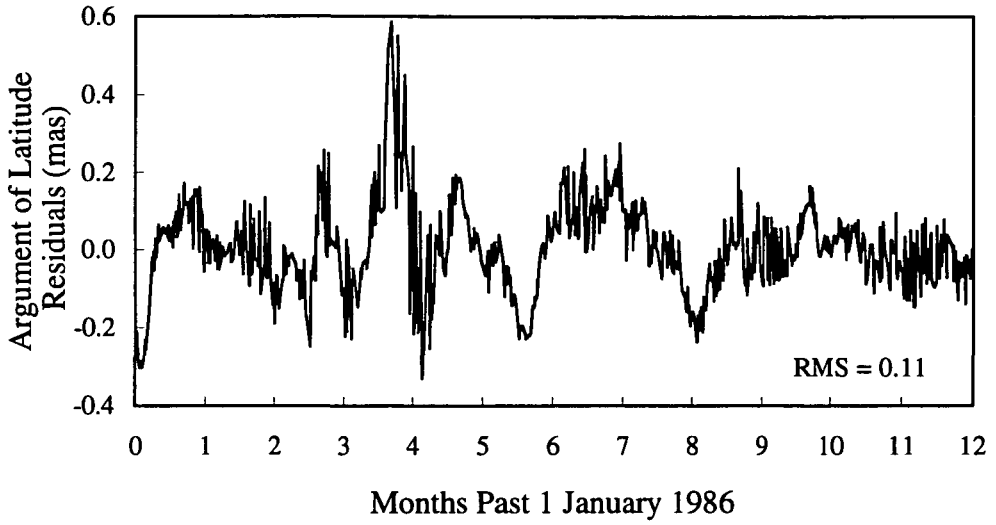

Figure B.6. Argument of Latitude Residuals Using Process Noise.

APPENDIX C

KEPLERIAN RESIDUALS FOR ONE YEAR BOXCAR ARC WITH C_t, J_2, J_3, J_4 AND J_5 MODEL DEVIATION SIGNALS

The following Figures are orbit differences (with respect to the truth) resulting from the one year arc with C_t, J_2, J_3, J_4, and J_5 model deviation signals present using the standard boxcar method. They are shown in terms of the Keplerian elements (semi-major axis a, eccentricity e, inclination i, argument of periapse ω, longitude of ascending node Ω, and argument of latitude $\omega + f$, where f is true anomaly).

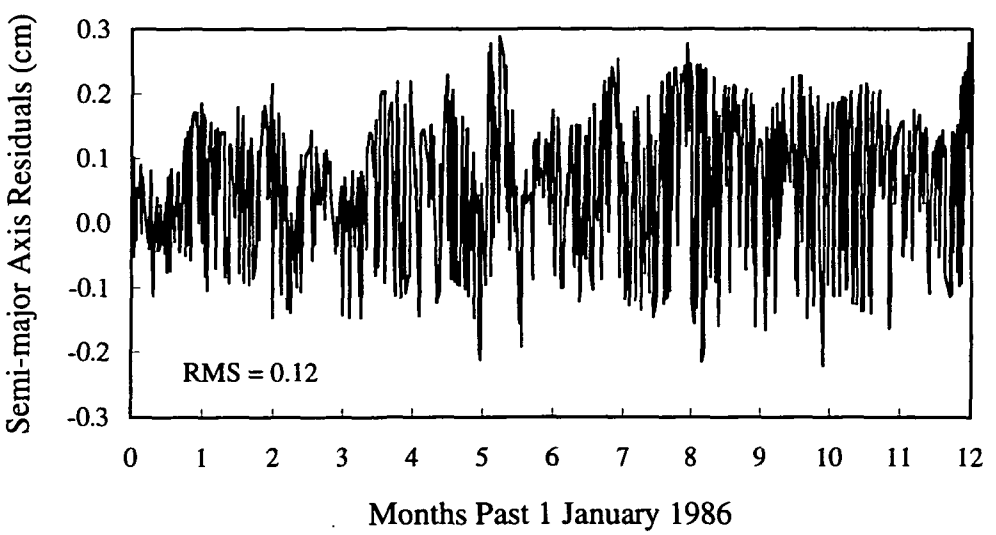

Figure C.1. Semi-Major Axis Residuals Using Boxcars with J_4 and J_5 Model Deviation Signals Present but not Estimated.

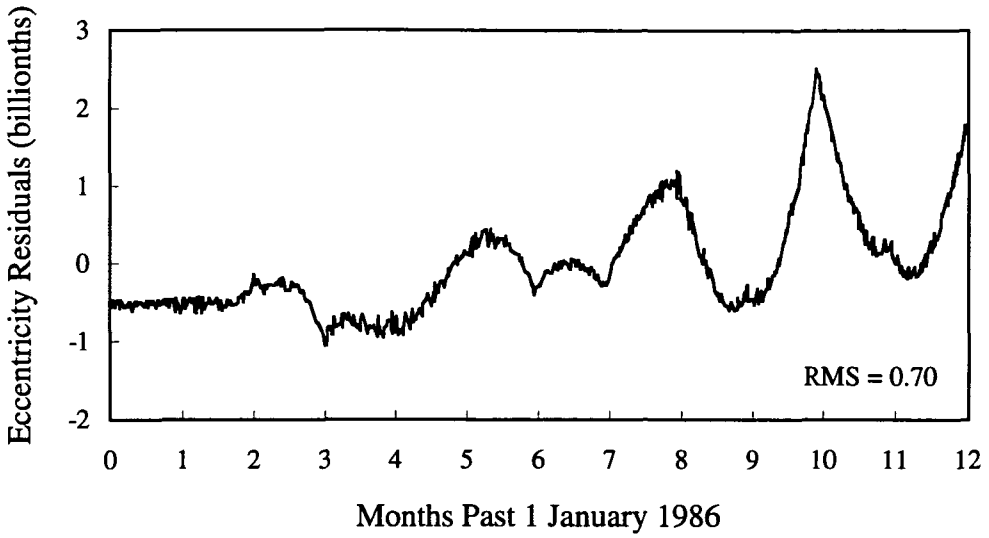

Figure C.2. Eccentricity Residuals Using Boxcars with J_4 and J_5 Model Deviation Signals Present but not Estimated.

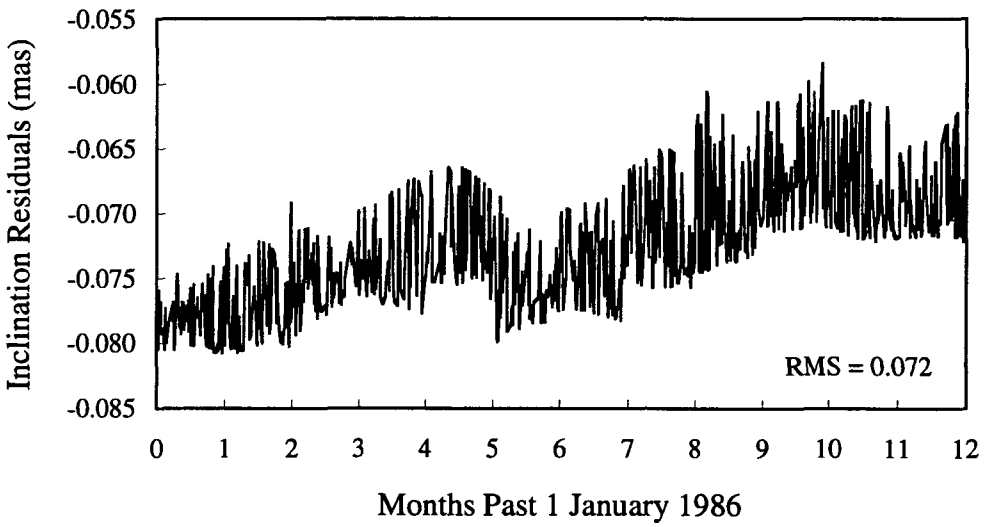

Figure C.3. Inclination Residuals Using Boxcars with J_4 and J_5 Model Deviation Signals Present but not Estimated.

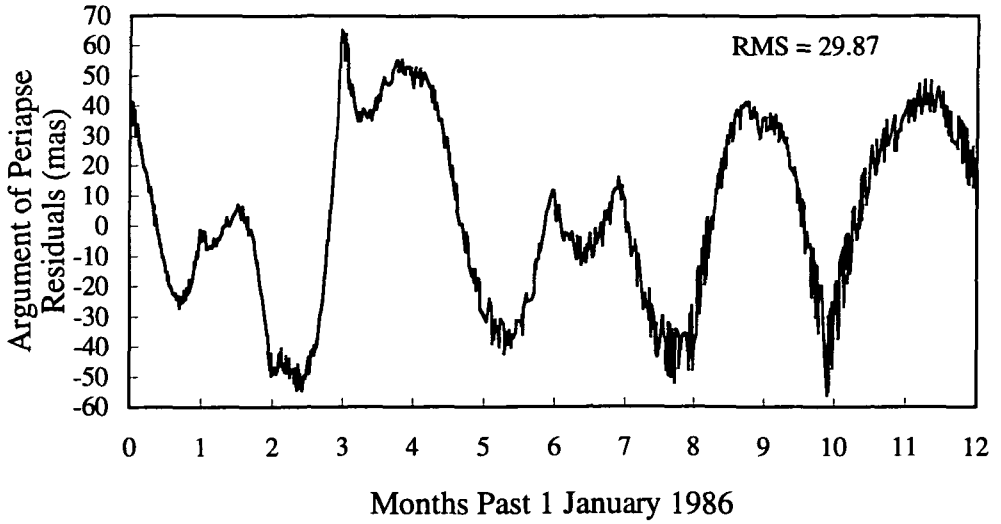

Figure C.4. Argument of Periapse Residuals Using Boxcars with J_4 and J_5 Model Deviation Signals Present but not Estimated.

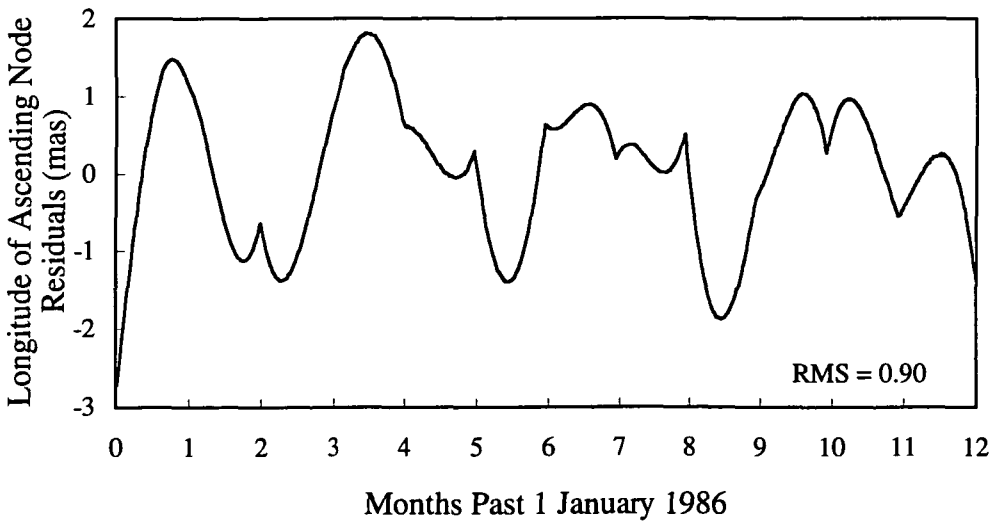

Figure C.5. Longitude of Ascending Node Residuals Using Boxcars with J_4 and J_5 Model Deviation Signals Present but not Estimated.

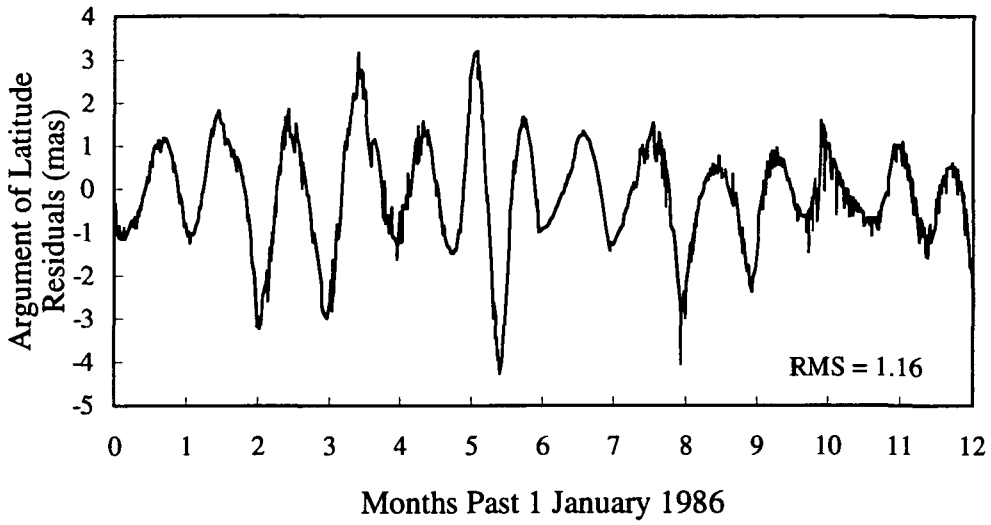

Figure C.6. Argument of Latitude Residuals Using Boxcars with J_4 and J_5 Model Deviation Signals Present but not Estimated.

APPENDIX D

KEPLERIAN RESIDUALS FOR ONE YEAR PROCESS NOISE ARC WITH C_t, J_2, J_3, J_4 AND J_5 MODEL DEVIATION SIGNALS

The following Figures are orbit differences (with respect to the truth) resulting from the one year arc with C_t, J_2, J_3, J_4, and J_5 model deviation signals present using the process noise method. They are shown in terms of the Keplerian elements (semi-major axis a, eccentricity e, inclination i, argument of periapse ω, longitude of ascending node Ω, and argument of latitude $\omega + f$, where f is true anomaly).

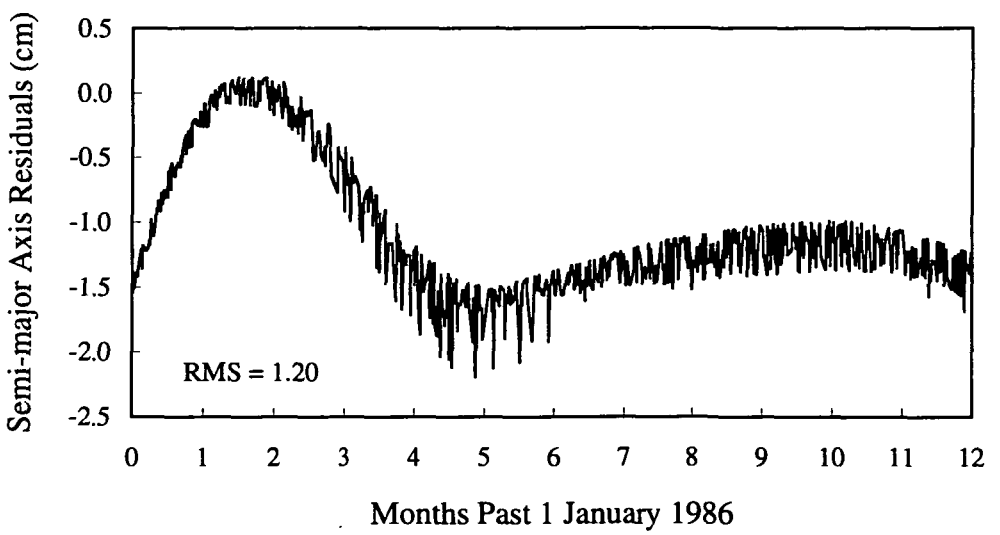

Figure D.1. Semi-Major Axis Residuals Using Process Noise with J_4 and J_5 Model Deviation Signals Present but not Estimated.

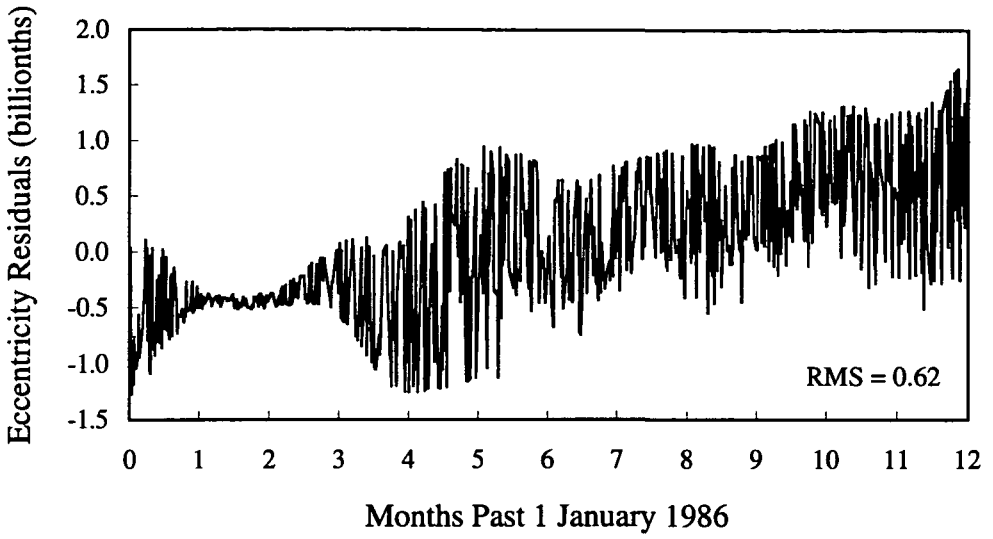

Figure D.2. Eccentricity Residuals Using Process Noise with J_4 and J_5 Model Deviation Signals Present but not Estimated.

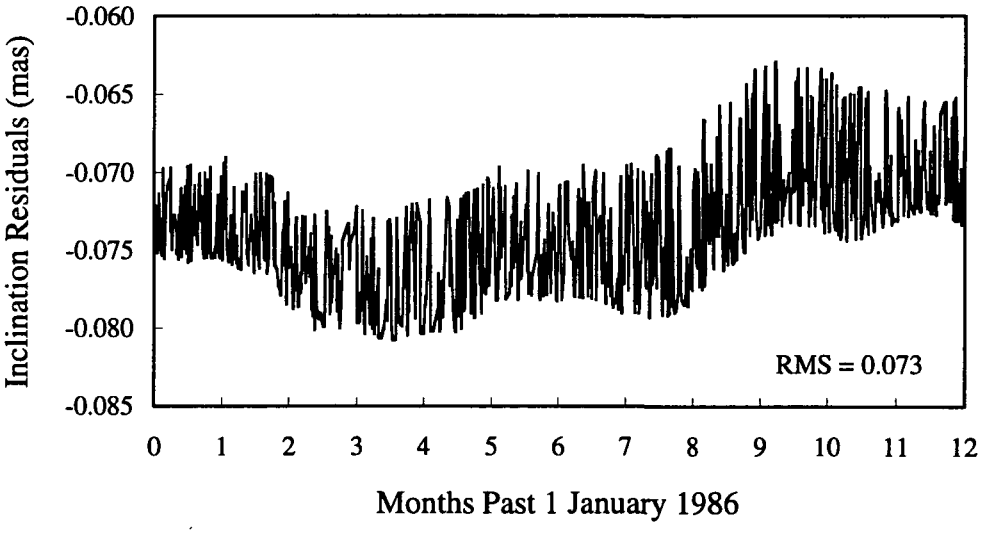

Figure D.3. Inclination Residuals Using Process Noise with J_4 and J_5 Model Deviation Signals Present but not Estimated.

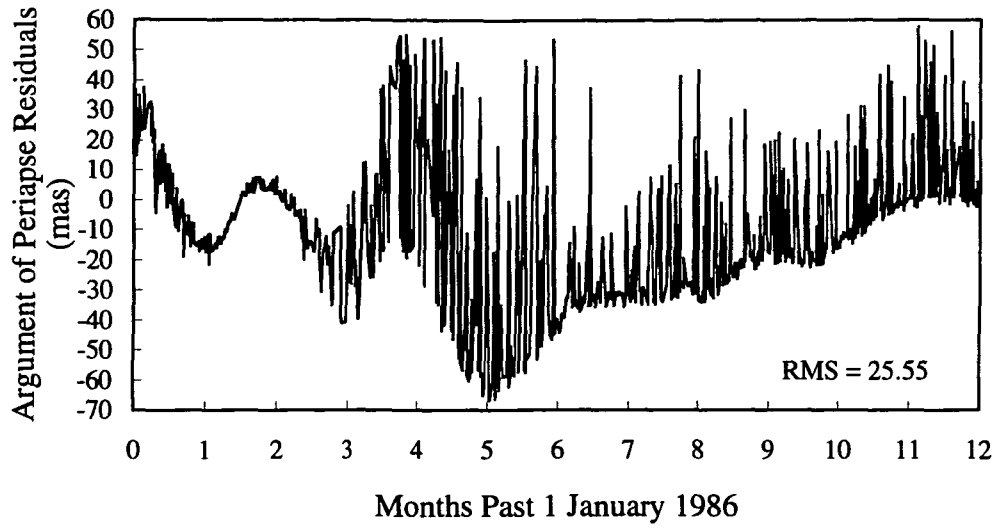

Figure D.4. Argument of Periapse Residuals Using Process Noise with J_4 and J_5 Model Deviation Signals Present but not Estimated.

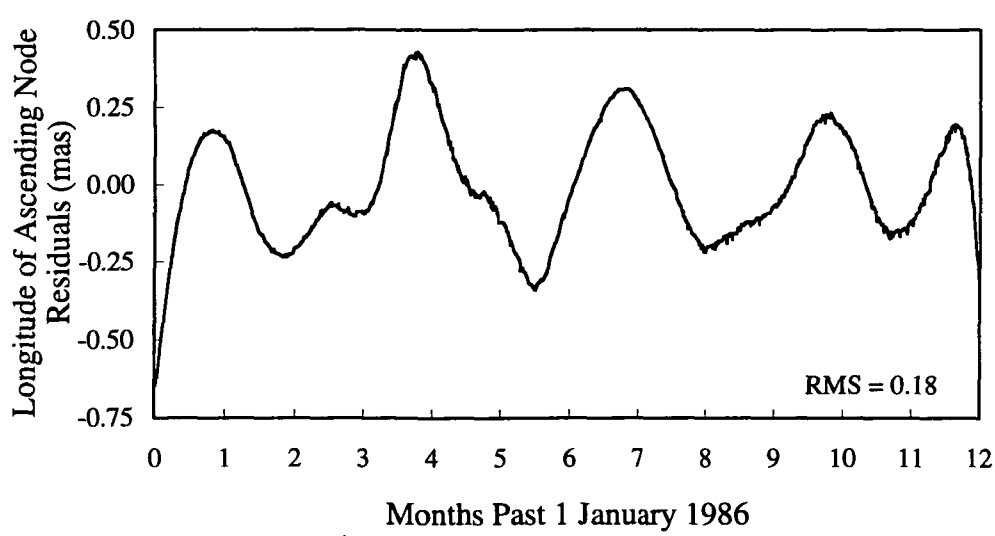

Figure D.5. Longitude of Ascending Node Residuals Using Process Noise with J_4 and J_5 Model Deviation Signals Present but not Estimated.

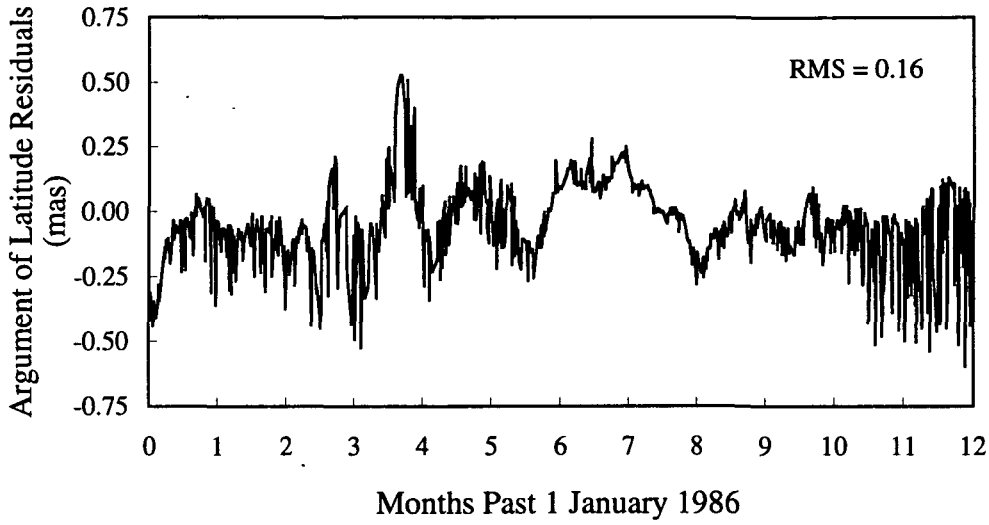

Figure D.6. Argument of Latitude Residuals Using Process Noise with J_4 and J_5 Model Deviation Signals Present but not Estimated.